Dynamic behaviour of elastic metamaterial system with negative effective mass and modulus

by

Zhengwei Li

A thesis submitted in partial fulfillment of the requirements for the degree of

Doctor of Philosophy

Department of Mechanical Engineering
University of Alberta

Abstract

Elastic metamaterials have received growing attention from the research community due to their unique properties and attractive engineering applications. The unusual elastic wave manipulation ability of the elastic metamaterials mainly comes from the delicately designed structural configuration. This thesis aims to developing elastic metamaterial systems with engineered representative cell featuring negative effective mass and/or modulus, and then conduct a systematic investigation of their dynamic behaviour, as well as their interesting applications.

To investigate the underlying mechanism of generating negative effective parameters, a two-dimensional elastic metamaterial model, consisting of a series of properly arranged rigid bodies and linear springs, is developed to exhibit both negative effective mass and modulus under specific frequencies. In this model, the translational resonance of the resonators can generate negative effective mass by inducing overall motion of the representative cells, whereas the translational resonance can generate negative effective modulus through giving rise to the local deformation of the representative cells without overall motion. By generating such controllable translational and rotational resonances in the representative cell, negative effective mass and modulus can be achieved independently. The effect of the generated negative effective mass and/or modulus on wave propagation of the elastic metamaterial has been studied.

Then, from this design strategy, a new one-dimensional elastic metamaterial is designed to possess negative effective mass and/or modulus through two types of local translational resonance introduced in the representative cell, to avoid the potential difficulties in fabrication associated with rotational motion. The unique feature of the representative cell endows the

elastic metamaterial model with great flexibility to generate these two negative effective parameters in different frequency ranges, the independent control of which is realized to some extent. Numerical analysis has been conducted to show its strong wave mitigation ability with single negative effective parameter and the phenomenon of negative phase velocity is observed when simultaneously negative effective mass and modulus exist.

Based on the one-dimensional elastic metamaterial, a new two-dimensional elastic metamaterial model is developed with simultaneously negative effective mass density, bulk modulus and shear modulus. Analytical study of the new metamaterial system is performed based on a simplified model to study the effect of the main material and geometric parameters. Numerical analysis is further conducted to simulate wave propagation in the current metamaterial. The results shows that this new elastic metamaterial can behave like solid with negative phase velocities for longitudinal and transverse waves and also can behave like fluid mainly supporting longitudinal waves with negative phase velocities.

For the new two-dimensional metamaterial designed, numerical analysis is performed to further study the wave propagation in the metamaterial system containing a large number of periodically distributed material cells. The phenomenon of negative refraction is observed at the frequency with negative phase velocity, which can potentially be utilized for sub-wavelength imaging. The numerical results clearly show the wave blocking ability of the anisotropic model in broad frequency ranges, which can be applied in vibration isolation and noise reduction.

The elastic metamaterial models and the investigations presented in this thesis shed new light on the design strategy of elastic metamaterials with negative effective parameters and provide insights into developing such metamaterials with various special functionalities.

Preface

The main body of this thesis is composed of four journal papers, which are published, submitted or in preparation. See below for details.

Chapter 2 of this thesis is mainly based on a published journal paper: Zhengwei Li and Xiaodong Wang, "On the dynamic behaviour of a two-dimensional elastic metamaterial system," *International Journal of Solids and Structures*, vol. 78-79, pp. 174-178, January 2016. The dissertation author was the primary investigator and author of this paper.

Chapter 3 of this thesis is mainly based on a submitted journal paper: Zhengwei Li, Chen Wang and Xiaodong Wang, "Modelling of elastic metamaterials with negative mass and modulus based on translational resonance." The dissertation author was the primary investigator and author of this paper.

Chapter 4 of this thesis is mainly based on a submitted journal paper: Zhengwei Li, Huan Hu and Xiaodong Wang, "A new two-dimensional elastic metamaterial system with multiple local resonances." The dissertation author was the primary investigator and author of this paper.

Chapter 5 of this thesis is mainly based on a journal paper in preparation: Zhengwei Li and Xiaodong Wang, "Wave propagation in a new two-dimensional elastic metamaterial." The dissertation author was the primary investigator and author of this paper.

Acknowledgements

This work has been carried out at the University of Alberta, Edmonton, in the department of Mechanical Engineering under the supervision of Dr. Xiaodong Wang. I would like to first express my most sincere appreciation to Dr. Xiaodong Wang for his continuous support, repeated encouragement, inspiration on the origin of the research and systematic guidance throughout my Ph.D. study. I greatly admire and respect the quiet humility of his immense wisdom, the spirit of exploration and the commitment to excellence on research. From him, I have not only gained valuable academic knowledge and methodology in the field of acoustic/elastic metamaterials but also obtained the right attitudes towards life and work. It is my great pleasure and honor to conduct research under his guidance.

I would like to express my deep gratitude to my Ph.D. supervisory committee members, Dr. Chong-Qing Ru and Dr. Ming J. Zuo for their precious help during my study. Their valuable support is sincerely appreciated. I also want to thank Dr. Zengtao Chen, Dr. Hossein Rouhani and Dr. Jeff Pieper for their valuable comments on my thesis.

Many thanks to the ASML Lab members, Dr. Huangchao Yu, Dr. Mohanmad Molavi Nojumi, Chen Wang and Shadi Abdel-Gawad. They have contributed tremendously to my personal and professional time at Alberta, being a great source of friendship as well as good advices. Working with them is an exciting and beneficial experience.

I also want to convey my heartfelt gratefulness to my friends, including but not limited to Dr. Xihui Liang, Dr. Feng Yu, Dr. Guanghan Bai, Dr. Guangfeng Chen, Dr. Jikai Liu, Dr. Lei Li, Dr. Zhengrong Chen, Dr. Wenjing Wang, Lei Zhang, Libin Liu, Yining Fang. For all the

happy time we spent together that will be always cherished and become my precious memory.

Finally, special thanks go to my family members. Words cannot express how grateful I am to my parents Wanyun Chen, Yanju Li for their unwavering love and support all along. I would like to extend my deep gratitude to my wife Huan Hu for her unconditional love, accompany and taking care of my daughter Jennifer Li and my son Daniel Li, who bring lots of joys and colors into my everyday life and drive me on during this long journey. Without their continued help and encouragement, all of these professional and personal developments would not have been possible.

Table of Contents

List of Tables

List of Figures

Chapter 1: Introduction

This Chapter mainly aims to introducing the development of metamaterials and bring out the objectives of this thesis. It is divided into four sections. The background and evolution of metamaterial are given in Section 1.1 and the motivation of the thesis topics is presented in Section 1.2. The detailed literature review of the development and challenges in the research area of acoustic/elastic metamaterials are provided in Section 1.3. Section 1.4 lists the research objectives and illustrates the main structure of the thesis.

1.1 Background

The properties of a conventional material are essentially determined by the chemical elements in the material. People have always kept on trying to better understand and manipulate the material properties with the accumulated knowledge of the nature. For instance, alloys were synthesized to improve the mechanical properties of metals over 3000 years ago. The slight doping can make the conductivity of silicone with orders of magnitude higher and this approach has laid the foundation for the whole semiconductor industry. With the aid of the rapidly developed technology, people can investigate the material properties in various scales for special functionalities. These efforts have strived to maximize the potential of existing materials and significantly enlarged the range of materials' functionalities available for human use (Liu and Zhang, 2011).

In the past several decades, attempts have also been made to pursue the desired material properties from the delicately designed subwavelength structures, rather than their composi-

tions. Termed metamaterial, these materials with artificial structures can exhibit unique properties, which are not commonly seen or physically inconceivable in nature. The materials with simultaneous negative permittivity and negative permeability under certain frequencies were first theoretically demonstrated to possess a negative refractive index (Veselago, 1968), from which the concept of metamaterial was proposed. Due to the limitation of technologies in synthesis and fabrication, this novel idea remained to be an academic curiosity at that time. A revolution started two decades ago with the experimental realization of the hypothetical materials with negative refractive index in the microwave frequency regime by mounting copper split-ring resonators and wires on interlocking sheets of fiberglass circuit board (Shelby et al., 2001; Smith et al., 2000). Ever since then, considerable interests have been sparked in the field of electromagnetic metamaterial and various unprecedented applications of this type of metamaterials have been proposed. The property of negative refraction was utilized to develop superlense with spatial resolution beyond the diffraction limit (Pendry, 2000; Shalaev, 2007; Zhang and Liu, 2008). The ability to adjust the permittivity and permeability independently and arbitrarily through the metamaterials makes the electromagnetic cloaks possible (Landy and Smith, 2012; Leonhardt, 2006; Pendry et al., 2006; Schurig et al., 2006). Many of these concepts, techniques and applications are not exclusive to electromagnetic waves and their counterparts exist in other areas of wave science.

Since the analogy between electromagnetic and acoustic waves was found to identify compliance with electric permittivity and relate mass density with magnetic permeability (Auld, 1973; Carcione and Cavallini, 1995; Chan et al., 2006), considerable attention has been placed on the research of acoustic metamaterials to explore the possible similar applications for acous-

tic waves (Craster and Guenneau, 2013; Cummer et al., 2016; Wu et al., 2018). Typical acoustic metamaterials have been developed to achieve negative effective mass and/or negative effective bulk modulus (Fang et al., 2006; Lee et al., 2017, 2010; Liu et al., 2000; Lu et al., 2009; Ma and Sheng, 2016). By making use of these unusual properties of the developed metamaterials, researchers are considering using acoustic metamaterials in advanced applications, such as acoustic wave mitigation (Jiang et al., 2014; Mei et al., 2012), acoustic superlens (Moleron and Daraio, 2015; Park et al., 2015), and acoustic cloaks (Bi et al., 2018; Zigoneanu et al., 2014). Despite these fabulous achievements already obtained, there are still growing efforts placed on the development of acoustic metamaterials to seek new functionalities.

Acoustic metamaterials have already been studied intensively. However, relatively less attention has been paid to elastic metamaterials, which can show richer dynamic behavior and offer more potential applications due to the coexisting and coupling of longitudinal and transverse waves in the elastic medium (Zhou et al., 2012; Zhu et al., 2015). These two kinds of metamaterials have developed along with each other by sharing two independent effective parameters, effective mass and bulk modulus, which are identified as the essential parameters in controlling acoustic wave propagation (Cummer et al., 2016; Ma and Sheng, 2016). Some classic elastic metamaterials have already been designed to possess negative effective parameters for elastic waves, such as negative effective mass, bulk modulus and shear modulus (Lai et al., 2011; Liu and Hu, 2016; Wu et al., 2011; Zhou and Hu, 2009; Zhu et al., 2014a). However, the potentials of elastic metamaterial have not been fully explored yet and the development of elastic metamaterial is still in its early stage. Most of the current elastic metamaterial models with negative effective parameters only provide theoretical guidance for further research of

elastic metamaterials and their potential applications.

1.2 Motivation

It is now well established that there are several ways to generate negative effective mass and modulus. The first negative effective mass has been achieved with the unit cell as shown in figure 1.1(a). The translational motion of the coated lead sphere will cause an overall motion of the cell, resulting in frequency-dependent effective mass and its working mechanism can be clearly illustrated with the spring-mass model in figure 1.1(b). This classic approach has been intensively implemented to design acoustic/elastic metamaterials with negative effective mass.

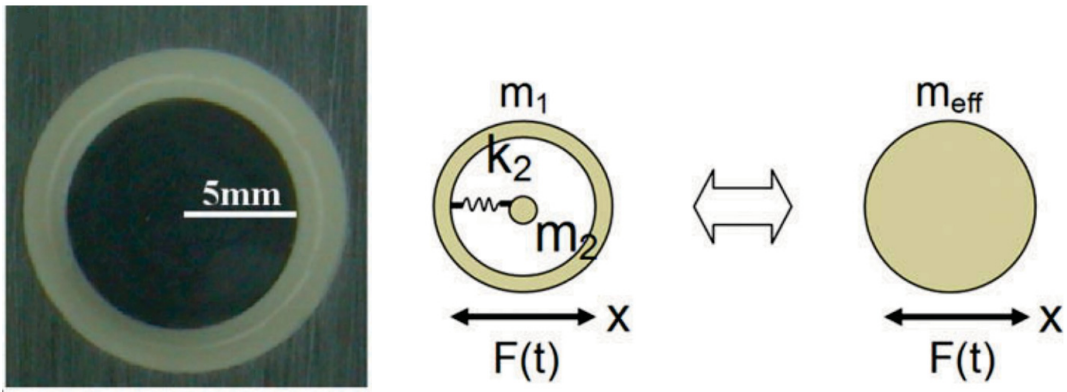

(a) (b)

Figure 1.1: (a) The cross section of the continuum representative cell ((Liu et al., 2000), image used with permission from The American Association for the Advancement of Science), (b) the single spring-mass system ((Huang et al., 2009a), image used with permission from Elsevier).

For negative effective modulus, the Helmholtz resonator in figure 1.2(a) was firstly used to induce resonance of the fluid in the neck section to generate negative effective bulk modulus (Fang et al., 2006). This approach can be just applied to acoustic metamaterials. A mechanical resonator, as shown in figure 1.2(b), was then introduced to generate negative effective modulus

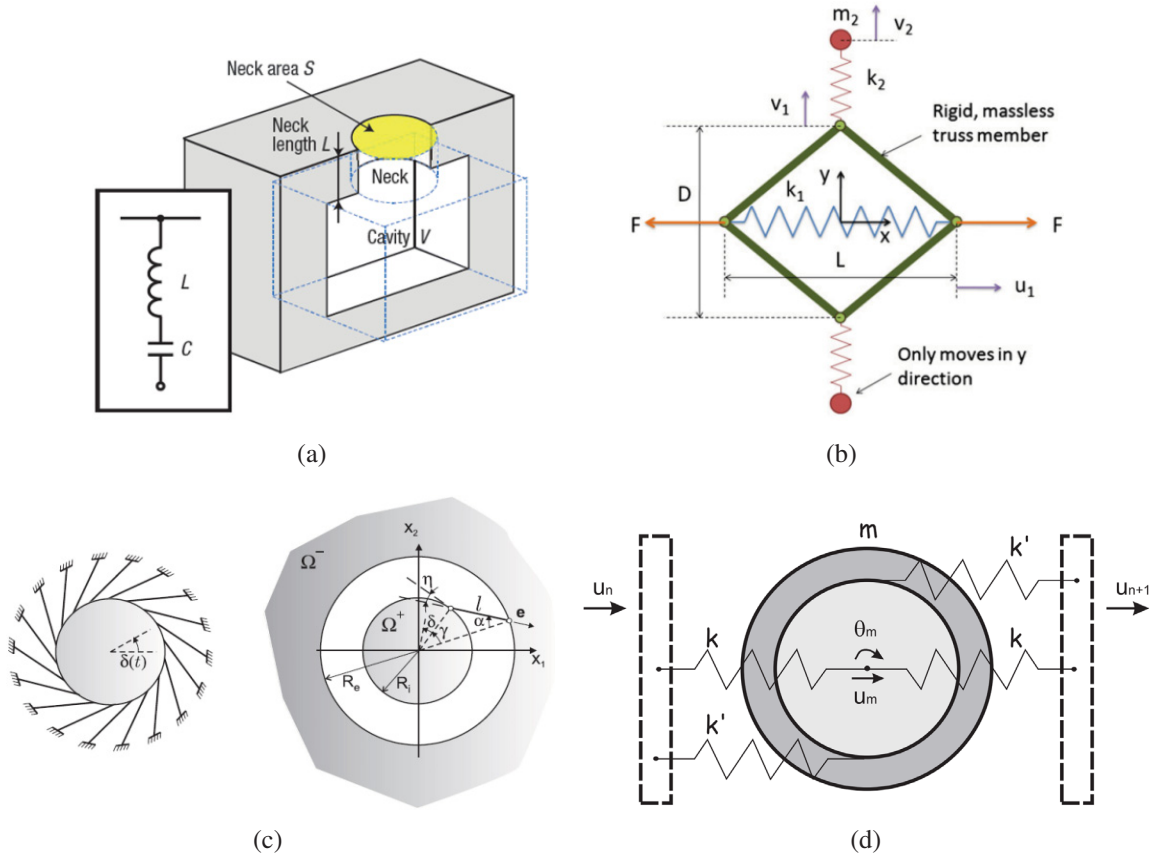

Figure 1.2: (a) Schematic corss-sectional view of a Helmholtz resonator ((Fang et al., 2006), image used with the permission from Springer Nature), (b) a unit of the mechanial model with negative modulus ((Huang and Sun, 2011a), image used with permission from Elsevier), (c) schematic view of the model ((Bigoni et al., 2013), image used with permission from The American Phyical Society), (d) part 1 of the unit cell ((Wang, 2014), image used with permission from Elsevier).

through translational resonance in the transverse direction (Huang and Sun, 2011a). However, this model cannot endure horizontal overall motions. Then, as depicted in figure 1.2(c), the centre resonator was connected to the matrix through beam ligaments and the rotation of the resonator can lead to compressive or tensile radial stress on the boundary of the void to cause similar effect of monopolar resonance, which can generate negative effective bulk modulus (Bigoni et al., 2013). This design is not easy to fabricate and use though. Most of the existing elastic metamaterials combined these approaches mentioned to generate double negative effec-

tive parameters, negative effective mass and bulk modulus. Then, a one-dimensional model, as shown in figure 1.2(d), obtained negative effective mass and modulus through rotational and translational motion of the resonators and the two effective parameters can be adjusted in a controllable manner (Wang, 2014). This simple spring-mass model clearly illustrated that the overall motion of the representative cell will generate effective mass and the local deformation of the representative cell will result in effective modulus, shedding a light on the fundamental understanding of manipulation of acoustic/elastic waves.

In light of the progress in elastic metamaterials, a spring-mass model has been developed as part of the work in this thesis to further illustrate the mechanism of generating effective parameters in two dimensions, as the extension of the one-dimensional model shown in figure 1.2(d). These two effective parameters in this two dimensional spring-mass model can be controlled independently and this model can provide guidance in designing two-dimensional elastic metamaterials (Li and Wang, 2016).

For the development of elastic metamaterials, the effective shear modulus plays an indispensable role. As discussed, negative effective shear modulus has already been achieved in several elastic metamaterial models. However, no triple negative elastic metamaterial exists, i.e., simultaneously negative effective mass, bulk modulus and shear modulus. Triple negative elastic metamaterial is of significant importance to the development of metamaterials due to the negative refraction of both longitudinal and transverse waves. To this end, based on the same approach that local deformation of the representative cell can induce effective modulus and overall motion of the representative cell can generate effective mass, a one-dimensional realistic metamaterial structure has been firstly developed with controllable negative effective mass

and modulus through translational resonances. Directly from this one-dimensional model, a two-dimensional elastic metamaterial is further developed with simultaneously negative effective mass, bulk modulus and shear modulus.

1.3 Literature review

This part provides a literature review of acoustic/elastic metamaterials featuring negative effective parameters including the development, the challenges and their attractive applications.

1.3.1 Metamaterials with negative effective mass

There has been significant attention paid to the development of acoustic/elastic metamaterials with negative effective mass (Bonnet and Monchiet, 2017; Ge et al., 2018; Islam and Newaz, 2012; Lu et al., 2017). It is a common sense that the mass density of a composite should be considered as the volume average of the constituent components with the implicit assumption that all the constituent components move in unison (Mei et al., 2007; Sheng et al., 2007). However, this theory does not hold when relative motion between the constituent components exists due to the local resonant behavior (Mei et al., 2006; Mitchell et al., 2014), and then the composite will display an exotic inertia response, different from that of a homogeneous material (Banerjee, 2011). The effective mass can deviate significantly from its static value and it will turn negative at frequencies where the sub-wavelength microstructure resonates and moves out of phase with the excitation (Deymier, 2013; Gan, 2018). It can be concluded that the negativity of the effective mass directly results from the attempt to use a single mass to represent a composite structure with more than one component and it describes the out-of-phase relation between the average acceleration and the external loading (Lee and Wright,

2016; Wang et al., 2004).

The initial experimental realization of acoustic/elastic metamaterials with negative effective mass has been achieved by embedding heavy lead spheres coated with soft silicon rubber in epoxy to activate the so-called dipolar resonance. This local resonance characterized by the relative motions of the constituents internal to the elementary building block can be activated as chosen frequencies with proper adjustment of the structural and material parameters, creating band gaps two orders of magnitude lower than that obtained by the Bragg scattering (Liu et al., 2000). In this pioneer work, the composite with randomly dispersed resonators still possessed negative effective mass to attenuate sound wave and break the conventional mass-density law, indicating the key role of the local resonance rather than the periodicity of the structure. In what follows, the general concept of local resonance has motivated further studies of acoustic/elastic metamaterials with negative effective mass and different local resonators have been fabricated based on the variation of the shape and materials of the components, such as distributing particles in water (Larabi et al., 2007; Zhao et al., 2005) and penetrating angularly anisotropic cylindrical scatters in rigid waveguide (Gracia-Salgado et al., 2013). For the metamaterials mentioned above, the negative effective mass only exhibits over a pretty narrow frequency region. To overcome this problem, thin membrane-type resonator has been proposed to control acoustic wave for broadband frequency range (Huang et al., 2016; Ma et al., 2013; Yang et al., 2010), and negative effective mass density below a cut-off frequency was achieved in such acoustic metamaterials consisting of an array of tubes with stretched rubber membranes fixed (Lee et al., 2009a). Similar results can be obtained in a continuum metamaterial model with clamped boundary conditions (Yao et al., 2010). Also, multilevel local resonators (An et al.,

2015; Huang and Sun, 2010; Xiao et al., 2012) and resonators with graded stiffness and/or masses (An et al., 2017; Banerjee et al., 2017; Baravelli and Ruzzene, 2013) have been considered to extend the widths of the frequency ranges with negative effective mass to some extent. Lattice structure with local resonators also has been reported as broadband elastic metamaterial since wave cannot propagate in lattice system above a certain frequency (Liu et al., 2015).

Thorough theoretical explorations with spring-mass systems consisting of mass-in-mass resonating units have also been conducted to investigate the mechanism of generating negative effective mass in acoustic/elastic metamaterials (Huang et al., 2009a; Lee and Wright, 2016). A rigorous theoretical framework has been formed to describe the harmonic motion of a spring-mass system with frequency-dependent effective mass developed from Newton's law (Milton and Willis, 2007). The relation between the negative effective mass, band gaps and dispersion curves has been clearly illustrated (Huang and Sun, 2009b). Specifically, negative effective mass will generate band gaps, in which only purely imaginary wave numbers exist. This relation is experimentally and numerically verified through wave transmission analysis for such a mass-in-mass system (Yao et al., 2008). Efforts have been made to describe the dynamic behavior of this kind of spring-mass systems, in the sense of an effective medium (Liu et al., 2012; Srivastava, 2015; Zhu et al., 2011).

It is now well established that properly designed local resonances in the representative cells can generate negative effective mass. In general, the effective mass will be highly frequency-dependent and become negative at certain frequencies (Liu et al., 2005; Ma and Sheng, 2016; Zhu et al., 2016a).

1.3.2 Metamaterials with negative effective modulus

It is intuitive to expect that the resulting displacement of a deformed elastic object will be in the same direction as the external force with implicit assumption of positive definite elasticity tensor, which indicates positive bulk modulus and shear modulus (Ting, 1996; Zadpoor, 2016). However, acoustic/elastic metamaterials with their inherent deep sub-wavelength nature have triggered exciting investigations on the abnormal dynamic properties regarding the effective modulus. It has been shown that negative effective bulk modulus is associated with the so-called monopolar resonance, whereas negative effective shear modulus is associated with the so-called quadrupolar resonance (Li and Chan, 2004; Wu et al., 2007; Zhou and Hu, 2009). Here, negative bulk modulus describes the out-of-phase relation between the volume deformation and the external triaxial loadings and negative shear modulus illustrates the out-of-phase relation between the antisymmetric deformation and loading (Zhou et al., 2012). Due to the local resonances, the resulting effective moduli will be highly frequency-dependent and can turn negative at certain frequencies.

Initially, a composite of soft rubber spheres suspended in water has been taken as a theoretical example to show that the volume dilation of the rubber sphere could be out of phase with pressure field applied near the monopolar resonance frequency, generating negative effective bulk modulus (Li and Chan, 2004). The first negative effective bulk modulus was demonstrated experimentally on ultrasound by a waveguide shunted with a chain of Helmholtz resonators (Fang et al., 2006). The Helmholtz resonance was characterized by the oscillation of the fluid in the narrow neck section, which can be considered to be incompressible due to the small volume of the neck compared to that of the cavity. In this scenario, the fluid in the neck section

played the role of mass whereas the cavity of the Helmholtz served as a spring. The resonant frequency can be adjusted by altering the geometrical parameters of the resonators and when the resulting bulk modulus turned negative, the sound waves were almost entirely reflected back, generating a broad band gap (Cheng et al., 2008; Fey and Robertson, 2011). Similar approaches have been applied in acoustic metamaterial systems consisting of an array of tubes with side holes (Lee et al., 2009b) or periodically arraying split hollow spheres in the sponge matrix (Ding and Zhao, 2011; Ding et al., 2010). Quasi-two-dimensional structure with drilled cylindrical boreholes has been reported to exhibit negative bulk modulus due to the interaction of the modes localized in the boreholes and the sound waves (Garcia-Chocano et al., 2012). The so-called double-fishnet metamaterial featuring a pair of closely spaced, periodically perforated plates, can attenuate sound waves for a wide range of frequencies and angles due to the negative bulk modulus generated (Bell et al., 2012; Christensen et al., 2010). These are typical approaches for acoustic metamaterials to obtain negative bulk modulus.

Also, the phenomenon of negative bulk modulus has been observed in the elastic metamaterials with bubble-contained-water spheres embedded in epoxy matrix (Ding et al., 2007), and negative effective shear modulus has been obtained by introducing the quadrupolar resonance (Lai et al., 2011). Chiral resonators featuring rotational resonance are implemented to induce negative effective bulk modulus (Bigoni et al., 2013; Liu et al., 2011a; Wang et al., 2016). To provide guidance for the design of elastic metamaterials with negative effective modulus, the dynamic response of simplified spring-mass models have been intensively investigated and the physical mechanism lies in that the translational resonance behaviour of the mass in the vertical direction induces an expansion of the structure in the horizontal direction when loaded under a

compressive force (Huang and Sun, 2011a; Zhou et al., 2012).

It should be noted that the negative effective modulus of acoustic/elastic metamaterials is distinct from the static negative stiffness of inclusions observed in the composites with stored energy from deformation (Drugan, 2007, 2017; Kochmann and Drugan, 2009; Lakes et al., 2001). The former one is induced by the local resonance effects from the designed representative cell and can be stable without constraint. However, the latter one should have constraint to be stable.

1.3.3 Metamaterials with simultaneously negative effective mass and modulus

It is now well established that realization of acoustic/elastic metamaterials with negative parameters needs local resonance within a certain frequency range. Then, it will be natural to obtain double negative dynamic behavior by overlapping the negative frequency ranges with negative mass or modulus from different types of local resonances (Ma and Sheng, 2016).

The possibility of acoustic metamaterials possessing simultaneously negative mass density and bulk modulus has been mathematically demonstrated for the first time (Li and Chan, 2004). The first successful experimental demonstration of acoustic double negativity was realized in the composite structure consisting of elements of negative mass density (thin membranes) and bulk modulus (side holes) (Lee et al., 2010). Similarly, a water based two-dimensional acoustic metamaterial combined Helmholtz and rod-spring resonators to make simultaneously negative mass density and bulk modulus occur (Fok and Zhang, 2011). A one-dimensional spring-mass model also was developed to illustrate the underlying mechanism of generating negative mass and negative modulus respectively (Huang and Sun, 2012). More recently, a three-dimensional

double negative acoustic metamaterial has been experimentally realized by embedding soft rubber microbeads in a water-based gel matrix to induce monopolar and dipolar resonances in an overlapping frequency range (Brunet et al., 2014). Most of the efforts have been focused on the acoustic metamaterials (Kaina et al., 2015) and the study of elastic metamaterials is relatively few due to its coupled waves.

For elastic waves, the frequency overlapping of monopolar resonance for bubble-contained water spheres and dipolar resonance for rubber-coated gold spheres in the epoxy matrix was realized in a composite with epoxy matrix (Ding et al., 2007). A chiral structure has been developed to gain double negative effective parameters at certain frequencies through translational and rotational motion of the resonators (Liu et al., 2011a), and the phenomenon of negative refraction for longitudinal wave is experimentally observed in an elastic metamaterial featuring chiral resonators (Zhu et al., 2014b). The chiral resonators have shown great potential in designing double elastic metamaterials. However, the translational and rotational motion of the resonators is coupled. To clearly clarify the working mechanism of generating negative effective parameters, one-dimensional and two-dimensional elastic metamaterials featuring springs and masses have been developed to generate independently controllable effective mass and modulus (Li and Wang, 2016; Wang, 2014). The theoretical possibility of negative effective shear modulus has been investigated (Wu et al., 2007; Zhou and Hu, 2009) and it was realized in a double negative elastic metamaterial comprising fluid-solid composite inclusions (Wu et al., 2011). Almost at the same time, a hybrid elastic solid showed dynamic behavior featuring simultaneously negative mass density and bulk modulus, or simultaneously negative mass density and shear modulus (Lai et al., 2011). After that, continuing efforts have

been paid to design elastic metamaterials with double negative effective parameters, such as a hybrid elastic metamaterial with integration of negative capacitance shunted piezoelectric patches to obtain negative effective mass density and tunable negative bending stiffness (Chen et al., 2017). However, no elastic metamaterial with simultaneously negative effective mass, bulk modulus and shear modulus exists yet.

1.3.4 Applications

The emerging of metamaterial has revolutionized the material design and strongly expedited the research of advanced materials with unprecedented properties. The concept of acoustic/elastic metamaterials extends far beyond negative effective mass and/or modulus, rather giving unprecedented opportunities of designing devices for various attractive applications, which are just beginning to be explored (Cummer et al., 2016; Ge et al., 2018). As the most popular applications, wave mitigation, wave negative refraction and wave cloaking have been illustrated in the following.

Wave mitigation

The need of blocking unwanted vibration is a long-standing subject in engineering and one of the prominent applications of acoustic/elastic metamaterials undoubtedly goes to their wave mitigation ability (Chen et al., 2016; Tan et al., 2014). The early effort started from trying to attenuate sound waves through periodic structures based on the underlying principle of impedance variation. In this case, their lattice constants are of the same order of the characteristic wavelengths (Hussein et al., 2014). Since the most common and devastating acoustic/elastic waves in the industries are usually in the low frequency ranges, blocking low frequency waves

is generally more desired than filtering those with high frequencies. In this scenario, periodic structures were not practical solutions for low frequency wave mitigation due to the large lattice constants needed. To address this limitation, localized resonance in acoustic/elastic metamaterials was exploited to show great potential in wave attenuation due to the superior performance in the low frequency frequency ranges. The local-resonance-induced band gap can reach to very low frequency range where the wavelength is much larger than the size of the microstructure and the band gap can be easily tuned through proper microstructure design in the acoustic/elastic metamaterials.

A composite has been firstly demonstrated to attenuate sound waves with wave lengths two orders larger than the lattice constant by introducing local resonance (Liu et al., 2000). After that, local resonance became a classic approach to mitigate acoustic/elastic waves and various acoustic/elastic models featuring negative effective mass or modulus have been developed to mitigate low-frequency waves (Song et al., 2015). Elastic metamaterials with anisotropic mass density also have been developed due to their various wave filtering ability along different wave propagation directions (Liu et al., 2015; Zhu et al., 2016b). However, due to the resonant nature of the metamaterial structures, the band gaps formed were usually of narrow bandwidths, which greatly limited their practical engineering applications. As discussed previously, several approaches have been made to extend the band gaps, such as membrane-type metamaterials (Ma and Sheng, 2016; Yang et al., 2008), multiple and graded resonators (An et al., 2015; Banerjee et al., 2017). Recently, the integration of active control technologies into the passive metamaterial structures started to show great potential in wave mitigation with reconfigurability and tunability (Cheer et al., 2017; Chen et al., 2017; Popa et al., 2015; Xiao et al., 2015).

Here, the band gap formation of the elastic metamaterials in the sense of an isotropic medium is explained as an example to illustrate the underlying mechanism of attenuating waves with single negativity. For the two-dimensional case, the phase velocities of the longitudinal and transverse waves can be calculated in terms of the effective material parameters as $c_p = \sqrt{(\kappa_e + \mu_e)/\rho_e}$ and $c_t = \sqrt{\mu_e/\rho_e}$, respectively. When either the effective bulk modulus κ_e and the effective mass density ρ_e turns negative due to the local resonance, the phase velocity of the longitudinal wave will be purely imaginary. It should be mentioned that in this scenario, the effective bulk modulus κ_e from local resonance plays a dominating role in controlling the wave phase velocities, rather than the effective shear modulus μ_e. Similarly, for transverse waves, the phase velocities are purely imaginary when one of the effective shear modulus μ_e and mass density ρ_e is negative. Imaginary phase velocity implies imaginary wave number, indicating that the waves will decay exponentially. In other words, in the frequency range for single negativity, wave cannot propagate through the effective medium, forming a band gap (Huang et al., 2009a; Mitchell et al., 2014). The formation of band gap can also be illustrated from the perspective of energy transfer mechanism. In a mass-in-mass lattice structure with negative effective mass, it has been shown that most of the work done by the external force is temporarily stored in the resonators and then the kinetic energy will be taken out by the external force in the form of negative work in a cyclic manner (Huang and Sun, 2009b).

Wave negative refraction

High-resolution acoustic/elastic imaging techniques are of significant importance for underwater sonar sensing, non-destructive evaluation and medical ultrasonic diagnostics (Craster and

Guenneau, 2013). However, the scattered waves from an object contain not only propagating waves but also evanescent waves, which carry the sub-wavelength features of the object. These evanescent waves decay exponentially and will be permanently lost before reaching the imaging plane of the conventional lens, which greatly limits the resolution of imaging. The first breakthrough was achieved in a flat slab with simultaneously negative permittivity and permeability, and the so-called perfect lens can focus the propagating waves and recover the evanescent waves through its negative refractive index to overcome the diffraction limit (Pendry, 2000). Since then, negative refraction has opened the door for realization of imaging and focusing with super spatial resolution (Zhang and Liu, 2008). Growing interests have been stimulated to develop acoustic/elastic metamaterials with double negative parameters featuring negative refraction (Brunet et al., 2014; Ge et al., 2018; Zhou et al., 2012). An acoustic superlense featuring Helmholtz resonators was experimentally realized to achieve negative refractive index with double negative effective parameters by breaking the structural symmetry and it showed sub-wavelength imaging with resolution 3.5 times better than the diffraction limit (Kaina et al., 2015). Besides negative refraction, similar effects for acoustic waves have been obtained with negative effective mass (Ambati et al., 2007; Park et al., 2011), or anisotropic effective mass (Ao and Chan, 2008; Li et al., 2009; Shen et al., 2015), which also can amplify the evanescent waves. A large amount of research work has been reported on negative refraction of the acoustic wave in fluid-like media (Cummer et al., 2016; Ma and Sheng, 2016). However, few attentions have been placed on the study of the negative refraction of elastic waves based on local resonance in solid media where the coupled longitudinal and transverse waves bring challenging but richer wave phenomena.

Wave cloaking

Wave cloaking, as an almost magic concept in metamaterials, is to redirect the incident wave around an object without scattering any of the wave energy through a spatially varying refractive index, rendering the object invisible (Chen et al., 2010). Earliest progress has been achieved in the field of electromagnetic metamaterials based on a coordinate transformation method, which is rooted in the form-invariance of Maxwell's equation (Cummer et al., 2006; Fleury et al., 2015; Pendry et al., 2006). This approach was then extended to manipulate acoustic waves due to the form-invariance of the acoustic wave equations under coordinate transformation with the implicit requirement of homogeneous and anisotropic mass density (Chen and Chan, 2007; Cummer and Schurig, 2007). Various models have been developed theoretically and experimentally, such as the broadband two-dimensional underwater ultrasound cloaking using a device with a network of acoustic circuit element (Zhang et al., 2011), the first omnidirectional ground cloak in air in three dimensions (Zigoneanu et al., 2014), and the recent three-dimensional broadband underwater acoustic carpet cloak (Bi et al., 2018).

Naturally, the coordinate transformation technique has been considered for elastic waves. However, there are two main barriers for this extensional work. For elastic waves, longitudinal waves are coupled with in-plane and anti-plane shear waves. Also, the Naiver equations cannot guarantee the form-invariance under generalized coordinate transformation (Colquitt et al., 2014; Graeme et al., 2006). Despite these barriers, a cylindrical cloak for in-plane coupled longitudinal and shear waves was developed through the material with heterogeneous isotropic density and heterogeneous anisotropic elastic stiffness tensor, showing the major symmetry, rather the minor symmetry (Brun et al., 2009). It was further demonstrated that transformation

elastodynamics for elastic cloaking requires the materials with stiffness tensor lacking the minor symmetry, indicating asymmetry stress (Norris and Shuvalov, 2011), which was found in hyperelastic solids under pre-deformation (Norris and Parnell, 2012). This special requirement limited the elastic wave cloaking to some complicated structures with the minor symmetry irrelevant (Sklan et al., 2018). There is still a long way for practical elastic wave cloaking. However, the unremitting efforts in this field make this goal touchable (Diatta et al., 2016; Parnell and Shearer, 2013; Zhang and Parnell, 2018).

1.4 Research objectives and outline

The objectives of this thesis are to develop realistic metamaterial structures with simultaneously negative effective mass and effective modulus and conduct a systematic investigation of the dynamic behavior of the elastic metamaterials under harmonic excitation.

In detail, this extensive investigation in this thesis is carried out by the following steps:

1. **Mechanism investigation:** modelling of a simplified two-dimensional elastic metamaterial structure, which consists of a series of properly arranged local resonators based on idealized massless linear springs and rigid masses. The underlying mechanism of generating negative effective mass and negative effective modulus has been intensively investigated. The key feature of the model lies in that the effective mass and modulus of the model can be adjusted independently.

2. **A new one-dimensional elastic metamaterial model:** developing a one-dimensional model and investigating its dispersion characteristics of wave propagation based on analytical and numerical methods. The dynamic behavior of this model has been studied

through its wave reduction functionality and the phenomenon of negative phase velocity with negative effective parameters under certain frequencies. This elastic metamaterial model can be directly used to design elastic metamaterial with controlled effective mass and modulus only based on translational resonances.

3. **A new two-dimensional elastic metamaterial model:** developing a two-dimensional elastic model with simultaneously negative effective mass, effective bulk modulus and effective shear modulus. The association of negative effective mass and moduli with the mode of local resonance, the eigenstate, is evaluated. This elastic metamaterial model can behave like solids or fluid for elastic waves with negative phase velocities in different wave propagating directions.

4. **Wave propagation of the new two-dimensional elastic metamaterial model:** studying the unusual dynamic properties of the new elastic metamaterial and its anisotropic case by conducting extensive numerical analysis. The attractive applications of the elastic metamaterial featuring negative refraction and wave attenuation have been discussed.

This thesis is prepared in the paper-based format except for Chapter 1 and Chapter 6. Chapter 1 provides an intensive introduction to the current research in the field of elastic metamaterials and illustrates the significance of the undertaking work with the objectives listed. Chapter 6 concludes the research of this thesis with highlights of its main contributions and propose future work for subsequent research. Chapters 2-5 are written in the form of a paper based on these four steps respectively.

Chapter 2: On the dynamic behaviour of a two-dimensional elastic metamaterial system

The current Chapter develops a two-dimensional mechanical system with local resonators to investigate the general mechanism of elastic metamaterials to generate negative effective material parameters. This system can exhibit simultaneously negative effective mass and modulus at certain frequencies through the controllable translational and rotatioal resonance induced in the representative cells. The dynamic behaviour of the developed system under different frequencies is evaluated in consideration of the effective mass and modulus.

2.1 Introduction

Metamaterials are engineered materials exhibiting unique properties, which are not commonly seen or physically inconceivable in nature. Early efforts in developing such unusual materials had been mostly focussed on new electromagnetic materials to control electromagnetic waves. It was demonstrated theoretically that materials with simultaneously negative permittivity and negative permeability under certain frequencies will possess a negative refractive index (Veselago, 1968), from which the concept of metamaterial was proposed. Due to the limitation of technologies in synthesis and fabrication, this novel idea remained to be an academic curiosity at that time. Only in recent years, the feasibility of designing this type of metamaterials, so-called left-handed electromagnetic materials, was justified and the new materials were successfully devised to achieve effectively negative permittivity and negative permeability (Pendry, 2000; Shelby et al., 2001; Smith et al., 2000). By making use of the unusual properties of the

developed materials, researchers are considering using metamaterials in advanced applications, which could not be achieved before, such as invisible cloak (Pendry et al., 2006; Schurig et al., 2006) and hyperlens (Liu et al., 2007) for electromagnetic waves.

As the counterpart of electromagnetic materials in mechanical engineering, in recent years, acoustic or elastic metamaterials, which exhibit negative effective mass or negative modulus, have also received significant attention. Many peculiar properties of these metamaterials have been predicted based on different material models, which provide the mathematical analogy between electromagnetic behaviour and mechanical behaviour. The main focus in the development of these materials is the design of engineered microstructures, which can generate the desired properties. The first design of such a material structure is by embedding heavy spheres coated with soft silicon rubber in epoxy to acquire, experimentally, negative mass at certain loading frequencies (Liu et al., 2000). The underlying mechanism of this material structure is the local mechanical resonance. This mechanism has been used in the design of other metamaterial systems, such as distributing local mechanical resonators in water (Larabi et al., 2007) to develop acoustic metamaterials, or using distributed membranes to generate periodic resonators in acoustic media to achieve negative mass (Cselyuszka et al., 2015; Lee et al., 2009a; Mei et al., 2012). It is now well-established that properly designed local resonance can generate negative effective mass for acoustic metamaterials. In general, the effective mass will be frequency-dependent and become negative at certain frequencies (Huang et al., 2009a; Liu et al., 2005; Milton and Willis, 2007; Movchan and Slepyan, 2007; Yao et al., 2008). Recently, multilevel resonators have also been considered in the generation of negative mass in a one-dimensional hierarchical metamaterial system (An et al., 2015).

Acoustic metamaterials with apparent negative modulus have also received increasing interests. A one-dimensional acoustic metamaterial system consisting of a chain of subwavelength Helmholtz resonators experimentally yields negative group velocity as a result of the negative bulk modulus (Fang et al., 2006). Similar results have also been achieved in a metamaterial system consisting of an array of tubes with side holes (Lee et al., 2009b). To develop elastic metamaterials, theoretical models have been developed based on spring-mass systems, mainly in one dimension cases, exhibiting frequency-dependent effective modulus (Huang and Sun, 2011a; Zhou et al., 2012). Attempts have also been made to achieve both negative mass and negative modulus (Bigoni et al., 2013; Liu et al., 2011a), using more general two-dimensional spring-mass models. However, in these works, negative mass and negative modulus cannot be adjusted independently in a controllable manner. It should be mentioned that one of the main issue in the development of this type of metamaterials is to precisely manipulate the dynamic behaviour and wave propagation in the metamaterials, and therefore, the desired negative mass and negative modulus should be reliably controlled. Recently, a one-dimensional metamaterial model formed with a special mass-spring system is proposed, with which the effective mass and effective modulus, depending on the loading frequency and structural parameters, can be easily tuned to desired positive or negative values by adjusting the geometry and material properties of the system (Wang, 2014).

The current paper, as the extension of the corresponding study of the one-dimensional model (Wang, 2014), presents a two-dimensional (2D) metamaterial system consisting of periodic cells formed by properly arranged mass-spring structures. The structure allows rather independent local translation motion and rotation motion, making effective mass and effective

modulus being easily controlled, with the translational motion directly dominating the effective mass and the rotational motion controlling the effective modulus. Numerical simulation is conducted to show the resulting negative mass and negative modulus under specific loading frequencies and geometries. The frequency response of the effective properties and the effects of geometric parameters are also presented to illustrate the feasibility of designing the desired effective properties by proper adjusting the metamaterial cell. The dynamic behaviour of such a two-dimensional metamaterial system is also studied by considering the elastic wave propagation in the effective medium under different conditions of the metamaterial cell. Some of the basic features of the current 2D model are similar to that of the previous 1D model, but significantly different dynamic behaviour in 2D cases is observed, such as Poisson's ratio effect, the direction dependence of wave propagation, and the complexity of the 2D model. More importantly, the 2D model will provide a guideline for designing realistic 2D metamaterials.

2.2 Formulation of a two-dimensional metamaterial model

Consider a two-dimensional metamaterial system formed by a periodic structure, as shown in figure 2.1(a). The representative cell of the system consists of two separate units, as shown schematically in figure 2.1(b and c). Each unit contains one circular rigid body, for linear springs attached to the centre, and four side springs wrapping around the rigid body with a radius R. These springs are attached to the boundary of the cell formed by four light rigid bodies, as shown by the dashed rectangles. In a cell, the arrangement of the two units is that one unit is in front of the other in the out-of-plane direction and the four boundary rigid bodies are shared by the two units, such that the two units move independently but having the same boundary displacements. It should be noted that because of the different wrapping directions

of springs in these two units when same displacements are applied to the boundary of the cell, the two rigid bodies of the two units will rotate in opposite directions.

The two units in the cell are geometrically similar, i.e. the second unit is formed by rotating the first unit by 180^{o} about the vertical axis (or horizontal axis). The two rigid bodies in the two units can freely move and rotate around their mass centres (the centres) with the same mass and moment of inertia, denoted as m and I, respectively. The only difference between the two units is in the directions of rotation of the respective rigid bodies. The spring constants of the springs are k and k', respectively, as identified in figure 2.1(b and c). The size of the cell, measured from left to the right, is assumed to be L, which is determined by the length of the springs.

The attention is focussed on the harmonic mechanical response of the two-dimensional metamaterial system. The effect of possible damping is not included in the formulation and the free vibration of the system has been ignored. Therefore, all field variables, such as displacement, acceleration and force, can be expressed in the general form of $\mathbf{A} = Ae^{-i\omega t}$ with ω being the circular frequency of the harmonic motion. For convenience, the time factor $e^{-i\omega t}$ will be suppressed and only the amplitudes of the variables A are kept in the formulation of the problem.

2.2.1 Effective modulus and effective mass

The dynamic response of the representative cell can be described in terms of forces and displacements at its boundary. For the current two-dimensional metamaterial system, a cell can be identified by its unit number (n,h) with n and h being the order of the cell in the horizontal and vertical direction, respectively. To determine the effective mass and effective modulus,

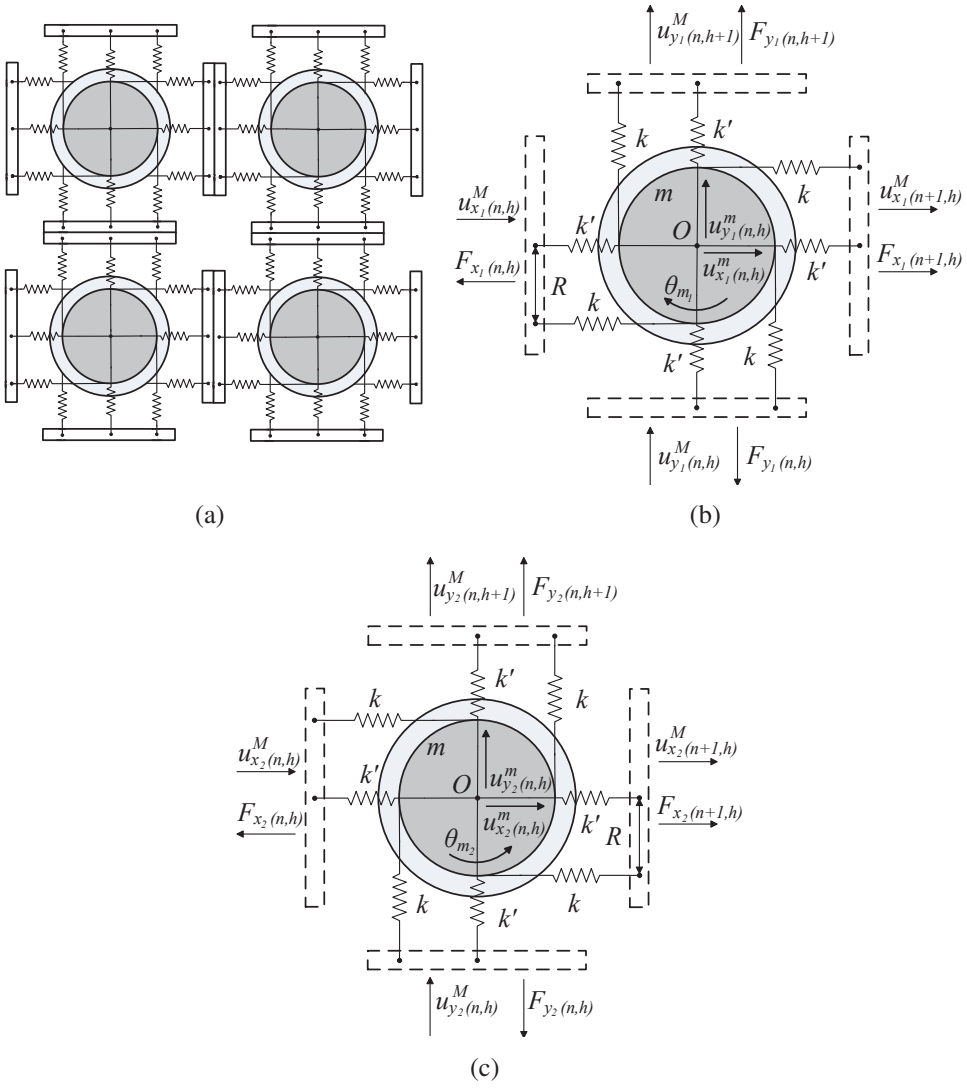

Figure 2.1: The two-dimensional metamaterial system, (a) periodic cells, (b) cell unit 1, (c) cell unit 2.

consider the case where the cell is deformed in both horizontal and vertical directions. For unit one, as shown in figure 2.1(b), the boundary forces are denoted as $F_{x1(n,h)}$, $F_{x1(n+1,h)}$, $F_{y1(n,h)}$, $F_{y1(n,h+1)}$, and the boundary displacements are $u^M_{x1(n,h)}$, $u^M_{x1(n+1,h)}$, $u^M_{y1(n,h)}$ and $u^M_{y1(n,h+1)}$. The motion of the central rigid bodies are governed by its translational displacement $u^m_{x1(n,h)}$ and $u^m_{y1(n,h)}$, and rotational displacement θ_{m1}.

It should be mentioned that the four boundary rigid bodies of the cell are actually allowed

to rotate in the model. The possible rotation of these boundary rigid bodies has been analysed and the results show that the rotation will affect both units in the cell but when the two units are superimposed into the final cell, the effect of this rotation disappears when the effective properties, as defined in the current paper, are evaluated. Therefore, in the formulation of the problem, the rotation of the boundary rigid bodies has been omitted to avoid trivial discussion associated with this rotation.

By considering the kinematic relation, in figure 2.1(b), the spring forces will be in the form of

$$F_{x1(n,h)} = \left(k+k'\right)\left(u^{m}_{x1(n,h)} - u^{M}_{x1(n,h)}\right) - kR\theta_{m1}, \tag{2.1}$$

$$F_{x1(n+1,h)} = \left(k+k'\right)\left(u^{M}_{x1(n+1,h)} - u^{m}_{x1(n,h)}\right) - kR\theta_{m1}, \tag{2.2}$$

$$F_{y1(n,h)} = \left(k+k'\right)\left(u^{m}_{y1(n,h)} - u^{M}_{y1(n,h)}\right) - kR\theta_{m1}, \tag{2.3}$$

$$F_{y1(n,h+1)} = \left(k+k'\right)\left(u^{M}_{y1(n,h+1)} - u^{m}_{y1(n,h)}\right) - kR\theta_{m1}. \tag{2.4}$$

By conducting the kinetic analysis of the central rigid body, the displacements of the central mass in unit one can be determined as

$$u^{m}_{x(n,h)} = \frac{u^{M}_{x(n,h)} + u^{M}_{x(n+1,h)}}{2}\frac{1}{1-\omega^2/\omega_1^2}, \tag{2.5}$$

$$u^{m}_{y(n,h)} = \frac{u^{M}_{y(n,h)} + u^{M}_{y(n,h+1)}}{2}\frac{1}{1-\omega^2/\omega_1^2}, \tag{2.6}$$

$$\theta_m = \frac{1}{2R}\frac{1}{1-\omega^2/\omega_0^2}\frac{u^{M}_{x(n+1,h)} - u^{M}_{x(n,h)} + u^{M}_{y(n,h+1)} - u^{M}_{y(n,h)}}{2}, \tag{2.7}$$

where ω_0 and ω_1 are the natural frequencies of the cell for rotation and translation motions, respectively, given by

$$\omega_0^2 = \frac{4R^2k}{G^2m}, \tag{2.8}$$

$$\omega_1^2 = \frac{2\,(k+k')}{m}, \tag{2.9}$$

with G being the radius of gyration of the central rigid body. Since the two units share the common displacements at the boundaries, subscript '1' has been omitted in equations (2.5)-(2.7) and these equations are also applicable to unit two, shown in figure 2.1(c).

As discussed before, to ensure that the rotational motion of the cell is symmetric, a second mass-spring system, unit two, is also added. For the second system, the direction of rotation of the central mass will be opposite to that of the first one and the motion of the central mass can be similarly represented by the displacements at the boundary of the cell, as shown in equations (2.5)-(2.7). The boundary displacements are commonly shared by the two units. The boundary forces acting at the cell are the superposition of that of the two units, which can be expressed as

$$F_{x(n,h)} = F_{x1(n,h)} + F_{x2(n,h)}, \tag{2.10}$$

$$F_{x(n+1,h)} = F_{x1(n+1,h)} + F_{x2(n+1,h)}, \tag{2.11}$$

$$F_{y(n,h)} = F_{y1(n,h)} + F_{y2(n,h)}, \tag{2.12}$$

$$F_{y(n,h+1)} = F_{y1(n,h+1)} + F_{y2(n,h+1)}, \tag{2.13}$$

where the forces with subscript '2' are that for unit two, which are similar to the forces for unit one given by equations (2.1)-(2.4). Accordingly, the relation between forces and displacements

at the boundary of the cell can then be determined as

$$F_{x(n+1,h)} - F_{x(n,h)} = -\omega^2 \left(\frac{2m}{1-\omega^2/\omega_1^2} \right) \frac{\left(u^M_{x(n,h)} + u^M_{x(n+1,h)} \right)}{2}, \tag{2.14}$$

$$\frac{1}{2}\left(F_{x(n,h)} + F_{x(n+1,h)} \right) = \left\{ \begin{array}{l} \left(k + k' - \dfrac{k}{2\left(1-\omega^2/\omega_0^2\right)} \right) \left(u^M_{x(n+1,h)} - u^M_{x(n,h)} \right) \\ -\dfrac{k}{2\left(1-\omega^2/\omega_0^2\right)} \left(u^M_{y(n,h+1)} - u^M_{y(n,h)} \right) \end{array} \right\}, \tag{2.15}$$

$$F_{y(n,h+1)} - F_{y(n,h)} = -\omega^2 \left(\frac{2m}{1-\omega^2/\omega_1^2} \right) \frac{\left(u^M_{y(n,h)} + u^M_{y(n,h+1)} \right)}{2}, \tag{2.16}$$

$$\frac{1}{2}\left(F_{y(n,h)} + F_{y(n,h+1)} \right) = \left\{ \begin{array}{l} -\dfrac{k}{2\left(1-\omega^2/\omega_0^2\right)} \left(u^M_{x(n+1,h)} - u^M_{x(n,h)} \right) \\ \left(k + k' - \dfrac{k}{2\left(1-\omega^2/\omega_0^2\right)} \right) \left(u^M_{y(n,h+1)} - u^M_{y(n,h)} \right) \end{array} \right\}. \tag{2.17}$$

In the horizontal direction, equation (2.14) establishes the relation between the net force applied to the cell and the average acceleration of it. Equation (2.15) shows the relation between the averaged force applied to the cell and its deformation. Equations (2.16) and (2.17) demonstrate the same relations of the representative cell in the vertical direction.

Considering the relation between the net forces and average accelerations in both directions, as described in equations (2.14) and (2.16), the effective mass of the representative cell under a specific frequency can be identified as

$$m_e = \frac{2m}{1-\omega^2/\omega_1^2}. \tag{2.18}$$

The effective strain ε_{ij} and stress σ_{ij} of the cell are defined, for a cell with a unit length in

the thickness direction, by

$$\varepsilon_{11} = \frac{u^M_{x(n+1,h)} - u^M_{x(n,h)}}{L}, \quad \varepsilon_{22} = \frac{u^M_{y(n,h+1)} - u^M_{y(n,h)}}{L}, \tag{2.19}$$

and

$$\sigma_{11} = \frac{F_{x(n,h)} + F_{x(n+1,h)}}{2L}, \quad \sigma_{22} = \frac{F_{y(n,h)} + F_{y(n,h+1)}}{2L}. \tag{2.20}$$

The effective stress-strain relation can be expressed as

$$\sigma_{11} = C_{11}\varepsilon_{11} + C_{12}\varepsilon_{22}, \quad \sigma_{22} = C_{21}\varepsilon_{11} + C_{22}\varepsilon_{22}, \tag{2.21}$$

where the effective elastic moduli are

$$C_{11} = C_{22} = k + k' - \frac{k}{2\left(1 - \omega^2/\omega_0^2\right)}, \tag{2.22}$$

$$C_{12} = C_{21} = -\frac{k}{2\left(1 - \omega^2/\omega_0^2\right)}. \tag{2.23}$$

It should be mentioned that there are other possible ways to determine the effective mass and modulus, such as using the mean motion or energy of the unit cell (Srivastava and Nemat-Nasser, 2012; Wang and Gan, 2002). For periodic media, a high-frequency homogenization method has been developed (Antonakakis et al., 2014) to capture the essential dynamic behaviour at high resonant frequencies for elastic lattices (Colquitt et al., 2015). In this study, the main concern is the dynamic response of the system. The current definition of the effective dynamic mass and modulus is used because it can provide an accurate description of the relation between forces and displacements at the end rigid bodies, and the wave propagation in the metamaterial system.

Compared with the corresponding 1D model (Wang, 2014), the main difference is the effect of Poisson's ratio. For the current 2D problem, the dynamic behaviour is naturally dominated by two elastic constants C_{11} and C_{12}, different from the 1D problem, which is controlled by the Young's modulus.

A comparison between the effective material properties from 1D (Wang, 2014) and 2D models is given in table 2.1. It should be noted that k and k' in the 1D problem correspond to k' and k in the 2D model, respectively. The natural frequencies of translation, ω_1 and the effective mass m_e are the same in the two models. The natural frequency of rotation ω_0 are different, due to the Poisson's effect. Two parameters C_{11} and C_{12}, which are not applicable in the 1D model, describe the stiffness property of the 2D model. The Poisson's ratio is the unique feature of the 2D model. The modulus for uniaxial loading (Young's modulus, E_e) can be determined from the 2D model, which is different from the corresponding modulus from the 1D model (k_e).

Table 2.1: Parameters comparison between 1D and 2D model

1D Model	2D Model
$\omega_0^2 = \frac{2R^2k'}{G^2m}$	$\omega_0^2 = \frac{4R^2k}{G^2m}$
$\omega_1^2 = \frac{2(k'+k)}{m}$	$\omega_1^2 = \frac{2(k+k')}{m}$
$m_e = \frac{2m}{1-\omega^2/\omega_1^2}$	$m_e = \frac{2m}{1-\omega^2/\omega_1^2}$
N/A	$C_{11} = k + k' - \frac{k}{2\left(1-\omega^2/\omega_0^2\right)}$
N/A	$C_{12} = -\frac{k}{2\left(1-\omega^2/\omega_0^2\right)}$
$k_e = k - \frac{M}{2}\omega^2 + \frac{k'}{1-\omega_0^2/\omega^2}$	$E_e = \frac{(k+k')-k'(\omega_0^2/\omega^2)}{1-(k+2k')(\omega_0^2/\omega^2)/(2k+2k')}$
N/A	$\nu = \frac{1}{1-2(1-\omega^2/\omega_0{}^2)(1+k'/k)}$

The results indicate that both effective mass and effective modulus are significantly affected by the resonance behaviour of the cell in both translation and angular motions, which is strongly frequency dependent. As clearly illustrated in equations (2.18), (2.22) and (2.23), the effective mass and effective modulus become negative at certain frequencies due to the resonance behaviour.

2.2.2 Negative mass and modulus

The effective mass is directly related to the translational resonance of the cell and it determined by equation (2.18). It can be easily observed that negative mass is achieved when

$$1 < \frac{\omega^2}{\omega_1^2}. \tag{2.24}$$

The effective moduli of the cell are mainly controlled by the rotational resonance as shown in equations (2.22) and (2.23). For modulus component C_{11}, its negative range is

$$1 - \frac{1}{2\,(1+k'/k)} < \frac{\omega^2}{\omega_0^2} < 1, \tag{2.25}$$

and negative modulus component C_{12} is achieved when

$$\omega < \omega_0. \tag{2.26}$$

To better evaluate the behaviour of the representative cell, two parameters, a modulus ratio λ_K and a length ratio λ_R, are introduced, which dominate the effective property and are defined as

$$\lambda_K = \frac{k'}{k}, \quad \lambda_R = \frac{R}{G}, \tag{2.27}$$

where k' and k, R and G are the elastic constants of the central spring and the side spring,

the distance between the central and side springs, and the radius of gyration of the central rigid bodies, as shown in figure 2.1(b and c). By using the relation between the translational resonance frequency ω_1 and the rotational resonance frequency ω_0, the ranges for negative mass and modulus can be rewritten as

Negative mass

$$\frac{1+\lambda_K}{2\lambda_R^2} < \frac{\omega^2}{\omega_0^2}, \tag{2.28}$$

Negative modulus C_{11}

$$1 - \frac{1}{2\left(1+\lambda_K\right)} < \frac{\omega^2}{\omega_0^2} < 1, \tag{2.29}$$

Negative modulus C_{12}

$$\frac{\omega^2}{\omega_0^2} < 1. \tag{2.30}$$

The negative range of $C_{11}\left(C_{22}\right)$ is completely covered by the negative range of $C_{12}\left(C_{21}\right)$, as shown in equations (2.29) and (2.30).

Depending on the property of the cell, governed by λ_K and λ_R, either positive or negative mass and/or modulus can be achieved. The system may show single negative (SN, negative mass or modulus) or double negative (DN, both negative mass and modulus). Evaluating the relation between the range of negative mass and that of negative modulus indicates that two critical condition exist, as illustrated in figure 2.2. The frequency range shaded with horizontal lines indicates that for negative effective mass, whereas the frequency range shaded with vertical lines indicates that for negative effective modulus. Figure 2.2(a) shows the first critical case where the lower bound of the negative mass range is $\omega/\omega_0 = \omega/\omega_1 = 1$, i.e. identical to the

upper bound of negative modulus range. The left rectangle in figure 2.2(a) shows the range of negative C_{11} (and C_{22}) and the range of negative mass is to the right without overlapping. The condition is given by

$$\lambda_R = \sqrt{\frac{1+\lambda_K}{2}}. \tag{2.31}$$

In this case, the effective mass and effective modulus can not be negative simultaneously, i.e. only single negative (SN) exists.

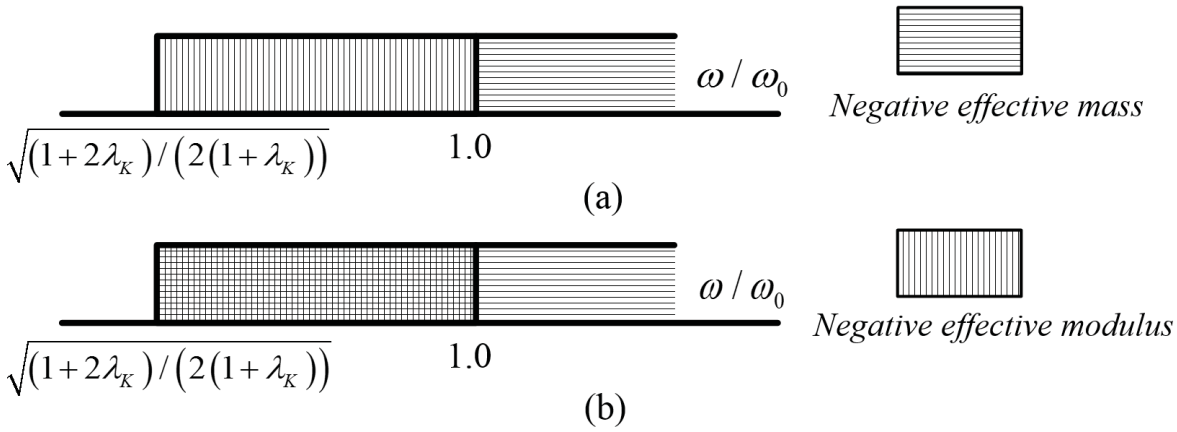

Figure 2.2: Critical positions for negative modulus and negative mass ranges, (a) the first critical condition, (b) the second critical condition.

The second critical case is shown in figure 2.2(b), where the lower bound of the negative mass range and that of the negative modulus range are identical. This condition is satisfied when

$$\lambda_R = \frac{1+\lambda_K}{\sqrt{1+2\lambda_K}}. \tag{2.32}$$

Obviously in this case, in the entire negative range of C_{11}, the effective mass will also be negative, showing double-negative property.

If λ_R is greater than the critical value provided by equation (2.31), the negative mass range

will move to the left relative to negative modulus range. Then, overlapping of the two ranges will be generated. The critical value given by equation (2.31) is shown as the first critical boundary in figure 2.3. Below the first critical boundary, no double negative behaviour can be observed. The other curve in figure 2.3 corresponds to the case where the lower bound of the negative mass range is identical to that of the negative modulus range, given by equation (2.32). Between the two critical curves, the double negative behaviour will exist from the low bound of the negative mass range to the upper bound of the negative modulus range. For the domain above the second critical boundary, the double negative range will be exactly the same as the negative modulus range.

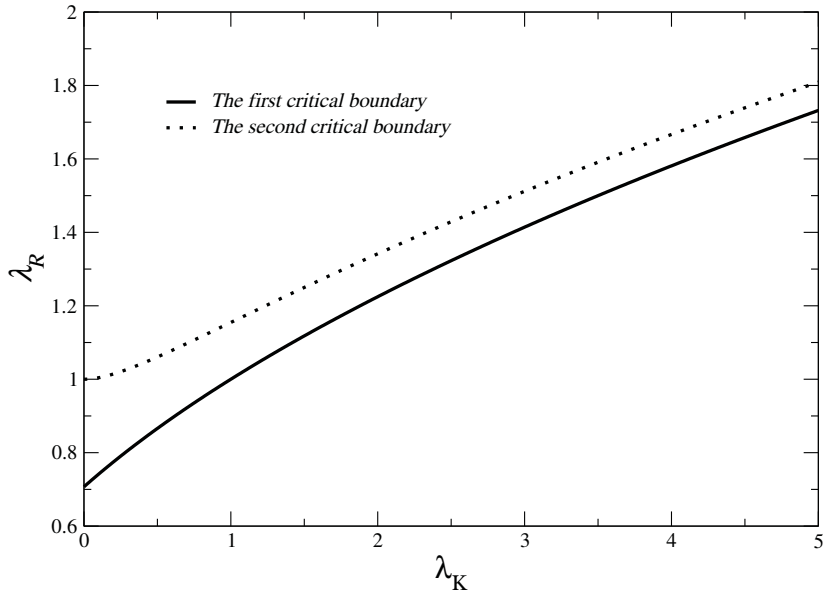

Figure 2.3: Domain for negative modulus and mass.

These results clearly indicate that the negative ranges of modulus and mass are governed by two parameters, the modulus ratio λ_K and the length ratio λ_R. Single negative (modulus or

mass) or double negative metamaterials can be generated with proper selection of the structural parameters. By controlling λ_K and λ_R, different material properties can be achieved.

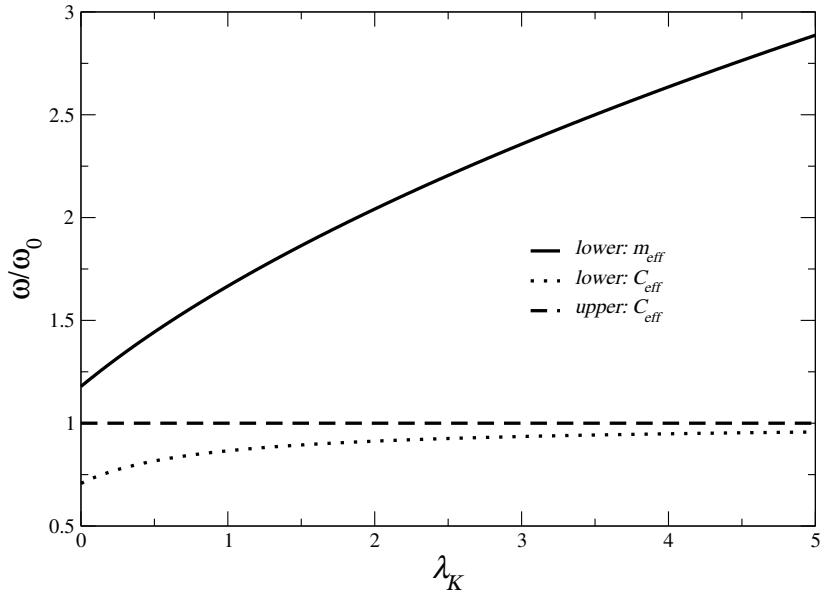

Figure 2.4: Negative modulus and mass for $\lambda_R = 0.6$.

Figure 2.4 shows the variation of the upper and lower bounds of the loading frequency for negative modulus and negative mass ranges with different λ_K for $\lambda_R = 0.6$. In this case, no overlapping of the two negative ranges exists. Figure 2.5 shows the corresponding results for $\lambda_R = 0.9$. Under this circumstance, only when $\lambda_K < 0.62$, the double negative behaviour can be achieved between the lower bound of negative mass (lower m_{eff}) and the upper bound of negative modulus (upper C_{eff}). Figure 2.6 shows the variation of the upper and lower bounds of the negative modulus and negative mass ranges for $\lambda_R = 1.5$. In this case, complicated behaviour of DN is observed, which is mostly dominated by the effective modulus. Two types of DN can be observed. The first is achieved for the range of negative modulus when $\lambda_K < 2.93$.

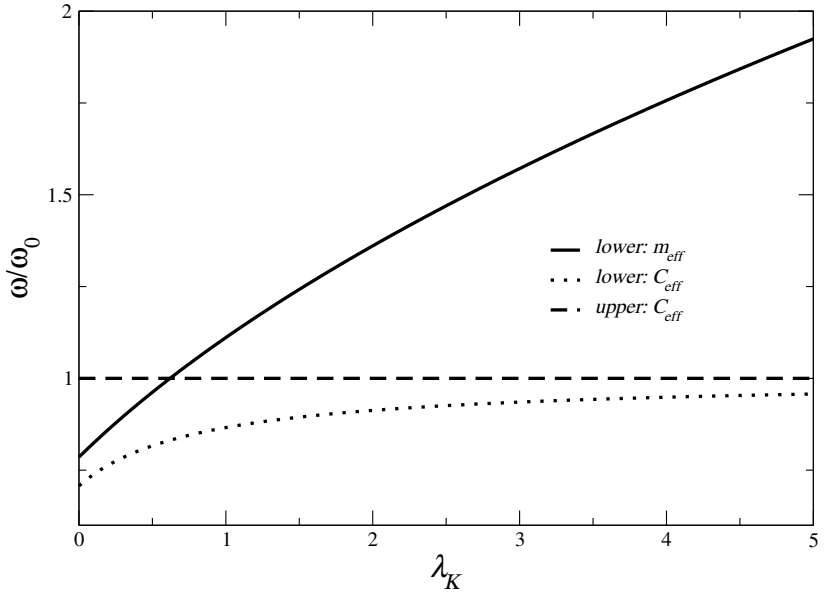

Figure 2.5: Negative modulus and mass for $\lambda_R = 0.9$.

The second is from lower m_{eff} to the upper C_{eff} for $0.293 < \lambda_K < 3.50$. When λ_K is increased to 2.0, DN is completely governed by the negative modulus range, as shown in figure 2.7. From these results, conclusion can be easily drawn that DN can be achieved in different ranges of frequencies with the selection of the mass, modulus and geometry of the system.

2.2.3 Behaviour of negative Poisson's ratio

Based on the generalized Hooke's law, the Poisson's ratio, defined as the ratio between C_{12} and C_{11}, is

$$\nu = \frac{1}{1 - 2\left(1 - \omega^2/\omega_0^2\right)(1 + \lambda_K)}. \tag{2.33}$$

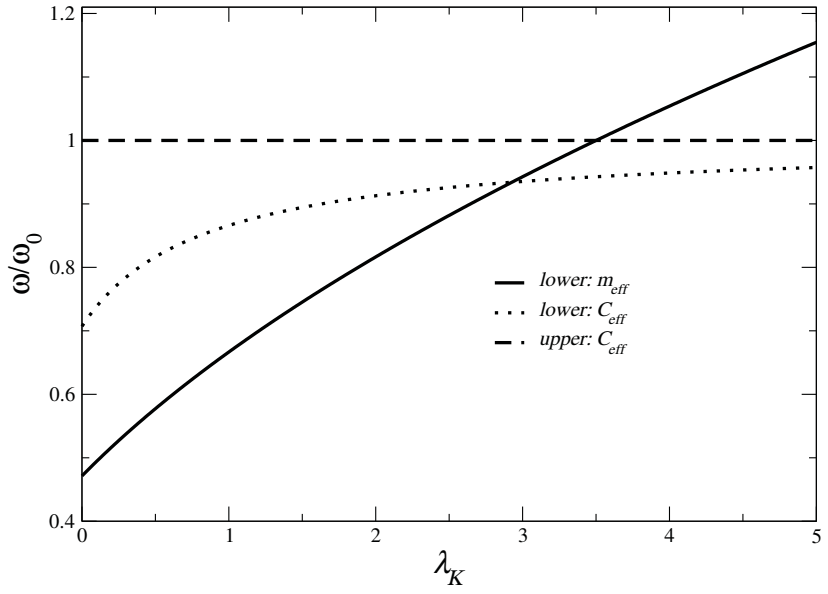

Figure 2.6: Negative modulus and mass for $\lambda_R = 1.5$.

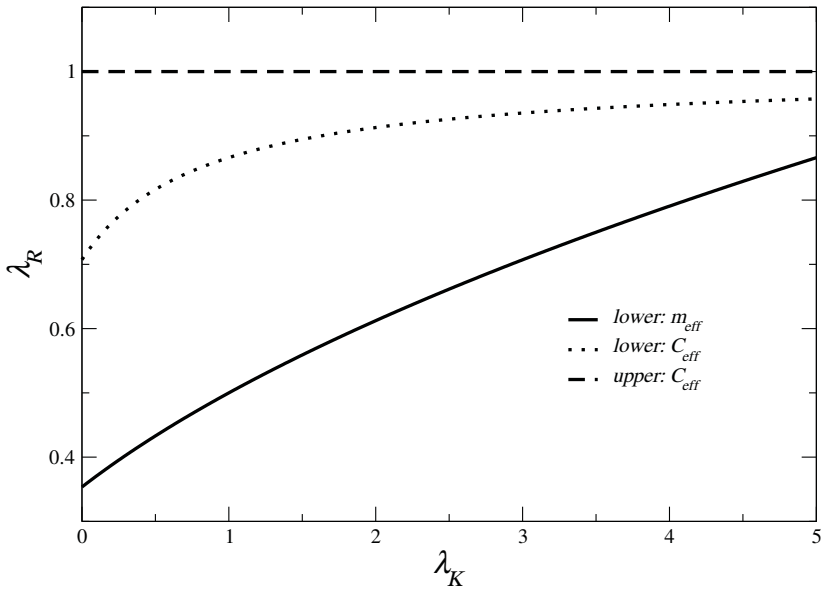

Figure 2.7: Negative modulus and mass for $\lambda_R = 2.0$.

Although a natural material usually has a positive Poisson's ratio, negative Poisson's ratio can be achieved in properly designed material system (Babaee et al., 2013). For the current metamaterial system, the Poisson's ratio can turn negative for certain structure parameters and frequencies.

Positive Poisson's ratio

$$\frac{1+2\lambda_K}{2(1+\lambda_K)} < \frac{\omega^2}{\omega_0^2}, \tag{2.34}$$

Negative Poisson's ratio

$$\frac{\omega^2}{\omega_0^2} < \frac{1+2\lambda_K}{2(1+\lambda_K)}. \tag{2.35}$$

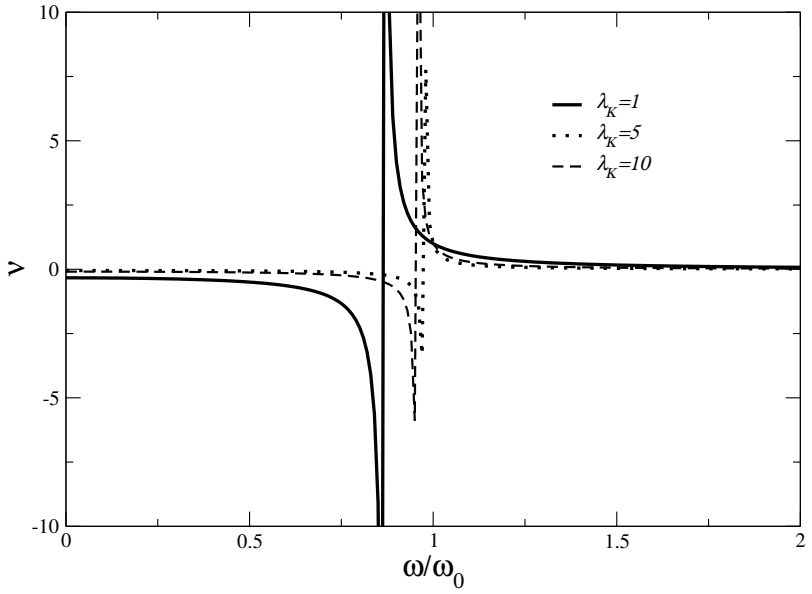

Figure 2.8: Poisson's ratio at different frequencies.

Figure 2.8 shows the variation of the Poisson's ratio with frequency for different λ_K. When $\lambda_K = 1$, the metamaterial obtains negative Poisson's ratio in the normalized frequency range

from 0 to 0.87. As λ_K increases, the upper bound of negative Poisson's ratio approaches 1, which can be easily observed from equation (2.35). As a special case, when $\omega = 0$, the Poisson's ratio will be

$$\nu = -\frac{1}{1+2\lambda_K}, \tag{2.36}$$

which is a function of λ_K and is negative, caused by the rotating motion in the representative cell.

2.3 Elastic wave propagation in the metamaterial system

Obviously, the dependence of effective mass and effective modulus upon loading frequency will affect the propagation of elastic waves in the material system. To study this effect, consider the harmonic wave propagation in the two-dimensional metamaterial system formed by repeated cells of length L, as shown in figure 2.1. By using equations (2.14) and (2.15), the force $F_{x(n+1,h)}$, acting on the right end of cell (n,h), can be expressed in terms of displacements as

$$F_{x(n+1,h)} = \left\{ \begin{array}{l} \frac{1}{4}\left(-4C_{11} - m_e\omega^2\right) u^M_{x(n,h)} + \frac{1}{4}\left(4C_{11} - m_e\omega^2\right) u^M_{x(n+1,h)} \\ +C_{12}\left(u^M_{y(n,h+1)} - u^M_{y(n,h)}\right) \end{array} \right\}. \tag{2.37}$$

The force acting on the left side of cell $(n+1,h)$ can also be obtained from equations (2.14) and (2.15) as

$$F_{x(n+1,h)} = \left\{ \begin{array}{l} \frac{1}{4}\left(-4C_{11} + m_e\omega^2\right) u^M_{x(n+1,h)} + \frac{1}{4}\left(4C_{11} + m_e\omega^2\right) u^M_{x(n+2,h)} \\ +C_{12}\left(u^M_{y(n+1,h+1)} - u^M_{y(n+1,h)}\right) \end{array} \right\}. \tag{2.38}$$

By combining equations (2.37) and (2.38), the following governing equation for the harmonic wave propagation is obtained

$$\left\{\begin{array}{l} \frac{1}{4}\left(-4C_{11}-m_e\omega^2\right)\left(u^M_{x(n,h)}+u^M_{x(n+2,h)}\right)+\frac{1}{2}\left(4C_{11}-m_e\omega^2\right)u^M_{x(n+1,h)} \\ +C_{12}\left(u^M_{y(n,h+1)}-u^M_{y(n,h)}+u^M_{y(n+1,h)}-u^M_{y(n+1,h+1)}\right) \end{array}\right\}=0. \tag{2.39}$$

Similarly, a second governing equation can be obtained based on the corresponding relations of the cell in the vertical direction,

$$\left\{\begin{array}{l} \frac{1}{4}\left(-4C_{11}-m_e\omega^2\right)\left(u^M_{y(n,h)}+u^M_{y(n,h+2)}\right)+\frac{1}{2}\left(4C_{11}-m_e\omega^2\right)u^M_{y(n,h+1)} \\ +C_{21}\left(u^M_{x(n+1,h)}-u^M_{x(n,h)}+u^M_{x(n,h+1)}-u^M_{x(n+1,h+1)}\right) \end{array}\right\}=0. \tag{2.40}$$

For a harmonic plane wave propagating in the two-dimensional metamaterial system, the wave field will have the general form of

$$\mathbf{u}=A\mathbf{d}e^{iK(\mathbf{xp}-ct)}, \tag{2.41}$$

$$\mathbf{d}=(d_x,d_y), \quad d_x=\cos\phi, \quad d_y=\sin\phi, \tag{2.42}$$

$$\mathbf{p}=(p_x,p_y), \quad p_x=\cos\theta, \quad p_y=\sin\theta, \tag{2.43}$$

where A is the amplitude of the displacement field, and $\mathbf{d}$ and $\mathbf{p}$ are unit vectors representing the directions of the displacement and the wave propagation, respectively, with the angles ϕ and θ being measured from the x-axis. K is the wave number, which can be complex in general. The x axis and y axis are selected such that the origin is at the intersection of the lower left corner of the zeroth cell $(n=0,h=0)$. The length of all the representative cells is identically L so that the coordinates of the lower left corner of cell (n,h) will be $x=nL$ and $y=hL$, for example. Following this definition of coordinates, the governing equations for the wave propagation,

equations (2.39) and (2.40) can be rewritten as

$$\left\{\begin{array}{l}\frac{1}{4}\left(-4C_{11}-m_e\omega^2\right)\cos\phi\left[1+e^{i(2KL\cos\theta)}\right]\\+\frac{1}{2}\left(4C_{11}-m_e\omega^2\right)\cos\phi e^{i(KL\cos\theta)}\\+C_{12}\sin\phi\left[e^{i(KL\sin\theta)}+e^{i(KL\cos\theta)}-e^{iKL(\cos\theta+\sin\theta)}-1\right]\end{array}\right\}=0, \tag{2.44}$$

$$\left\{\begin{array}{l}\frac{1}{4}\left(-4C_{11}-m_e\omega^2\right)\sin\phi\left[1+e^{i(2KL\sin\theta)}\right]\\+\frac{1}{2}\left(4C_{11}-m_e\omega^2\right)\sin\phi e^{i(KL\sin\theta)}\\+C_{12}\cos\phi\left[e^{i(KL\sin\theta)}+e^{i(KL\cos\theta)}-e^{iKL(\cos\theta+\sin\theta)}-1\right]\end{array}\right\}=0. \tag{2.45}$$

Eliminating $\sin\phi$ and $\cos\phi$ from equations (2.44) and (2.45), the following dispersion relation for the wave propagation can be determined,

$$\begin{aligned}&\frac{-\left(C_{11}+m_e\omega^2/4\right)\left(1+e^{i2KL\cos\theta}\right)+2\left(C_{11}-m_e\omega^2/4\right)e^{iKL\cos\theta}}{C_{21}\left(1-e^{iKL\cos\theta}\right)\left(1-e^{iKL\sin\theta}\right)}\\&=\frac{C_{21}\left(1-e^{iKL\cos\theta}\right)\left(1-e^{iKL\sin\theta}\right)}{-\left(C_{11}+m_e\omega^2/4\right)\left(1+e^{i2KL\sin\theta}\right)+2\left(C_{11}-m_e\omega^2/4\right)e^{iKL\sin\theta}}.\end{aligned} \tag{2.46}$$

The metamaterial structure presented has three axes of symmetry at 0, $\pi/4$, $\pi/2$ directions. Therefore, the dynamic behaviour of the wave propagation will be the same for two complementary directions, such as in 0 and $\pi/2$ directions. In the following discussion, waves in different directions will be considered.

The most interested issue here is the wave propagation in the metamaterial system so only the real part of the wave number is provided. In general, positive KL indicates that the wave propagates along the direction defined by θ for the cases where both effective mass and modulus are positive, and negative KL indicates waves in the opposite direction, corresponding to

negative mass and modulus (DN). This phenomenon is generated by the condition that the applied power for a specific cell must be positive (Wang, 2014).

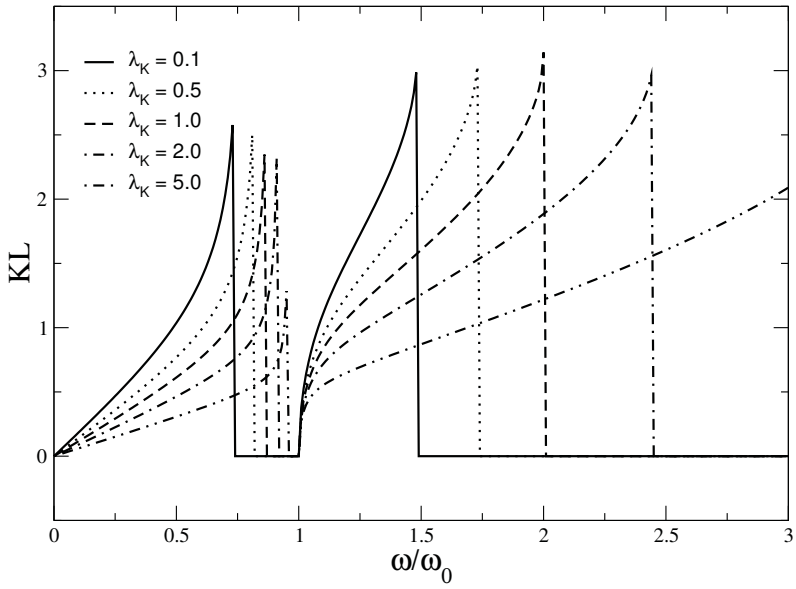

Figure 2.9: Wave number at different frequencies for $\theta = 0.0, \lambda_R = 0.5$.

Figure 2.9 shows the variation of the normalized wave number KL with frequency when $\lambda_R = 0.5$ for different λ_K, for a horizontal wave with $\theta = 0^o$. In this case, the wave number is either real or imaginary so the results shown in this figure represent all possible waves for the frequency range considered. Positive KL is found in two different ranges of frequency but no negative KL is observed, indicating that there is no overlapping between the negative mass and negative modulus ranges. The positive KL is formed by the gaps between these ranges. Figure 2.10 shows the corresponding result for $\lambda_R = 1.0$. In this case, depending on the value of λ_K, different phenomena can be observed. For lower λ_K $(0.1, 0.5)$, negative KL exists for a specific frequency range, which indicates backward wave propagation. For $\lambda_K = 1.0$, there is only one positive KL range. While for $\lambda_K = 2.0, 5.0$, positive KL appears in two separate ranges.

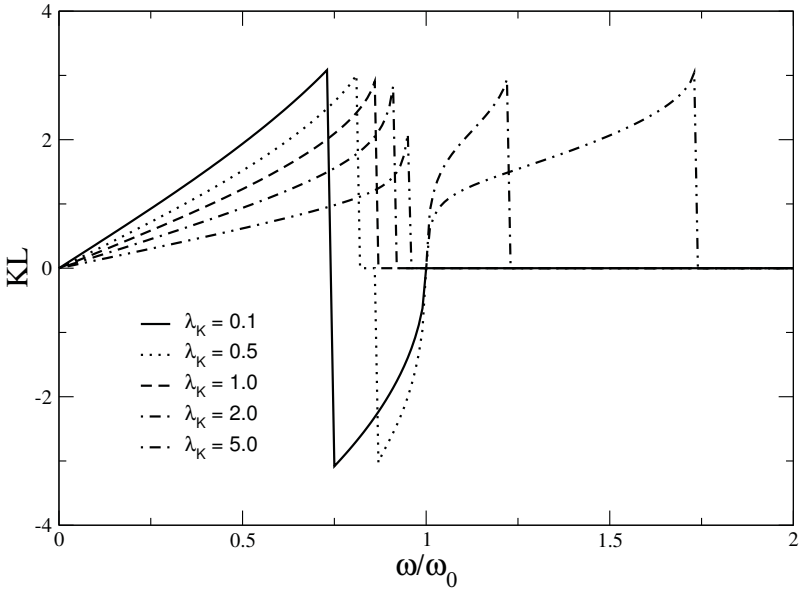

Figure 2.10: Wave number at different frequencies for $\theta = 0.0, \lambda_R = 1.0$.

The KL for $\lambda_R = 2.0$ is given in figure 2.11. In this case, there is always a negative KL range following positive KL with increasing frequency. The wave number for a wave propagating at $\theta = 45^{\text{o}}$ for the case where $\lambda_R = 1.0$ is given in figure 2.12. The result is similar to that given in figure 2.10, i.e. for lower λ_K values there are one positive KL range and one negative KL range, but for higher λ_K, there are only two positive KL ranges. For the case of $\lambda_R = 2.0$, a wave at $\theta = 45^{\text{o}}$ shows a similar property to that of the horizontal wave presented in figure 2.13. These results show clearly how the metamaterial system can be adjusted to generate different properties for wave propagation. It should also be mentioned that the current model is based on the simple mass-spring system so it can provide a clear idea about the mechanism of generating negative mass and modulus.

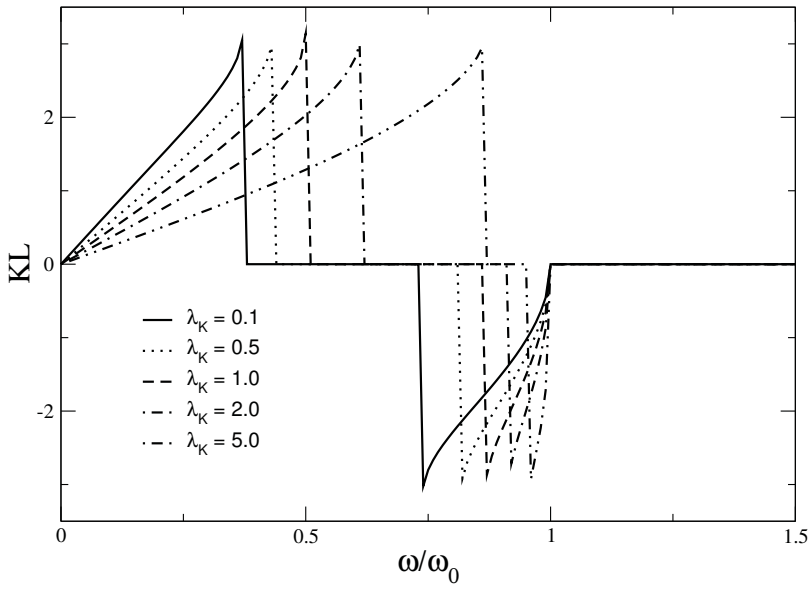

Figure 2.11: Wave number at different frequencies for $\theta = 0.0, \lambda_R = 2.0$.

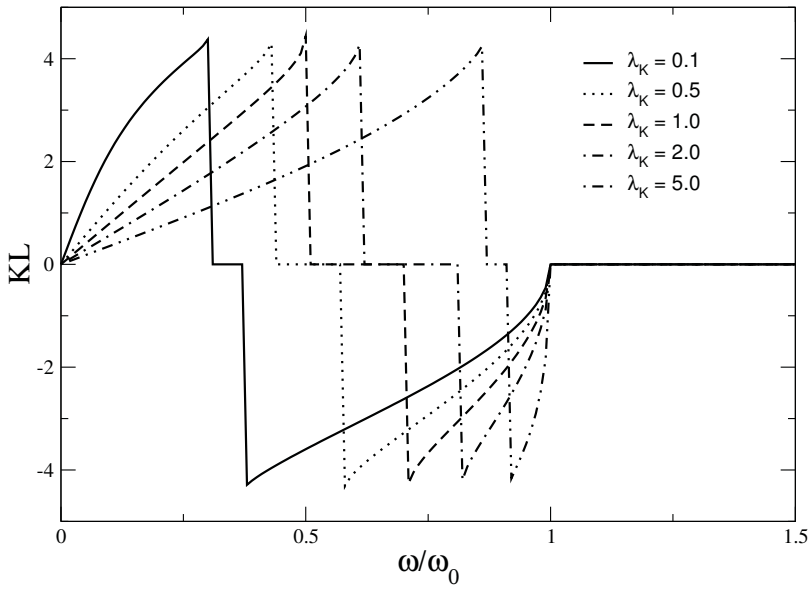

Figure 2.13: Wave number at different frequencies for $\theta = \pi/4, \lambda_R = 2.0$.

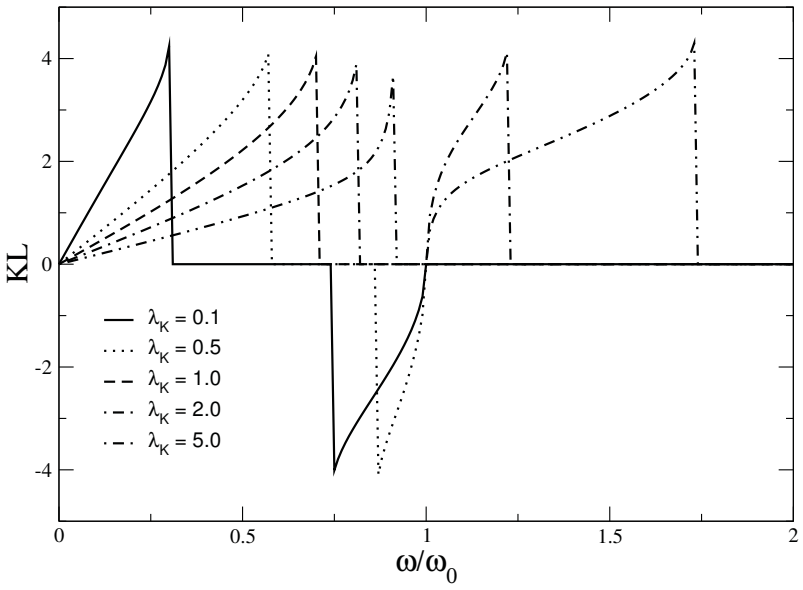

Figure 2.12: Wave number at different frequencies for $\theta = \pi/4, \lambda_R = 1.0$.

2.4 Conclusion

The general mechanism of generating negative effective material parameters in elastic metamaterials is revealed in this chapter. In the developed metamaterial system, the translational resonance of the resonators can generate negative effective mass by inducing overall motion of the representative cells, whereas the translational resonance can generate negative effective modulus through giving rise to the local deformation of the representative cells without overall motion. Through controllable translational and rotational resonances in the representative cell, negative effective mass and modulus can be achieved independently and simultaneously. The current work will provide a guideline for designing more general elastic metamaterials by incorporating both translational and rotational resonance in the material system.

Chapter 3: Modelling of elastic metamaterials with negative mass and modulus based on translational resonance

This Chapter develops a new elastic metamaterial exhibiting simultaneously negative effective mass and modulus through only translational motion of the resonators in the representative cells, without using the rotational motion as one of the fundamental mechanism, to avoid potential difficulties in fabrication. Based on the mechanism revealed in the previous work, this model can induce overall motion of the representative cells to generate negative effective mass and give rise to the local deformation of the representative cells to yield negative effective modulus. The effect of the structural parameters of the representative cell on the frequency ranges with single negativity (negative mass or negative modulus) or double negativity (negative mass and negative modulus) has been evaluated in detail. Typical examples are presented to illustrate the dynamic property of this developed elastic metamaterial.

3.1 Introduction

Recently, significant progress has been achieved in the design of new materials engineered to gain unique dynamic effective properties, which are physically inconceivable in nature. Termed as metamaterials, these complex composites acquire their special features from the delicately designed sub-wavelength structures, not from the chemical compositions. Earlier efforts have been made to explore the theoretical possibility of electromagnetic materials with negative re-

fractive index generated by negative electric permittivity and magnetic permeability (Veselago, 1968). By following this initial proposal, many practical concepts have been proposed and realized, such as superlenses with sub-wavelength spatial resolution and invisible cloak based on designed gradient-index (Kundtz and Smith, 2010; Pendry, 2000).

These features are based on the realization of the double negative properties of the electromagnetic metamaterials, which are bestowed by the special resonance of their unique unit cells (Shelby et al., 2001; Smith et al., 2000). This idea of local resonance is equally valid for acoustic/elastic metamaterials due to the analogy between acoustic and electromagnetic fields. The successful manipulation of electromagnetic waves has stimulated substantial interests of the research community in the acoustic/elastic metamaterials. One of the main objectives of the study of acoustic/elastic metamaterials is to achieve negative effective mass and/or negative effective modulus through the design of local unit cells. Negative effective mass and negative effective modulus are realized as the results of the vibration of different kinds of resonators in the local unit cells (Huang and Sun, 2011a; Huang et al., 2009a). The first design of such a structure with negative effective mass was investigated and fabricated by embedding soft silicon rubber coated heavy spheres in epoxy acting as the local mechanical resonators (Liu et al., 2000). The mechanism of local resonance has been used to generate negative effective mass for acoustic/elastic metamaterials (Liu et al., 2005; Milton and Willis, 2007; Yao et al., 2008) and different local resonators have been designed, such as periodically distributed membranes and organized hollow plastic tubes in acoustic media (Chen et al., 2014; Lee et al., 2009a). There are also considerable attention paid to the development of acoustic/elastic metamaterials with negative effective modulus. The first experimental realization of negative bulk modulus has

been achieved with a one-dimensional acoustic metamaterial system, which consists of a chain of sub-wavelength Helmholtz resonators (Fang et al., 2006). Acoustic metamaterials formed by a tube with an array of side holes have been devised to generate similar phenomenon (Lee et al., 2009b). It is now well-established that the effective mass and modulus can be highly frequency-dependent in acoustic/elastic metamaterials and can turn negative for certain frequency ranges. The realization of negative mass and/or modulus in acoustic/elastic metamaterials have been extensively studied based on various physical schemes (An et al., 2015; Ding et al., 2007; Lai et al., 2011; Lee et al., 2010; Liang et al., 2012; Zhu et al., 2014a).

The unique properties of acoustic/elastic metamaterials make them very attractive for many novel applications. The imaginary phase velocity due to single negativity has been effectively implemented to vibration shielding and noise elimination (Chen et al., 2016; Liu et al., 2015; Mitchell et al., 2014). Moreover, the property of negative refractive index obtained from double negative metamaterials can be utilized for superlensing beyond the diffraction limit (Kaina et al., 2015; Li et al., 2009; Wu et al., 2011).

One of the major issues in the development of elastic metamaterials is the proper design of the local unit cells. Previous studies indicate that translational and rotational resonances of resonators in the local unit cell will play their unique roles in achieving negative mass and modulus (Bigoni et al., 2013; Liu et al., 2011a,b). The independent control of negative mass and modulus has been realized by properly designing the translational and rotational resonance properties of the mechanical resonators (Li and Wang, 2016; Wang, 2014). Based on a different mechanism, a metamaterial model has been developed based on translational resonance of local unit cells, which can generate simultaneously negative effective mass and modulus (Huang and

Sun, 2012; Su and Sun, 2015). This model has later been modified by adding more resonators to broaden the single negative frequency ranges (band gaps) (Pai and Huang, 2015). In the unit cells of these models, multiple resonators move in different directions and the coupling of the motion of these resonators significantly affect the properties of the unit cells.

In the current paper, a new metamaterial model based on only translational resonance is proposed. In the new model, a simpler local structure is used for the representative cell and two types of translational resonance are introduced. One resonance controls the negative effective modulus and the coupled effect of the two resonances can generate negative effective mass, providing more flexibility for controlling the generation of negative mass and modulus. The effect of the structural parameters of the representative cell on the distribution of the frequency ranges with single negativity or double negativity is investigated and broad band gap can be generated in this model. The harmonic dynamic behaviour of periodic elastic metamaterials based on such representative cells is studied. The wave mitigating ability of the proposed material model within the band gaps and the phenomenon of negative phase velocity in double negative frequency ranges are demonstrated. Typical examples are presented to exhibit the dynamic property of the current metamaterial. Finite Element Method analysis is also conducted to study the property of the proposed metamaterial model and to evaluate the simplified spring-mass model.

3.2 Formulation of the metamaterial model

The properties of metamaterials are governed by their representative cells and the design of the structure of these cells is a very important issue in developing acoustic/elastic metamate-

rials. In our previous works, spring-mass models for one-dimensional and two-dimensional metamaterials have been proposed, which can achieve controlled negative mass and modulus through localized mechanical vibrations (Li and Wang, 2016; Wang, 2014). In these models, the localized translational motion of the resonators controls the overall motion of the representative cell, generating negative effective mass. The localized rotational motion of the resonators dominates the deformation of the representative cell, giving rise to negative effective modulus. The two effective parameters, mass and modulus, can be easily controlled in these models. In the current study, a new metamaterial model is designed to achieve negative mass and modulus through only translational motion of the resonators in the representative cells, without using the rotational motion as one of the fundamental mechanism, to avoid potential difficulties in fabrication.

3.2.1 The proposed representative cell

The proposed representative cell of the model is depicted in figure 3.1(a), in which three different materials are used. The current model aims to generate negative mass and/or modulus along the horizontal direction. It should be mentioned that materials I and II, which can be identical, are materials with higher mass densities and high moduli. Material III is designed to possess lower mass density and lower modulus.

To better illustrate the underlying mechanism of the metamaterial model for generating the single negative and double negative behaviour, the representative cell of the elastic model is simplified as a structure built with springs and masses, as illustrated in figure 3.1(b). This simplified representative cell consists of two end rigid bodies and four masses, internal resonators, connected with six massless linear springs. The two end rigid bodies with the same mass M

(a)

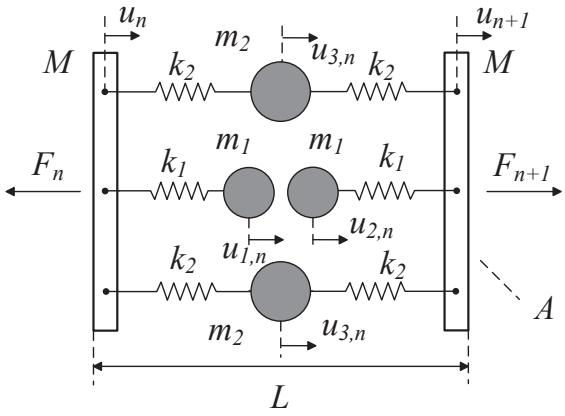

(b)

Figure 3.1: (a) The representative cell of the one-dimensional elastic metamaterial model, (b) the n^{th} representative cell of the simplified spring-mass model.

form the boundary of the cell. As shown in figure 3.1(b), for each end rigid body, a mass m_1 is attached through a spring with stiffness k_1. Two masses, m_2, are attached to the end rigid bodies through springs with an elastic constant k_2. In this model, the rigid bodies and the internal masses represent materials I and II and the linear springs represent material III. It is of interest to note that the springs and rigid bodies are assembled in such a manner to make the structure symmetrical in the vertical direction. The length of the cell is assumed to be L and the area of its transverse cross section is defined as A. The overall motion of the system considered is limited to the horizontal direction.

Based on the proposed model, a periodic elastic metamaterial can be formed by assembling the representative cells in the horizontal direction. The harmonic response of such a one-dimensional metamaterial is controlled by the property of the representative cell. When an excitation with a circular frequency ω is applied, the resulting displacements, accelerations and forces can be expressed in the general form of $\mathbf{A} = Ae^{-i\omega t}$ in the following discussion. For convenience, the common time factor $e^{-i\omega t}$ will be suppressed and only the amplitudes of the variables are evaluated, unless otherwise specified. The effect of the possible damping of the system is ignored.

3.2.2 Effective mass and effective modulus

The effective mass and effective modulus of the metamaterial system are determined by the dynamic response of the representative cell, which is governed by the relation between displacements and forces at its boundaries. As shown in figure 3.1(b), the boundary displacements and forces of the n^{th} representative cell are denoted as u_n and u_{n+1}, F_n and F_{n+1}, respectively. The motion of the rigid resonators inside the cell is dominated by their translational displacements $u_{1,n}$, $u_{2,n}$ and $u_{3,n}$. Based on the kinematic relation illustrated in figure 3.1(b), the equations of motion for the six rigid bodies, the left mass M, the right mass M, the left mass m_1, the right mass m_1 and the masses m_2, can be obtained in the form of, respectively,

$$-M\omega^2 u_n = 2k_2\left(u_{3,n} - u_n\right) + k_1\left(u_{1,n} - u_n\right) - F_n, \tag{3.1}$$

$$-M\omega^2 u_{n+1} = 2k_2\left(u_{3,n} - u_{n+1}\right) + k_1\left(u_{2,n} - u_{n+1}\right) + F_{n+1}, \tag{3.2}$$

$$-m_1\omega^2 u_{1,n} = k_1\left(u_n - u_{1,n}\right), \tag{3.3}$$

$$-m_1\omega^2 u_{2,n} = k_1(u_{n+1} - u_{2,n}), \tag{3.4}$$

$$-m_2\omega^2 u_{3,n} = k_2(u_n - u_{3,n}) + k_2(u_{n+1} - u_{3,n}). \tag{3.5}$$

Making use of equations, (3.3), (3.4) and (3.5), the displacements of the four resonators with masses m_1 and m_2 can be represented in terms of the boundary displacements of the representative cell as

$$u_{1,n} = \frac{u_n}{1 - \omega^2/\omega_1^2}, \tag{3.6}$$

$$u_{2,n} = \frac{u_{n+1}}{1 - \omega^2/\omega_1^2}, \tag{3.7}$$

$$u_{3,n} = \frac{1}{2}\left(\frac{u_n + u_{n+1}}{1 - \omega^2/\omega_2^2}\right), \tag{3.8}$$

where ω_1 and ω_2 are the natural frequencies of the rigid resonators m_1 and m_2, respectively, given by

$$\omega_1^2 = \frac{k_1}{m_1}, \quad \omega_2^2 = \frac{2k_2}{m_2}. \tag{3.9}$$

Substitution of equations (3.6), (3.7) and (3.8) into equations (3.1) and (3.2) will yield

$$F_{n+1} - F_n = -\omega^2 m_e\left(\frac{u_{n+1} + u_n}{2}\right), \tag{3.10}$$

$$\frac{1}{2}(F_{n+1} + F_n) = \frac{E_e A}{L}(u_{n+1} - u_n). \tag{3.11}$$

Equation (3.10) establishes the relation between the net force applied to the cell and the average acceleration of it. Equation (3.11) represents the relation between the average force applied to the cell and its deformation. Based on these relations, m_e and E_e are the effective mass and

modulus of the representative cell with

$$m_e = 2M + \frac{2m_1}{1-\omega^2/\omega_1^2} + \frac{2m_2}{1-\omega^2/\omega_2^2}, \tag{3.12}$$

$$E_e = \left(k_2 - \frac{M}{2}\omega^2 - \frac{k_1}{2}\frac{\omega^2/\omega_1^2}{1-\omega^2/\omega_1^2}\right)\frac{L}{A}. \tag{3.13}$$

It is clearly shown in equations (3.12) and (3.13) that effective modulus is dominated by ω_1, which is controlled by the vibration of the central masses m_1, and both ω_1 and ω_2 affect the effective mass. The effective mass and modulus of the representative cell are highly frequency-dependent and will become negative under certain frequencies due to the local resonance behaviour.

3.2.3 Negative effective mass and modulus

The dynamic behaviour of the representative cell of the metamaterial structure is controlled by three parameters, the modulus ratio η, and two mass ratios λ_1 and λ_2, defined as

$$\eta = \frac{k_1}{k_2}, \quad \lambda_1 = \frac{m_1}{M}, \quad \lambda_2 = \frac{m_2}{M}. \tag{3.14}$$

Based on the results given in equations (3.12) and (3.13), frequency ranges, in which negative effective mass or modulus is achieved, can be determined in terms of these three parameters.

Negative effective mass

From equation (3.12), the condition for negative effective mass is

$$F_{m1}\left(\frac{\omega}{\omega_1}\right) \bullet F_{m2}\left(\frac{\omega}{\omega_1}\right) < 0, \tag{3.15}$$

where the functions, $F_{m1}(\omega/\omega_1)$ and $F_{m2}(\omega/\omega_1)$, are given by

$$F_{m1}\left(\frac{\omega}{\omega_1}\right) = \begin{cases} \left(\frac{\omega}{\omega_1}\right)^4 - \left(1+\frac{2\lambda_1}{\eta}+\frac{2\lambda_1}{\lambda_2\eta}+\lambda_1\right)\left(\frac{\omega}{\omega_1}\right)^2 \\ +\frac{2\lambda_1}{\lambda_2\eta}(1+\lambda_1+\lambda_2) \end{cases}, \tag{3.16}$$

$$F_{m2}\left(\frac{\omega}{\omega_1}\right) = \left(\frac{2\lambda_1}{\lambda_2\eta} - \left(\frac{\omega}{\omega_1}\right)^2\right)\left(1-\left(\frac{\omega}{\omega_1}\right)^2\right). \tag{3.17}$$

The property of negative effective mass is controlled by the positions of the roots of $F_{m1}(\omega/\omega_1) = 0$ and $F_{m2}(\omega/\omega_1) = 0$. Two positive roots of $F_{m1}(\omega/\omega_1) = 0$, ζ_1 and ζ_2 ($\zeta_1 > \zeta_2$), can be determined from equation (3.16), as given in appendix A, and the two positive roots of $F_{m2}(\omega/\omega_1) = 0$, $\bar{\zeta}_1$ and $\bar{\zeta}_2$, are

$$\bar{\zeta}_1 = \max(\theta, 1), \quad \bar{\zeta}_2 = \min(\theta, 1), \tag{3.18}$$

with

$$\theta = \frac{\omega_2}{\omega_1} = \sqrt{\frac{2\lambda_1}{\lambda_2\eta}}, \tag{3.19}$$

being the resonance frequency ratio.

Detailed analysis indicates, as shown in Appendix A, that the four roots will satisfy

$$\zeta_1 > \bar{\zeta}_1 \geq \zeta_2 \geq \bar{\zeta}_2, \tag{3.20}$$

and both F_{m1} and F_{m2} are positive when $|\omega/\omega_1|$ approaches infinity. The frequency ranges for negative mass can then be determined to be

$$\zeta_1 > \frac{\omega}{\omega_1} > \bar{\zeta}_1, \quad \zeta_2 > \frac{\omega}{\omega_1} > \bar{\zeta}_2. \tag{3.21}$$

For the special case where $\omega_2/\omega_1 = 1$, $\bar{\zeta}_1 = \zeta_2 = \bar{\zeta}_2 = 1$ and $\zeta_1 = \sqrt{1+\lambda_1+\lambda_2}$, the frequency

range for negative mass is

$$\zeta_1 > \frac{\omega}{\omega_1} > 1. \tag{3.22}$$

Negative effective modulus

From equation (3.13), negative effective modulus can be achieved when

$$F_e\left(\frac{\omega}{\omega_1}\right) < 0 \quad and \quad \frac{\omega}{\omega_1} < 1, \tag{3.23}$$

or

$$F_e\left(\frac{\omega}{\omega_1}\right) > 0 \quad and \quad \frac{\omega}{\omega_1} > 1, \tag{3.24}$$

where the function $F_e(\omega/\omega_1)$ is

$$F_e\left(\frac{\omega}{\omega_1}\right) = \left(\frac{\omega}{\omega_1}\right)^4 - \left(1+\lambda_1+\frac{2\lambda_1}{\eta}\right)\left(\frac{\omega}{\omega_1}\right)^2 + \frac{2\lambda_1}{\eta}. \tag{3.25}$$

Two positive roots of $F_e(\omega/\omega_1) = 0$, as shown in Appendix A, satisfy $\xi_1 > 1 > \xi_2$. Following the property that F_e is positive when $|\omega/\omega_1|$ approaches infinity, the condition for negative effective modulus is

$$\frac{\omega}{\omega_1} > \xi_1 \quad or \quad 1 > \frac{\omega}{\omega_1} > \xi_2. \tag{3.26}$$

The variation of the three structural parameters, η, λ_1 and λ_2, provides rich possibilities of frequency ranges with negative effective mass and/or modulus. The positions and sizes of the frequency ranges for negative mass/modulus can be adjusted through these three parameters. To further investigate the effect of these parameters on the dynamic behaviour of the proposed metamaterial, the coupling of the frequency ranges between that for negative effective mass

and modulus is evaluated in the following discussion.

Overlapping of negative mass and negative modulus

The ranges for negative mass and modulus are controlled by the six roots of F_{m1}, F_{m2} and F_e, ζ_1, ζ_2, $\bar{\zeta}_1$, $\bar{\zeta}_2$, ξ_1 and ξ_2. These ranges are illustrated in figure 3.2 for three different cases, (a) $\theta = \omega_2/\omega_1 > 1$, (b) $\theta = \omega_2/\omega_1 = 1$, and (c) $\theta = \omega_2/\omega_1 < 1$. The horizontal axis represents the normalized loading frequency. The frequency ranges formed by black solid lines indicate those of negative mass and the ranges formed by dashed lines illustrate those of negative modulus. Shaded ranges indicate double negative behaviour, in which both mass and

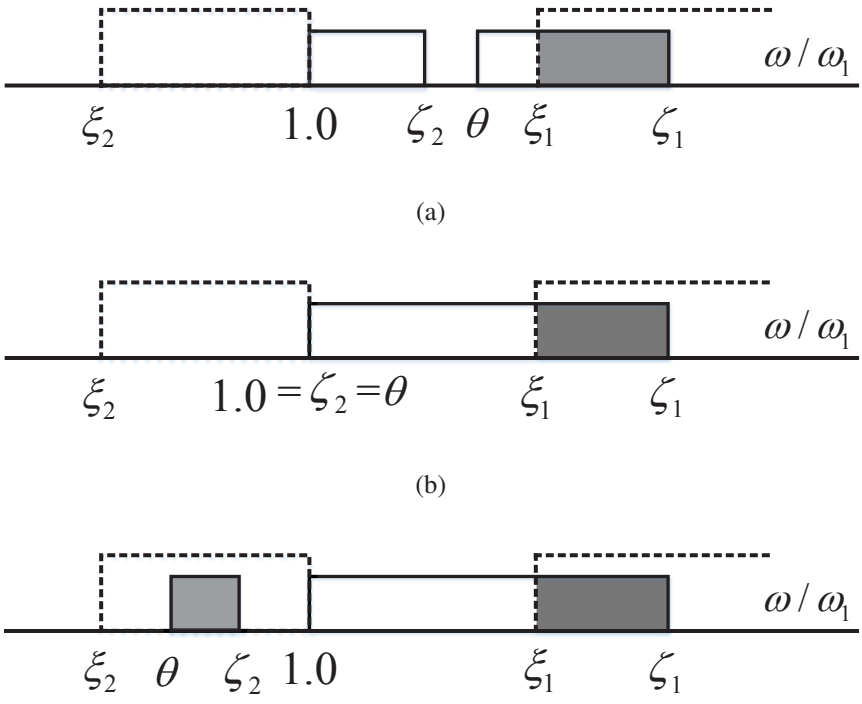

Figure 3.2: Negative mass and negative modulus ranges for: (a) $\theta > 1, \theta < \xi_1$, (b) $\theta = 1$, (c) $\theta < 1, \theta > \xi_2$.

modulus are negative. Figure 3.2 will be explained with details in the following discussion and these single or double negative ranges are investigated in terms of the structural parameters, η, λ_1 and λ_2.

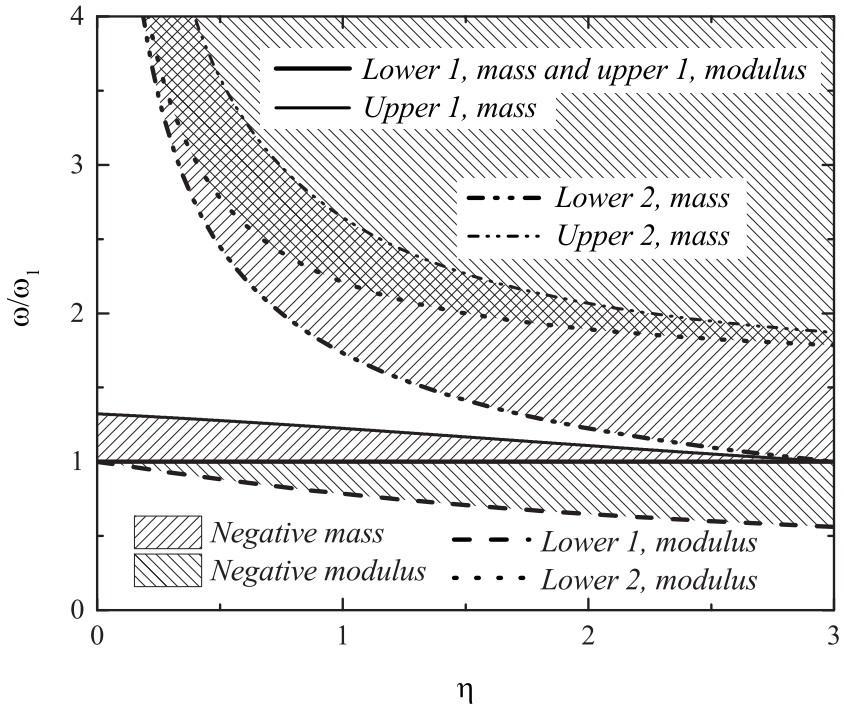

Figure 3.3: Frequency ranges for negative effective parameters for $\lambda_1 = 1.5$ and $\lambda_2 = 1.0$ with $\theta > 1$.

Case 1: $\boldsymbol{\theta = \omega_2/\omega_1 > 1}$

For $\theta = \omega_2/\omega_1 > 1$, detailed evaluation shows that $\zeta_1 > \xi_1 > \zeta_2 > 1 > \xi_2$ and $\zeta_1 > \theta > \zeta_2$ are satisfied. Three frequency ranges for single negativity can be determined as

$$\frac{\omega}{\omega_1} > \zeta_1, \quad \max(\theta, \xi_1) > \frac{\omega}{\omega_1} > \min(\theta, \xi_1), \quad \zeta_2 > \frac{\omega}{\omega_1} > \xi_2, \tag{3.27}$$

and a frequency range of double negativity exists when

$$\zeta_1 > \frac{\omega}{\omega_1} > \max(\theta, \xi_1). \tag{3.28}$$

Figure 3.2(a) shows the distribution of the frequency ranges for negative effective mass and/or modulus for this case with $\theta < \xi_1$. The effect of the structural parameters, η, λ_1 and λ_2, has been further analyzed. Figure 3.3 shows the frequency ranges of negative effective mass and negative effective modulus for different $\eta = k_1/k_2$ with $\lambda_1 = m_1/M = 1.5$ and $\lambda_2 = m_2/M = 1.0$. In this figure, domains 1 and 2 (noted as 1 and 2) are used to represent the two frequency ranges showing negative parameters. As shown in the figure, solid and dot-dashed lines indicate the bounds (lower and upper) for negative mass for domains 1 and 2, respectively. The

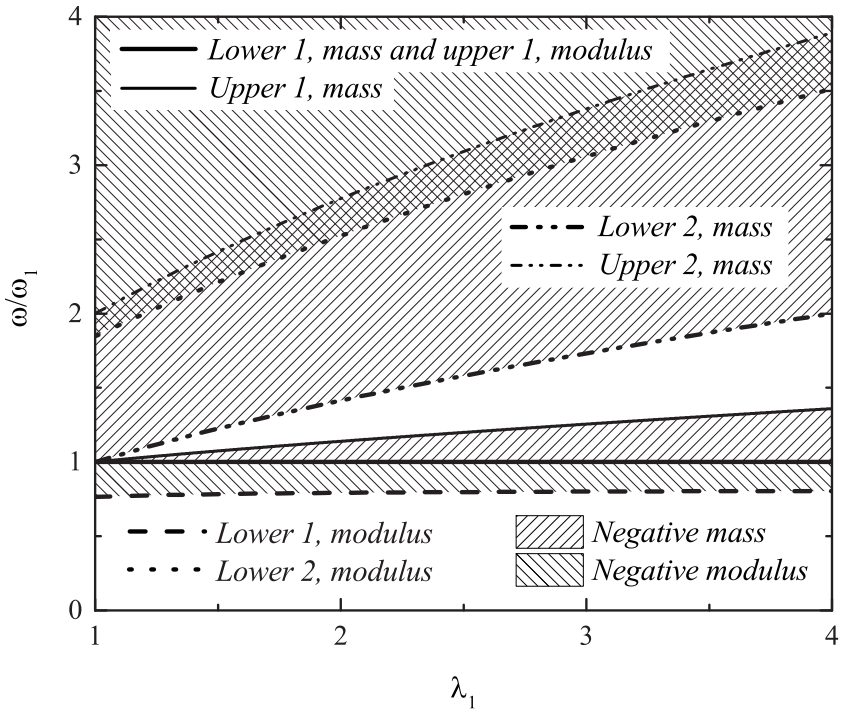

Figure 3.4: Frequency ranges for negative effective parameters for $\eta = 1.0$ and $\lambda_2 = 2.0$ with $\theta > 1$.

dotted and dashed lines form the bounds for negative effective modulus. Domain 1 for negative effective modulus exists just below $\omega/\omega_1 = 1$ and domain 2 for negative effective modulus is that above the dotted line (up to infinity). For better demonstration, the areas with negative mass effective or modulus have been shaded differently. It can be observed that, for a given ω, single or double negative behaviour can be achieved by adjusting ω_1 and η. When $\eta = 1.0$ and $\lambda_2 = 2.0$, the effect of λ_1 on the distribution of frequency ranges with negative parameters is shown in figure 3.4 and the effect of λ_2 on the frequency ranges when $\eta = 1.0$ and $\lambda_1 = 1.5$ is shown in figure 3.5. The existence of single or double negative domains can be easily observed. In this case, λ_2 has no effect on the effective modulus. As λ_2 increases, the widths of domain

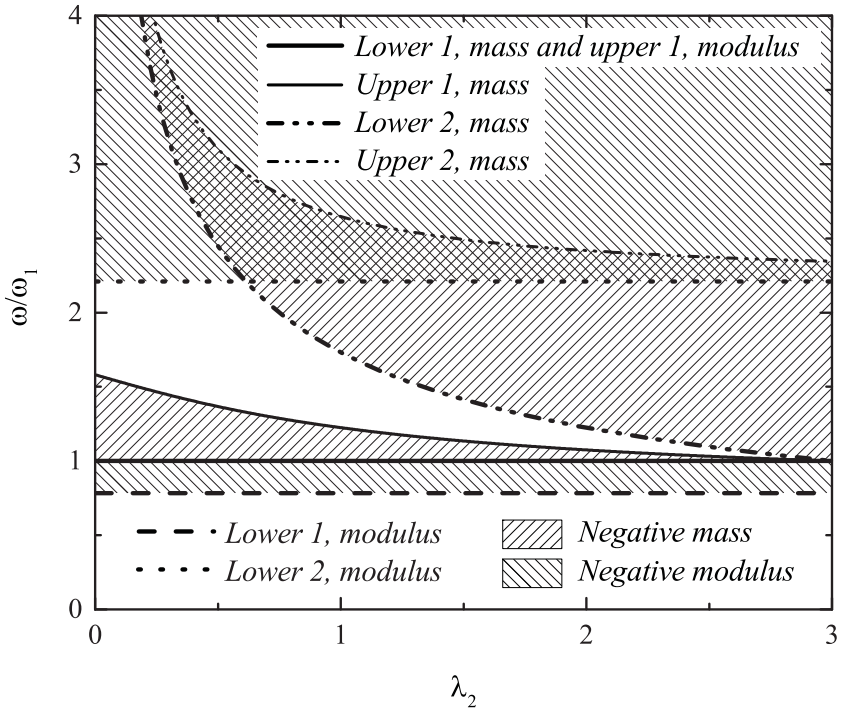

Figure 3.5: Frequency ranges for negative effective parameters for $\eta = 1.0$ and $\lambda_1 = 1.5$ with $\theta > 1$.

1 and domain 2 for negative mass decreases and increases respectively.

Case 2: $\theta = \omega_2/\omega_1 = 1$

For $\theta = 1$, the frequency ranges for single negativity will be

$$\frac{\omega}{\omega_1} > \zeta_1, \quad \xi_1 > \frac{\omega}{\omega_1} > \xi_2, \tag{3.29}$$

and the frequency range for double negativity is

$$\zeta_1 > \frac{\omega}{\omega_1} > \xi_1, \tag{3.30}$$

which have been clearly demonstrated in figure 3.2(b). Figure 3.6 shows the variation of the bounds for the frequency ranges of negative effective mass and negative effective modulus with

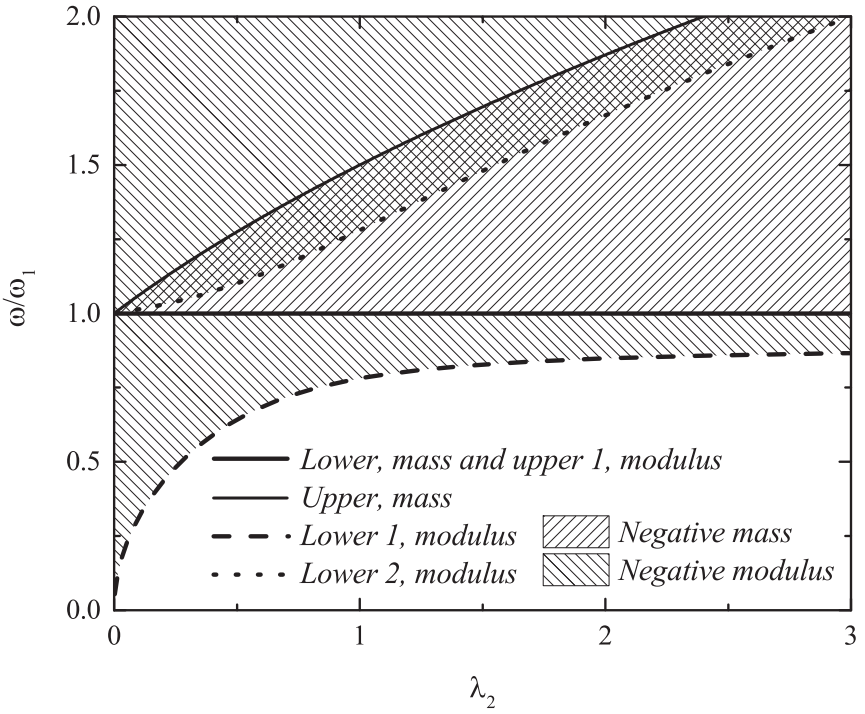

Figure 3.6: Frequency ranges for negative effective parameters for $\eta = 0.5$ with $\theta = 1$.

$\lambda_2 = m_2/M$ for $\eta = k_1/k_2 = 0.5$ ($\lambda_1 = \lambda_2/4$ in this case). The double negative frequency range, which is from the dotted line to the upper solid line, increases slightly with λ_2. A band gap is formed by the single negative domain from the dashed line to the dotted line. The band gaps formed, when $\eta = k_1/k_2$ is increased to 1.0 and 3.0, are shown in figures 3.7 and 3.8 between dashed and dotted lines . The frequency ranges for double negativity are relatively smaller in these cases.

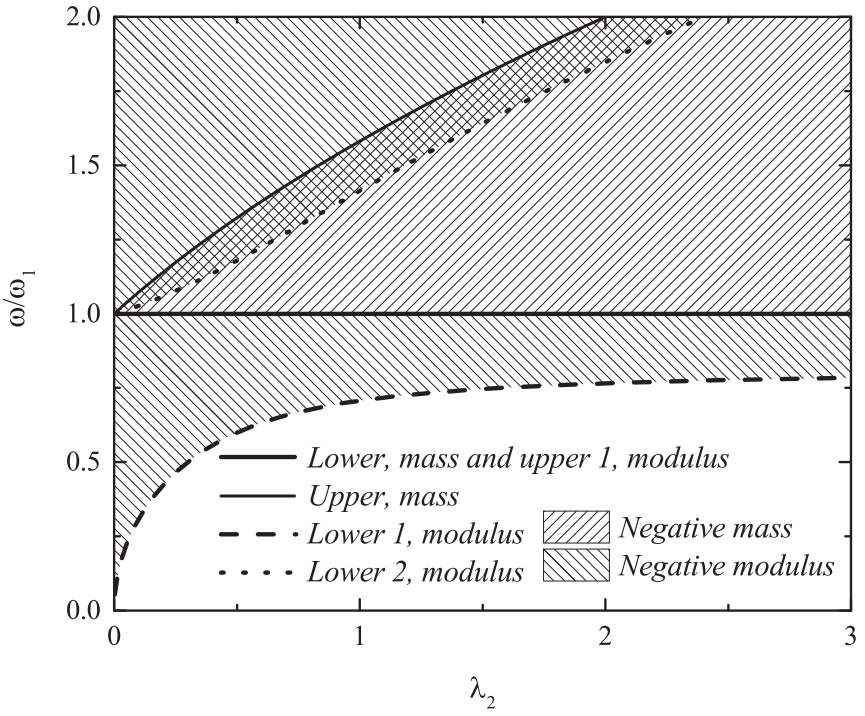

Figure 3.7: Frequency ranges for negative effective parameters for $\eta = 1.0$ with $\theta = 1$.

Case 3: $\theta = \omega_2/\omega_1 < 1$

For the case where $\theta < 1$, the relation $\zeta_1 > \xi_1 > 1 > \zeta_2 > \max(\theta, \xi_2)$ is satisfied. In this case,

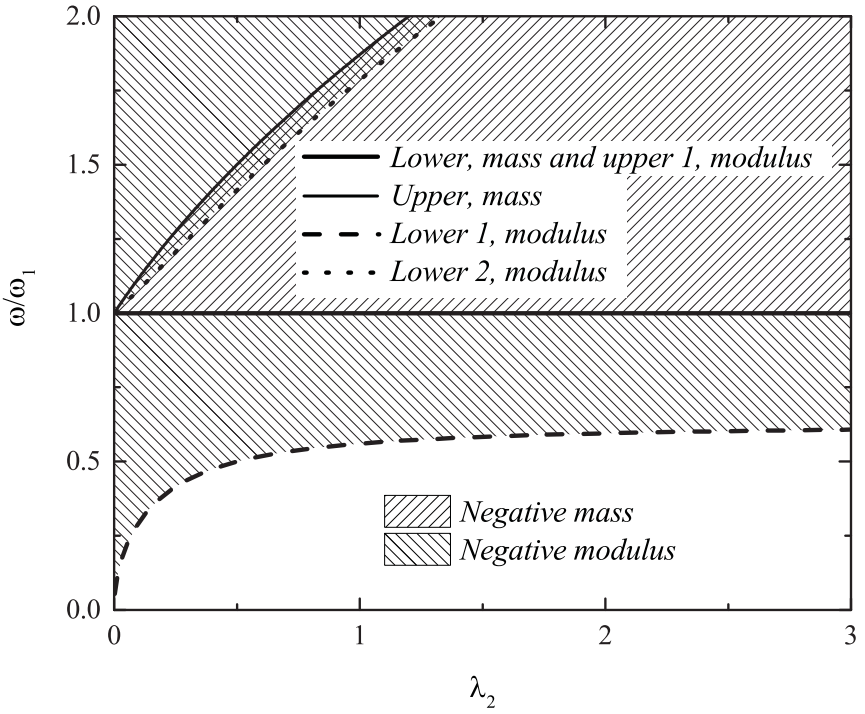

Figure 3.8: Frequency ranges for negative effective parameters for $\eta = 3.0$ with $\theta = 1$.

the frequency ranges of single negativity are

$$\frac{\omega}{\omega_1} > \zeta_1, \quad \xi_1 > \frac{\omega}{\omega_1} > \zeta_2, \quad \max(\theta, \xi_2) > \frac{\omega}{\omega_1} > \min(\theta, \xi_2), \tag{3.31}$$

and the frequency ranges of double negativity are

$$\zeta_1 > \frac{\omega}{\omega_1} > \xi_1, \quad \zeta_2 > \frac{\omega}{\omega_1} > \max(\theta, \xi_2). \tag{3.32}$$

These properties are illustrated in figure 3.2(c) for $\theta > \xi_2$, showing two frequency ranges with double negative effective parameters. The effect of the structural parameter $\eta = k_1/k_2$ is shown in figure 3.9 for the case where $\lambda_1 = 0.5$ and $\lambda_2 = 1.0\,(\theta > \xi_2)$. Two domains for both negative mass and negative modulus are observed (domain 1 and domain 2). The negative effective mass

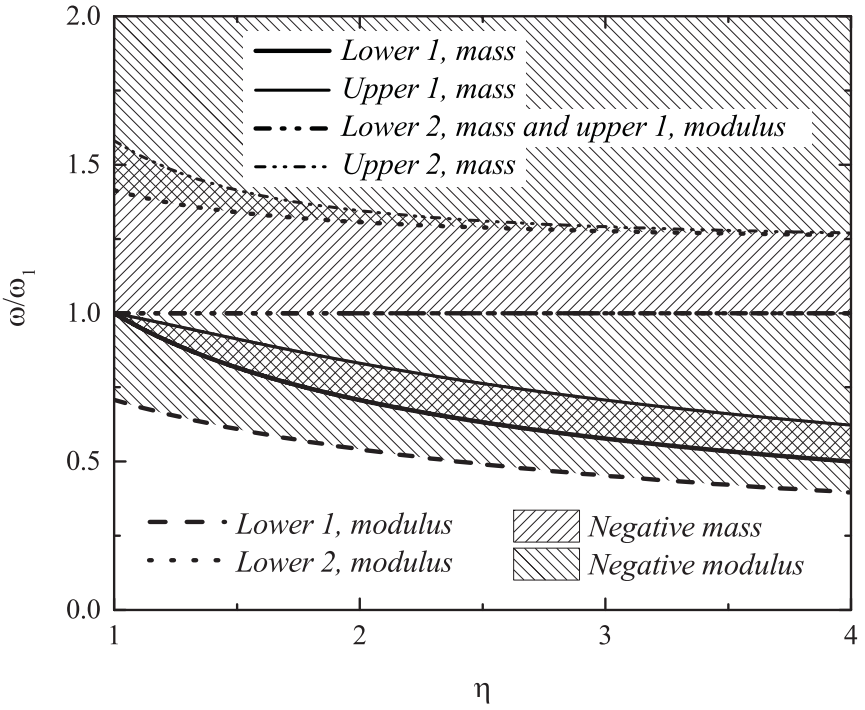

Figure 3.9: Frequency ranges for negative parameters for $\lambda_1 = 0.5$ and $\lambda_2 = 1.0$ with $\theta < 1$.

associated with domain 1 (lower frequency) will always generate double negativity. For domain 2 (higher frequency), small overlapping range of negative effective mass and modulus exists, leading to a broadened band gap (single negative). Figures 3.10 and 3.11 show the effects of λ_1 and λ_2 respectively on the frequency ranges of negativity. Similar to previous examples, while domain 1 of the frequency range generates double negative behaviour, domain 2 provides mainly a wide band gap.

The current results indicate that the three structural parameters, η, λ_1 and λ_2, have significant effect on frequency ranges of negativity. Adjusting these parameters will provide the flexibility to suit different working frequencies for potential applications.

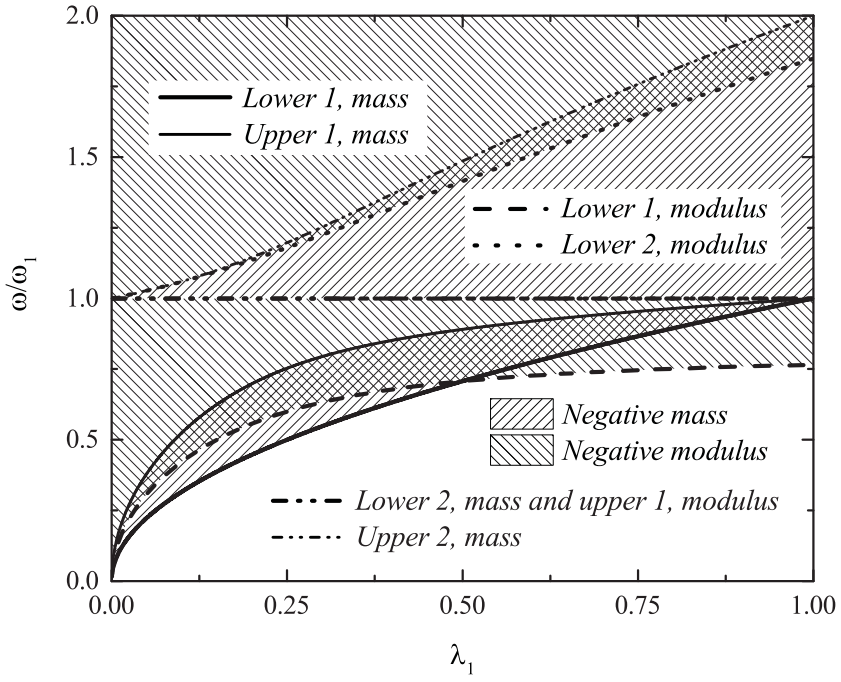

Figure 3.10: Frequency ranges for negative parameters for $\eta = 1.0$ and $\lambda_2 = 2.0$ with $\theta < 1$.

3.3 Dispersion characteristics of propagating waves

For the developed metamaterial system, the effective mass and modulus show strong dependence on the loading frequency, as discussed in the previous section. To further evaluate the frequency response of the system, lets consider the propagation of a harmonic longitudinal elastic wave in a one-dimensional mechanical system consisting of infinite number of the developed representative unit cells, as illustrated in figure 3.1(b). The wave can be generally expressed as

$$u(x,t) = u_0 e^{i(Kx-\omega t)}, \tag{3.33}$$

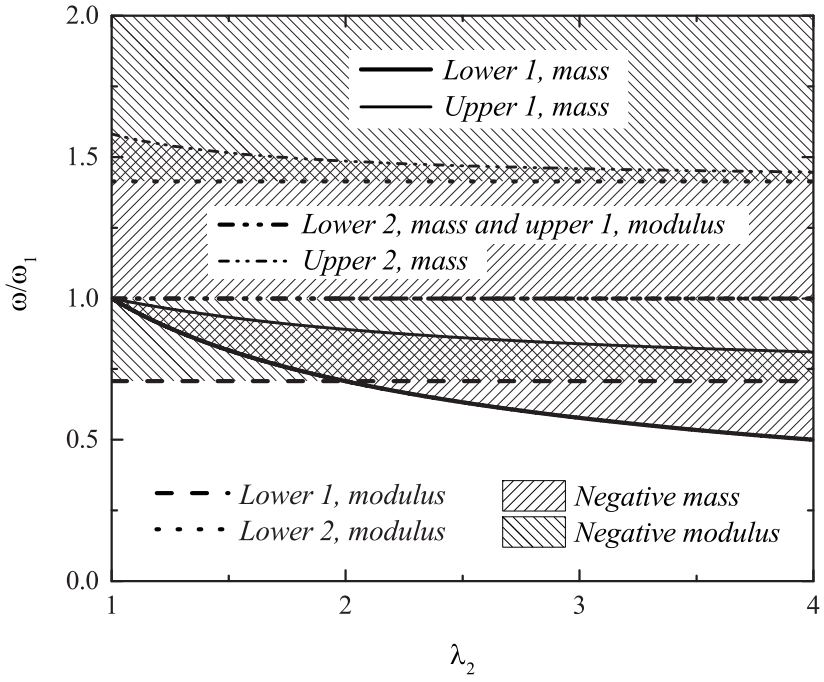

Figure 3.11: Frequency ranges for negative parameters for $\eta = 1.0$ and $\lambda_1 = 0.5$ with $\theta < 1$.

where ω and K are the circular frequency and the wave number of the wave, x is the axis along the longitudinal direction of the metamaterial and u_0 is the displacement amplitude at $x = 0$. The left end of the 0^{th} cell $(n = 0)$ is set as the origin of x axis $(x = 0)$. $x = nL$ indicates the distance of the left end of the n^{th} cell to the origin.

The dispersion relation for the wave propagation can be established by considering the continuity condition between adjacent unit cells. The boundary forces acting on the left and the right end of the n^{th} unit cell, F_n and F_{n+1}, respectively, can be determined from equations (3.10) and (3.11), as

$$F_n = \frac{E_e A}{L}(u_{n+1} - u_n) + \frac{m_e \omega^2}{4}(u_{n+1} + u_n), \tag{3.34}$$

$$F_{n+1} = \frac{E_e A}{L}(u_{n+1} - u_n) - \frac{m_e \omega^2}{4}(u_{n+1} + u_n). \tag{3.35}$$

From equation (3.34), the force acting on the left end of the $(n+1)^{th}$ cell, can be similarly determined as

$$F_{n+1} = \frac{E_e A}{L}(u_{n+2} - u_{n+1}) + \frac{m_e \omega^2}{4}(u_{n+2} + u_{n+1}). \tag{3.36}$$

By combining equations (3.35) and (3.36), the governing equation for the wave propagation can be expressed in terms of the boundary displacements of the unit cells as

$$\frac{E_e A}{L}(u_{n+2} - 2u_{n+1} + u_n) + \frac{m_e \omega^2}{4}(u_{n+2} + 2u_{n+1} + u_n) = 0. \tag{3.37}$$

Substitution of equation (3.33) into equation (3.37) will yield the dispersion relation between between the wave number and the frequency of the wave as

$$\frac{e^{iKL} - 2 + e^{-iKL}}{e^{iKL} + 2 + e^{-iKL}} + \frac{m_e \omega^2 L}{4E_e A} = 0. \tag{3.38}$$

3.3.1 Double positivity or double negativity

When both m_e and E_e are positive or negative, $m_e/E_e > 0$, the wave number K can be determined from equation (3.38) as (Wang, 2014),

$$KL = \cos^{-1}\left(\frac{1-\delta}{1+\delta}\right), \tag{3.39}$$

with $\delta = |m_e \omega^2 L/(4E_e A)|$. Substituting the expressions for the effective mass and modulus given in equations (3.12) and (3.13), this dispersion relation can be further expressed in terms

of the three structural parameters, η, λ_1 and λ_2, as

$$\begin{aligned}&\lambda_2\eta^2\gamma^6-\eta\left(2\lambda_1+\lambda_2\left(\eta+\lambda_1\left(2+\eta\right)\right)\right)\gamma^4\\&+2\left(\lambda_1^2\left(1-\cos\psi\right)+\lambda_1\eta\left(1+\lambda_1+\lambda_2\right)\right)\gamma^2-2\lambda_1^2\left(1-\cos\psi\right)=0,\end{aligned}\tag{3.40}$$

with $\psi = KL$ being the normalized wave number and $\gamma = \omega/\omega_1$ being the normalized frequency. It has been shown that (Wang, 2014) for both double positive and negative cases, $KE_e > 0$ since the the power input at the left end of the metamaterial by the external excitation must be positive to provide the energy to the system. Therefore, for double positivity, the sign of K will be positive, $KL = \mathrm{Re}\left(KL\right) > 0$, indicating a direction of wave propagation to the right. For double negativity, K will be negative, $KL = \mathrm{Re}\left(KL\right) < 0$, indicating a backward wave propagation to the left.

3.3.2 Single negativity

When only negative m_e or E_e is negative, the dispersion relation in equation (3.38) becomes

$$e^{iKL} = \frac{1 \pm \sqrt{\delta}}{1 \mp \sqrt{\delta}}.\tag{3.41}$$

The solution of KL is represented by an imaginary number, i.e., $KL = i\beta$ with β being a positive real number given by $\beta = \ln\left|\frac{1+\sqrt{\delta}}{1-\sqrt{\delta}}\right|$. The wave motion described in equation (3.33) can be recast in the form of

$$u(x,t) = u_0 e^{-\beta x/L} e^{-i\omega t},\tag{3.42}$$

in which a positive β represents an exponentially decaying field along the x direction. Therefore, β serves as the attenuation factor for the system. In this case, wave can not propagate in the elastic metamaterials.

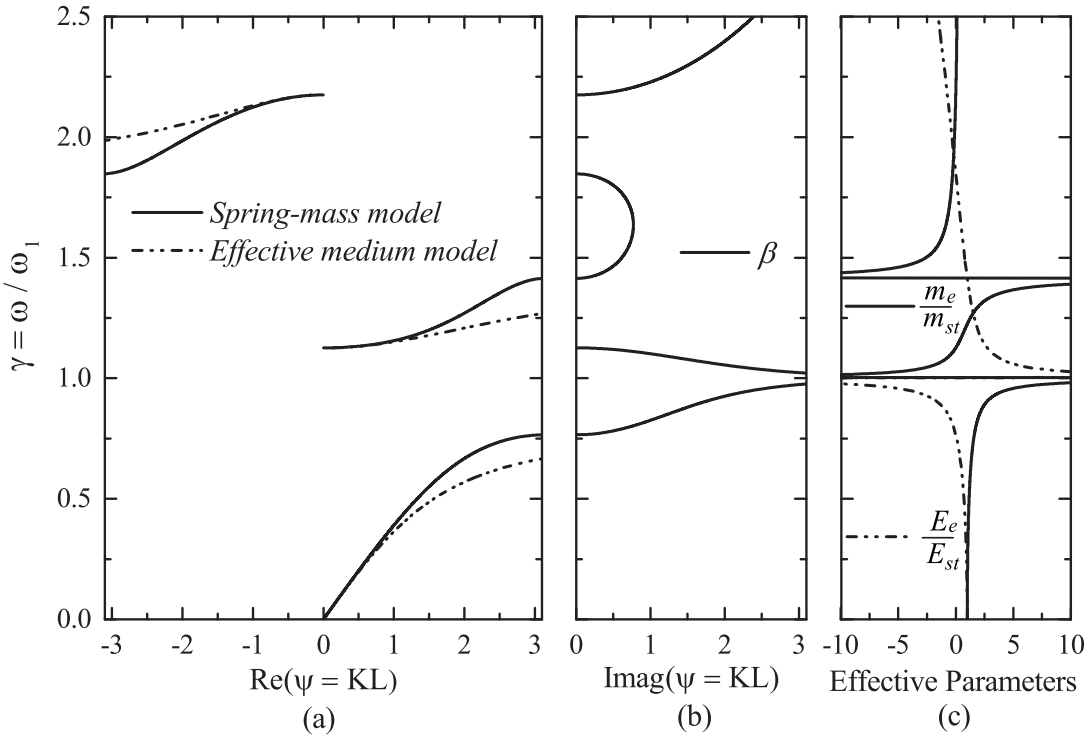

Figure 3.12: Frequency response for case 1, (a) the real part of the wave number, (b) the imaginary part of the wave number, (c) the effective mass and modulus.

3.3.3 Effective medium model

If the metamaterial structure is modelled as an equivalent one-dimensional homogeneous material with effective mass and effective modulus, given in equations (3.12) and (3.13), the equation of motion of the effective medium is

$$E_e \frac{\partial^2 u}{\partial x^2} = \rho_e \frac{\partial^2 u}{\partial t^2}, \tag{3.43}$$

where $\rho_e = m_e/AL$ is the effective mass density. A harmonic wave propagating in such an effective medium will have a wave number $\bar{K}$, given by

$$\bar{K}^2 = \frac{\rho_e \omega^2}{E_e}, \tag{3.44}$$

which provides the dispersion relation.

The dispersion relation and the effective mass and modulus for the new metamaterial structure are illustrated in figures 3.12, 3.13 and 3.14 for the following three cases, for $\lambda_1 = \lambda_2 = 1.0$,

- *Case* 1: $\eta = 1.0$, $\theta^2 = 2\lambda_1/(\eta\lambda_2) = 2.0$,
- *Case* 2: $\eta = 2.0$, $\theta^2 = 2\lambda_1/(\eta\lambda_2) = 1.0$,
- *Case* 3: $\eta = 2.5$, $\theta^2 = 2\lambda_1/(\eta\lambda_2) = 0.8$.

The dispersion relation for the effective homogeneous medium is also shown in figures $3.12(a)$, $3.13(a)$ and $3.14(a)$ for comparison. It can be observed that the dispersion curves of the two

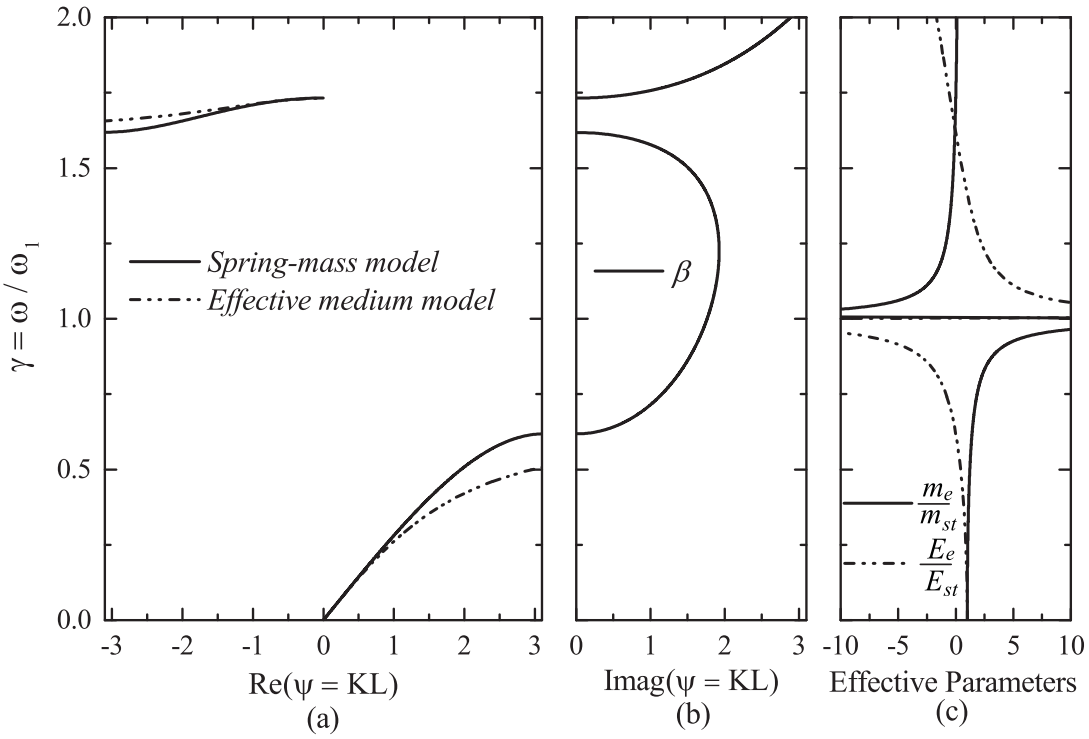

Figure 3.13: Frequency response for case 2, (a) the real part of the wave number, (b) the imaginary part of the wave number, (c) the effective mass and modulus.

models are very close to each other for low wave number, indicating that effective homogeneous medium can provide excellent approximation of the metamaterial structure for cases involving long-wavelength.

For case 1 ($\theta > 1$) and case 3 ($\theta < 1$), three band gaps are generated. For case 2, there are two band gaps. In the band gap, no real solution of wave number exists and the wave number is purely imaginary with positive attenuation factor, β, as shown in figures 3.12(b), 3.13(b) and 3.14(b). The normalized effective mass and modulus, m_e/m_{st} and E_e/E_{st}, are shown in figures 3.12(c), 3.13(c) and 3.14(c), in which m_{st} and E_{st} are the static mass and modulus of the representative unit cell given by $m_{st} = (2M + 2m_1 + 2m_2)$ and $E_{st} = k_2 L/A$, respectively.

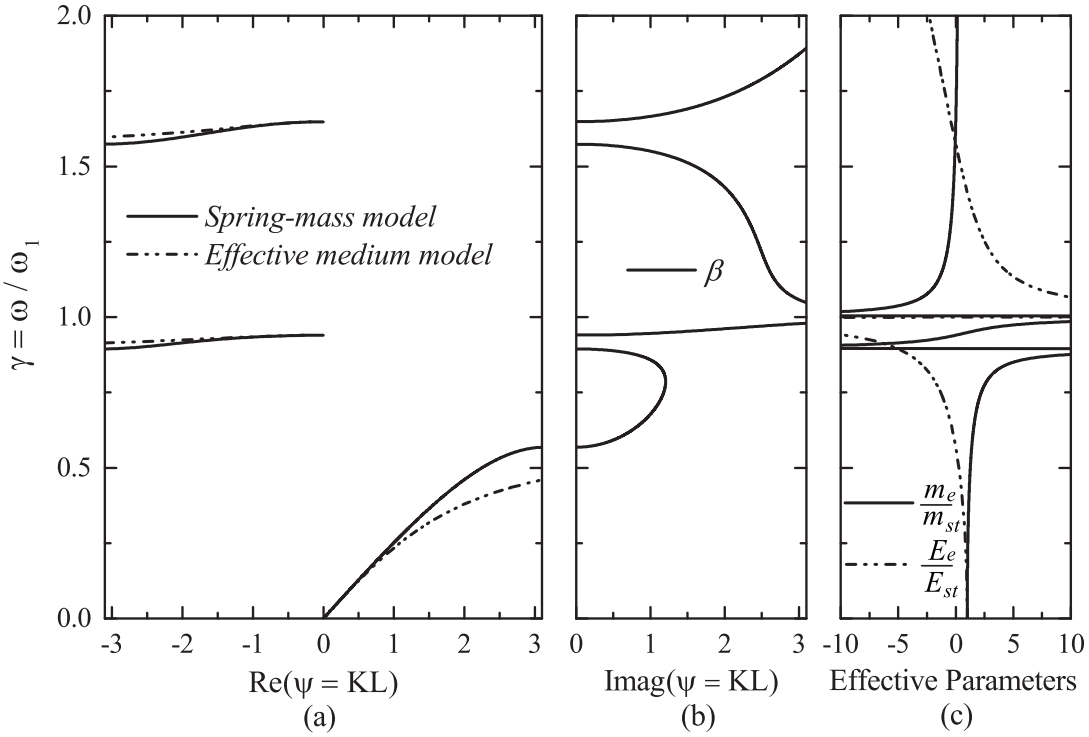

Figure 3.14: Frequency response for case 3, (a) the real part of the wave number, (b) the imaginary part of the wave number, (c) the effective mass and modulus.

3.4 Numerical analysis of the metamaterial model

In the previous sections, the proposed representative unit cell, figure 3.1(a), has been simplified as a cell consisting of a series of rigid bodies and massless linear springs, figure 3.1(b). This section provides a numerical study of the developed metamaterial model using Finite Element (FE) analysis to evaluate the suitability of the spring-mass unit cell used. A periodic metamaterial is formed by repeating the original unit cell of length L, as shown in figure 3.15. For the three materials used for the unit cell, labeled as materials I, II and III, materials I and II should possess higher mass densities and higher moduli. Material III should be much lighter and softer to generate local resonance. Materials I and II can be identical or different to realize various mass ratio λ_1. From a design perspective, more types of materials can be employed in the unit cell to generate desired parameters η, λ_1 and λ_2 with wider variations.

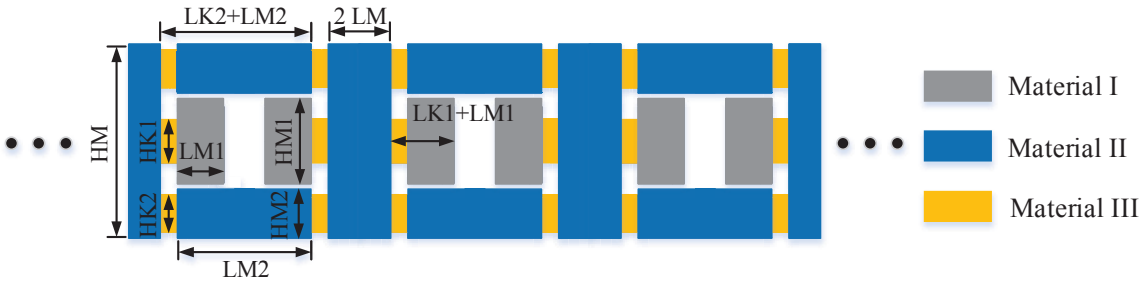

Figure 3.15: The periodic elastic metamaterial model.

In the current FE analysis, a one-dimensional elastic metamaterial structure consisting of 100 unit cells is used, with geometrical configuration and material properties being given in tables 3.1 and 3.2, respectively. The commercial software package COMSOL Multiphysics

5.2a is utilized to conduct the dynamic elastic analysis of the metamaterial system. Free quad element is used in the analysis with the element size being around $1.50 \times 10^{-2} L$, as depicted in figure 3.16(a). Because the one-dimensional model is mostly under simple tension, the model is not sensitive to the number of meshing elements. Actually, the simulation results converge when the number of meshing elements is larger than 100. Linear elastic material properties are used in the simulations and damping is not considered.

Table 3.1: Geometrical parameters

	LM	HM	LM_1	HM_1	LM_2	HM_2	LK_1	HK_1	LK_2	HK_2
Values (mm)	5.0	34.0	7.5	16.0	24.0	8.0	3.0	7.0	2.0	6.0

Table 3.2: Material parameters (Liu et al., 2015; Torrent et al., 2014)

	Material	Density $(\mathrm{Kg/m^3})$	Young's Modulus (Pa)	Poisson's ratio
Material I	Lead	11340	16E9	0.44
Material II	Steel	7850	210E9	0.29
Material III	Foam	115	8E6	0.33

As shown in table 3.2, lead is selected as the material of the resonators with mass m_1 and steel is used for the other four mass components in the representative unit cell. Foam, as a very light and soft material, is selected as material III. By using the geometrical parameters and the mass densities in tables 3.1 and 3.2, the exact values of m_1, m_2 and M can be determined. The values of k_1 and k_2 are obtained by conducting a FE analysis of the unit cell under static loading,

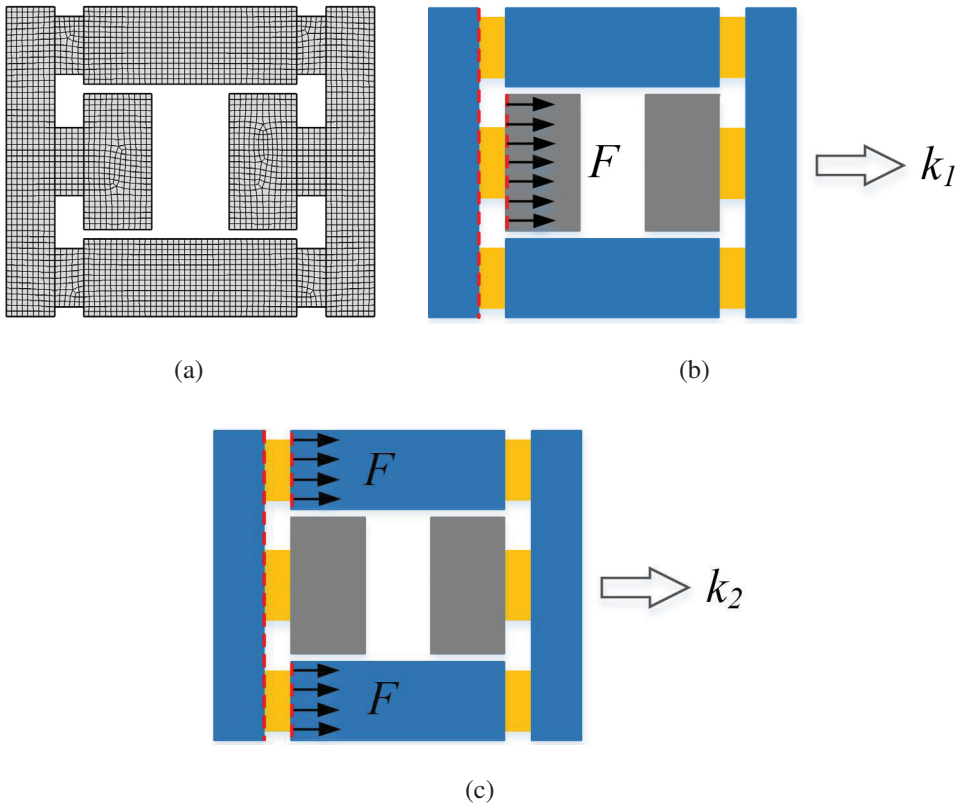

Figure 3.16: Numerical calculation, (a) FEM mesh, (b) calculating stiffness k_1, (c) calculating stiffness k_2.

where tensile forces are properly applied with the left boundary of the unit cell being fixed, as shown in figures 3.16(b) and 3.16(c). The determined masses and spring constants from FE anslysis are, $m_1 = 1.3608$ Kg, $m_2 = 1.5072$ Kg, $M = 1.3345$ Kg, $k_1 = 2.4409 \times 10^7$ N/m and $k_2 = 3.2256 \times 10^7$ N/m. In comparison, if uniform deformation in material III is assumed, k_1, k_2 can be directly calculated as 1.8667×10^7 N/m and 2.4×10^7 N/m, which show 23.5% and 25.6% difference with the FE results, respectively. In the following discussion, the k_1 and k_2 predicted by FE analysis will be used. According to these parameters, the two natural frequencies are determined to be $f_1 = \omega_1/2\pi = 674.06$ Hz, $f_2 = \omega_2/2\pi = 1041.25$ Hz. The θ value can then be calculated as $\theta = \omega_2/\omega_1 = 1.54 > 1$. According to equation (3.28), for this

case, only one frequency range with double negative behaviour will exist.

3.4.1 Dispersion relation

The dispersion characteristics of the periodic simplified spring-mass model is first compared with that from the FE analysis of the elastic model. For the spring-mass model, the dispersion curve, i.e., relation between wave number and loading frequency, is obtained from equation (3.38) for the current materials, as shown in figure 3.17(a). For the elastic model, FE modal analysis is conducted to determine the longitudinal natural frequencies and the corresponding mode shapes. The wave numbers are extracted by evaluating the model shapes using the least square method. The dispersion relation is then obtained, which is plotted with black dots in 3.17(a). In this figure, the areas filled with light grey indicate band gaps and the dark grey area represents the double negative range. It can be easily observed from figure 3.17(a) that the dispersion relations from these two models agree well, indicating that the spring-mass model can accurately predict the dispersion property of the proposed metamaterial system. Different from the property of elastic waves in traditional materials, the negative wave number shows negative phase velocity. The corresponding effective mass and modulus are shown in figure 3.17(b), which are determined from the metamaterial model by using the spring constants from the FE analysis and the masses. The band gaps predicted by the metamaterial model in 3.17(b) correspond very well with the band gaps determined from FE results in 3.17(a).

3.4.2 FE simulation of wave propagation

The dynamic response and wave propagation in periodic metamaterials, as shown in figure 3.15, is studied numerically using FE. The left end of the metamaterial, at $x = 0$, is excited by

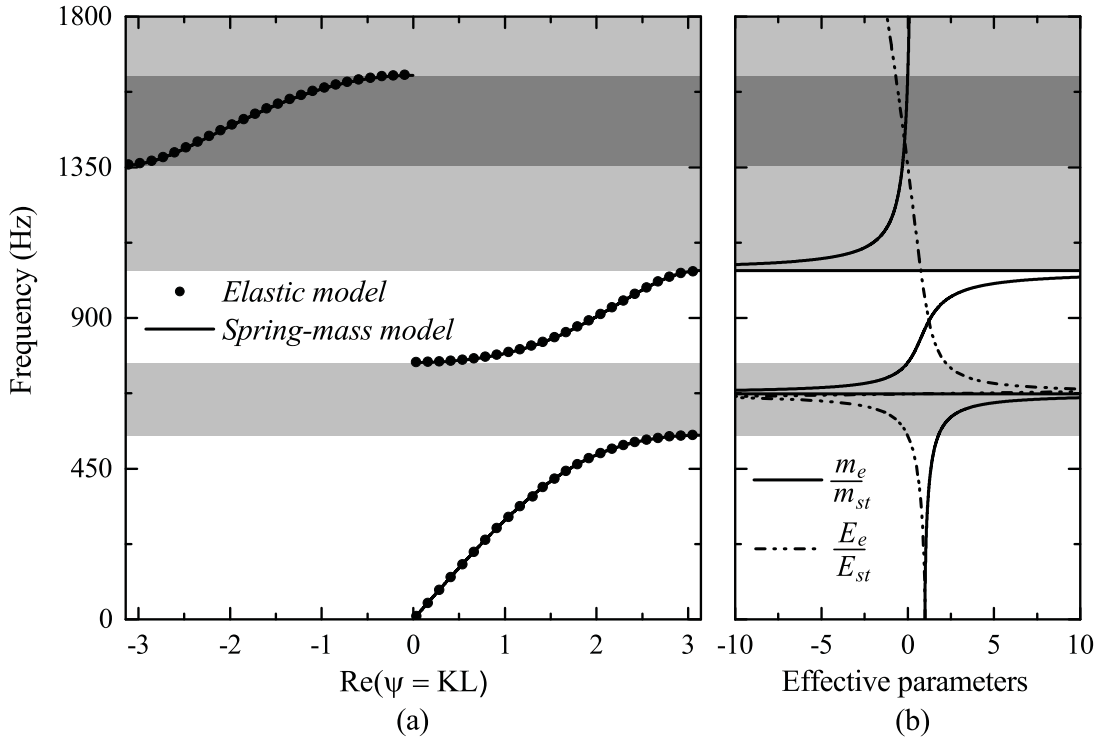

Figure 3.17: Frequency response of the elastic model and the spring-mass model, (a) dispersion relation, (b) the normalized effective parameters.

a harmonic prescribed displacement

$$U(t) = u_0 \sin(2\pi f t), \tag{3.45}$$

where f is the loading frequency in Hz and u_0 is selected to be 1 mm. The right end is set as traction free. Transient response of the material is calculated for a frequency $f = 700$ Hz, which is in the band gap based on the metamaterial model, associated negative effective mass, as shown in 3.17(b). Figure 3.18(a) shows the net force and average acceleration of the second cell from the left to this excitation. It can be observed that the net force applied to the second cell is exactly out of phase with its average acceleration, indicating negative mass. Also, in figure 3.18(b), the phase of the averaged force applied to the second cell perfectly matches

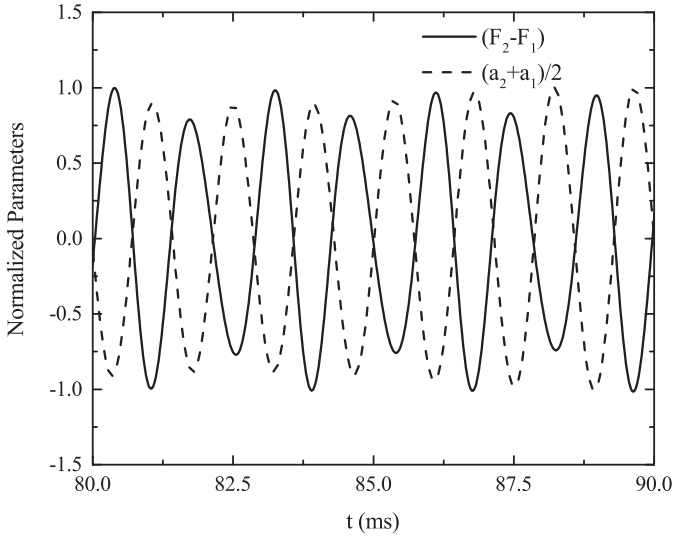

(a)

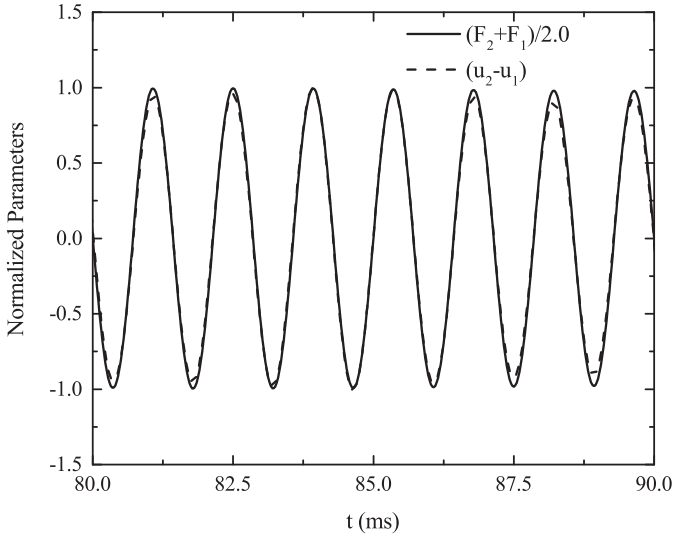

(b)

Figure 3.18: Normalized response of the second cell when $f = 700$ Hz, (a) net force and average acceleration, (b) average force and deformation.

that of its deformation, showing positive effective modulus. The results for $f = 650$ Hz are shown in figure 3.19, which generates positive effective mass and negative effective modulus,

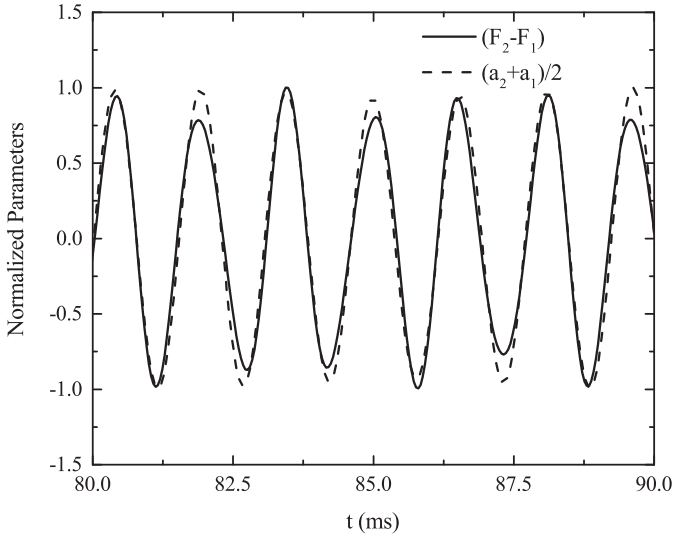

(a)

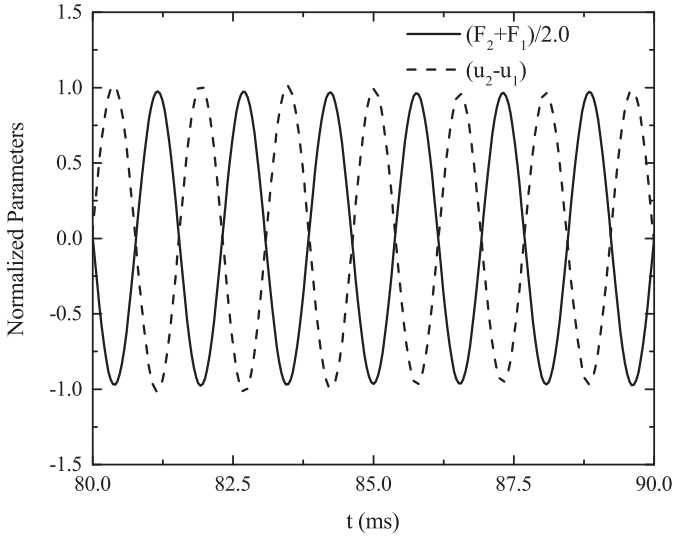

(b)

Figure 3.19: Normalized response of the second cell when $f = 650$ Hz, (a) net force and average acceleration, (b) average force and deformation.

as indicated by $3.17(b)$. Figure 3.20 shows the dynamic response of the second cell for $f =$ 1610 Hz. In this case, the corresponding effective mass and modulus are both negative, as

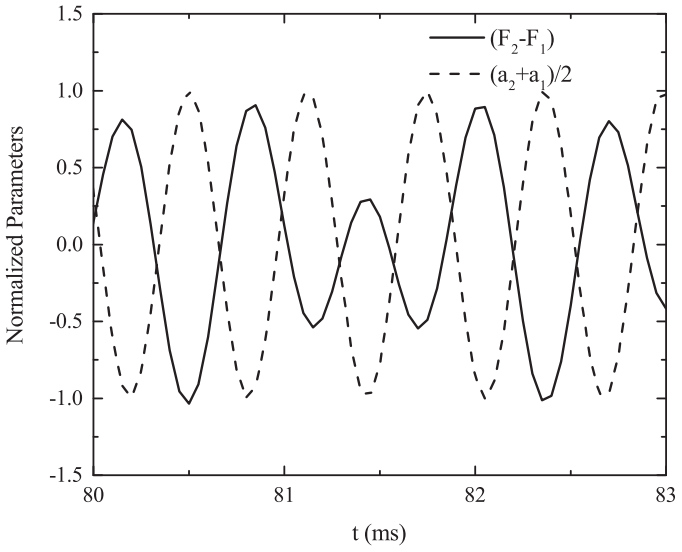

(a)

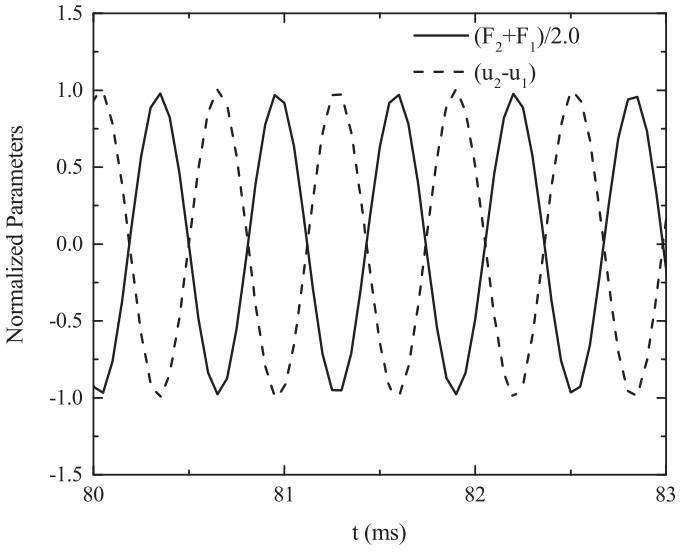

(b)

Figure 3.20: Normalized response of the second cell when $f = 1610$ Hz, (a) net force and average acceleration, (b) average force and deformation.

shown in figure 3.17(b). Both net force - average acceleration and average force - deformation relations are out of phase, as predicted, caused by the double negativity.

To further study the wave mitigation property of the metamaterial in the band gap, a frequency domain simulation is conducted. Transmission coefficients at different frequencies, which are defined as the amplitude ratios of the output displacement at the right end to that of the input at the left end, are determined. The variation of the transmission coefficients with frequency is shown in figure 3.21. Three passing bands in the low frequency range can be observed, which correspond to frequency ranges of double positivity or double negativity. There are also three frequency ranges with very low transmission coefficients, corresponding to band gaps, which are approximately from 551.4Hz to 768.4Hz, from 1044.4Hz to 1357.2Hz, and from 1627.1Hz to 39792.3Hz.

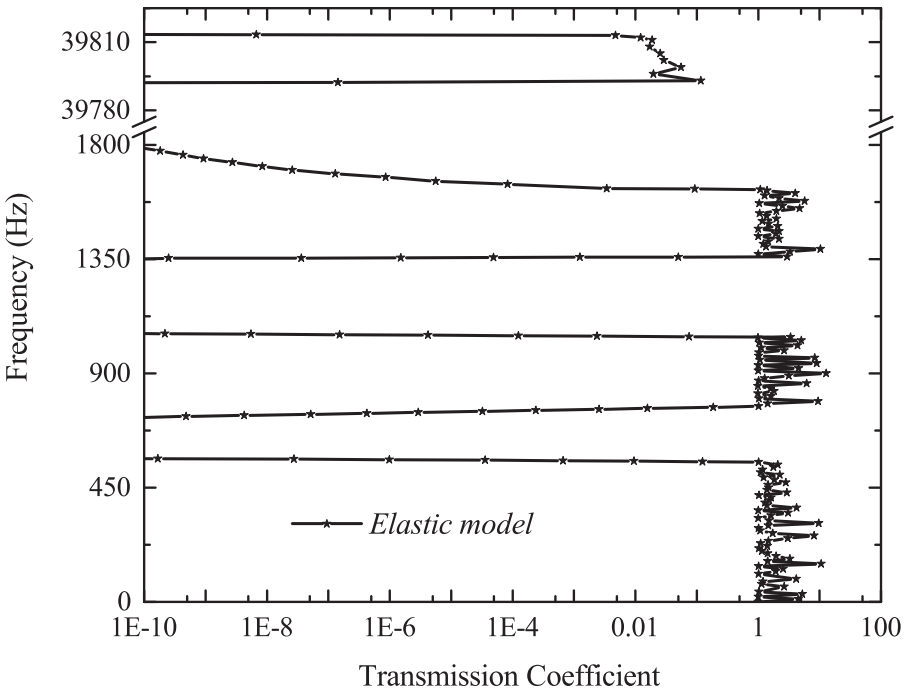

Figure 3.21: The transmission coefficients of the structure.

To illustrate the negative phase velocity, the transient response of the metamaterial with

$f = 1610$Hz is evaluated, at which both effective mass and modulus are negative, as shown in figure 3.17(b). To accurately capture the dynamic behaviour of the metamaterial, the time increments between the curves is selected to be less than $T/8$ with T as the period of the excitation in the following figures. Figure 3.22 shows the displacement distribution in the metamaterial at the initial stage of the loading. The peaks of the displacement move to the left, showing negative phase velocity. Figure 3.23 shows the displacement distribution at a later stage when steady wave motion is established. Backward motion of the peaks is clearly observed.

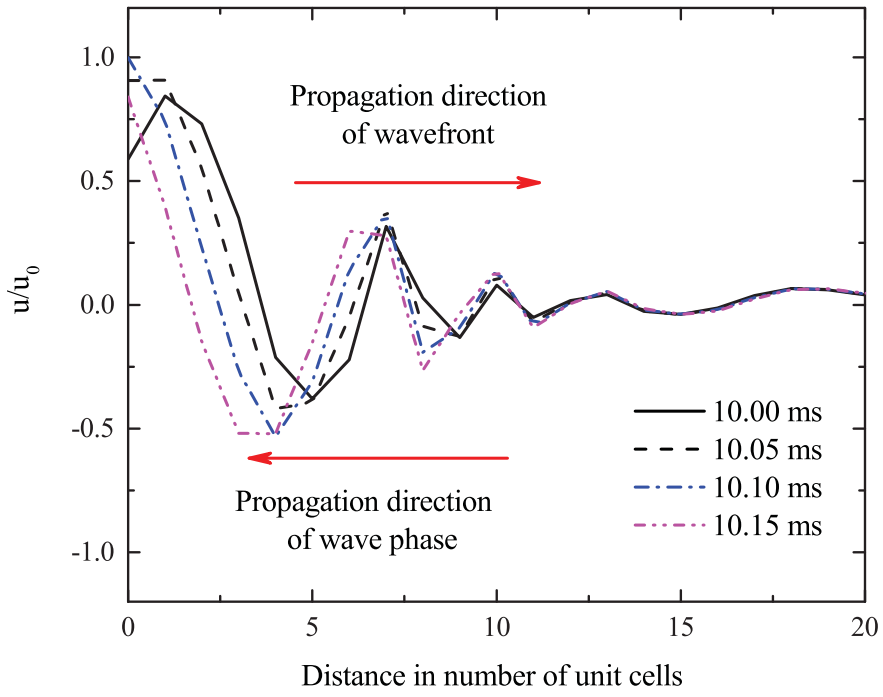

Figure 3.22: Snapshots of wave propagation of the wavefront in the elastic metamaterial model with an excitation frequency 1610 Hz.

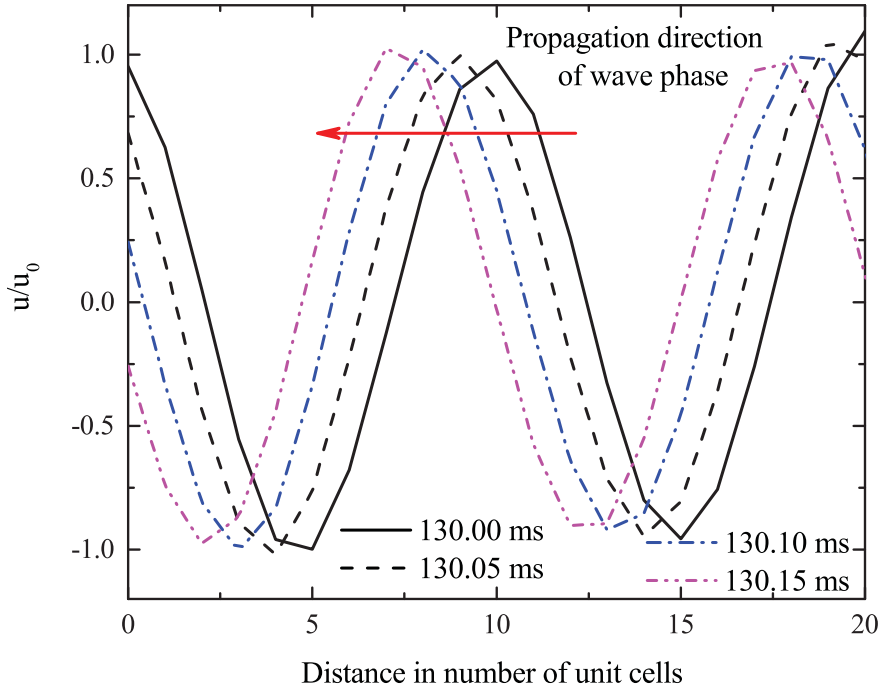

Figure 3.23: Snapshots of wave propagation in the elastic model around 130 ms with an excitation frequency 1610 Hz.

3.5 Conclusion

An elastic metamaterial model is designed based on translational resonance to obtain simultaneously negative effective mass and modulus within specific frequency ranges. Two different translational resonances exist in the metamaterial representative cell. One resonance contributes directly to the negative effective modulus and the coupled effect of the two resonances can generate negative effective mass, which endows the elastic metamaterial with great flexibility to generate negative effective parameters in different frequency ranges. Due to the unique feature of the developed representative cells, the independent control of the effective

mass and modulus can be realized to some extent. Wave propagation in such metamaterials is studied and the phenomenon of negative phase velocity is observed in the frequency range with double negative parameters. This model can shed new light on designing elastic metamaterial with negative effective material parameters.

Appendix A

In the discussion of the frequency ranges with negative effective mass, two positive roots of $F_m(\omega/\omega_1) = 0$, ζ_1 and ζ_2, are given by

$$\zeta_1^2 = \frac{1}{2}\left\{\begin{array}{l}\left(1+\dfrac{2\lambda_1}{\eta}+\dfrac{2\lambda_1}{\lambda_2\eta}+\lambda_1\right) \\ +\sqrt{\left(1+\dfrac{2\lambda_1}{\eta}+\dfrac{2\lambda_1}{\lambda_2\eta}+\lambda_1\right)^2-\dfrac{8\lambda_1}{\lambda_2\eta}(1+\lambda_1+\lambda_2)}\end{array}\right\}, \tag{A.1}$$

$$\zeta_2^2 = \frac{1}{2}\left\{\begin{array}{l}\left(1+\dfrac{2\lambda_1}{\eta}+\dfrac{2\lambda_1}{\lambda_2\eta}+\lambda_1\right) \\ -\sqrt{\left(1+\dfrac{2\lambda_1}{\eta}+\dfrac{2\lambda_1}{\lambda_2\eta}+\lambda_1\right)^2-\dfrac{8\lambda_1}{\lambda_2\eta}(1+\lambda_1+\lambda_2)}\end{array}\right\}. \tag{A.2}$$

For the root, ζ_1, it can be recast in the form of

$$\zeta_1^2 = \frac{1}{2}\left\{\begin{array}{l}\left(1+\dfrac{2\lambda_1}{\eta}+\dfrac{2\lambda_1}{\lambda_2\eta}+\lambda_1\right) \\ +\sqrt{\left(1-\dfrac{2\lambda_1}{\eta}-\dfrac{2\lambda_1}{\lambda_2\eta}+\lambda_1\right)^2+\dfrac{8\lambda_1^2}{\eta}}\end{array}\right\}, \tag{A.3}$$

which directly navigates to the relation that

$$\zeta_1^2 > \frac{1}{2}\left\{\begin{array}{l}\left(1+\dfrac{2\lambda_1}{\eta}+\dfrac{2\lambda_1}{\lambda_2\eta}+\lambda_1\right) \\ +\left|1-\dfrac{2\lambda_1}{\eta}-\dfrac{2\lambda_1}{\lambda_2\eta}+\lambda_1\right|\end{array}\right\} > 1. \tag{A.4}$$

According to equation (A.2), the second positive root, ζ_2, can be rearranged as

$$\zeta_2^2 = \frac{1}{2}\left\{\begin{array}{l}\left(1+\dfrac{2\lambda_1}{\eta}+\dfrac{2\lambda_1}{\lambda_2\eta}+\lambda_1\right)\\ -\sqrt{\left(1-\dfrac{2\lambda_1}{\eta}-\dfrac{2\lambda_1}{\lambda_2\eta}-\lambda_1\right)^2+4\lambda_1\left(1-\dfrac{2\lambda_1}{\lambda_2\eta}\right)}\end{array}\right\}. \tag{A.5}$$

Equations (A.1) and (A.2) can also be further rewritten as

$$\zeta_1^2 = \frac{1}{2}\left\{\begin{array}{l}\left(1+\dfrac{2\lambda_1}{\eta}+\dfrac{2\lambda_1}{\lambda_2\eta}+\lambda_1\right)\\ +\sqrt{\left(-1-\dfrac{2\lambda_1}{\eta}+\dfrac{2\lambda_1}{\lambda_2\eta}-\lambda_1\right)^2+\dfrac{8\lambda_1}{\eta}\left(\dfrac{2\lambda_1}{\lambda_2\eta}-1\right)}\end{array}\right\}, \tag{A.6}$$

$$\zeta_2^2 = \frac{1}{2}\left\{\begin{array}{l}\left(1+\dfrac{2\lambda_1}{\eta}+\dfrac{2\lambda_1}{\lambda_2\eta}+\lambda_1\right)\\ -\sqrt{\left(-1-\dfrac{2\lambda_1}{\eta}+\dfrac{2\lambda_1}{\lambda_2\eta}-\lambda_1\right)^2+\dfrac{8\lambda_1}{\eta}\left(\dfrac{2\lambda_1}{\lambda_2\eta}-1\right)}\end{array}\right\}. \tag{A.7}$$

When $\theta = \sqrt{\frac{2\lambda_1}{\lambda_2\eta}} > 1$, the following relations can be readily obtained from equations (A.5), (A.6) and (A.7), as

$$\zeta_1^2 > \frac{1}{2}\left\{\begin{array}{l}\left(1+\dfrac{2\lambda_1}{\eta}+\dfrac{2\lambda_1}{\lambda_2\eta}+\lambda_1\right)\\ +\left|-1-\dfrac{2\lambda_1}{\eta}+\dfrac{2\lambda_1}{\lambda_2\eta}-\lambda_1\right|\end{array}\right\} \geq \theta^2, \tag{A.8}$$

$$\zeta_2^2 < \frac{1}{2}\left\{\begin{array}{l}\left(1+\dfrac{2\lambda_1}{\eta}+\dfrac{2\lambda_1}{\lambda_2\eta}+\lambda_1\right)\\ -\left|-1-\dfrac{2\lambda_1}{\eta}+\dfrac{2\lambda_1}{\lambda_2\eta}-\lambda_1\right|\end{array}\right\} \leq \theta^2, \tag{A.9}$$

$$\zeta_2^2 > \frac{1}{2}\left\{\begin{array}{l}\left(1+\dfrac{2\lambda_1}{\eta}+\dfrac{2\lambda_1}{\lambda_2\eta}+\lambda_1\right)\\ -\left|1-\dfrac{2\lambda_1}{\eta}-\dfrac{2\lambda_1}{\lambda_2\eta}-\lambda_1\right|\end{array}\right\} = 1, \tag{A.10}$$

which directly leads to

$$\zeta_1 > \bar{\zeta}_1 > \zeta_2 > \bar{\zeta}_2. \tag{A.11}$$

When $\theta = \sqrt{\frac{2\lambda_1}{\lambda_2\eta}} < 1$, similar results can be obtained as

$$\zeta_2^2 < \frac{1}{2}\left\{\begin{array}{l}\left(1+\dfrac{2\lambda_1}{\eta}+\dfrac{2\lambda_1}{\lambda_2\eta}+\lambda_1\right)\\ -\left|1-\dfrac{2\lambda_1}{\eta}-\dfrac{2\lambda_1}{\lambda_2\eta}-\lambda_1\right|\end{array}\right\} \leq 1, \tag{A.12}$$

$$\zeta_2^2 > \frac{1}{2}\left\{\begin{array}{l}\left(1+\dfrac{2\lambda_1}{\eta}+\dfrac{2\lambda_1}{\lambda_2\eta}+\lambda_1\right)\\ -\left|-1-\dfrac{2\lambda_1}{\eta}+\dfrac{2\lambda_1}{\lambda_2\eta}-\lambda_1\right|\end{array}\right\} = \theta^2. \tag{A.13}$$

The relation in equation (A.11) can then be obtained for this case as well. When $\theta = \sqrt{\frac{2\lambda_1}{\lambda_2\eta}} = 1$, the following relation can be obtained as

$$\zeta_1 > \bar{\zeta}_1 = \zeta_2 = \bar{\zeta}_2. \tag{A.14}$$

Equations (A.11) and (A.14) directly navigate to equation (3.20).

For determination of the frequency ranges for negative effective modulus, the two positive roots of $F_e(\omega/\omega_1) = 0$, ξ_1 and ξ_2, are given by

$$\xi_1^2 = \frac{1}{2}\left\{\left(1+\lambda_1+\frac{2\lambda_1}{\eta}\right)+\sqrt{\left(1+\lambda_1+\frac{2\lambda_1}{\eta}\right)^2-\frac{8\lambda_1}{\eta}}\right\}, \tag{A.15}$$

$$\xi_2^2 = \frac{1}{2}\left\{\left(1+\lambda_1+\frac{2\lambda_1}{\eta}\right)-\sqrt{\left(1+\lambda_1+\frac{2\lambda_1}{\eta}\right)^2-\frac{8\lambda_1}{\eta}}\right\}. \tag{A.16}$$

For ξ_1, it can have a new form of

$$\xi_1^2 = \frac{1}{2}\left\{\left(1+\lambda_1+\frac{2\lambda_1}{\eta}\right)+\sqrt{\left(1-\frac{2\lambda_1}{\eta}\right)^2+\left(2\lambda_1+\lambda_1^2+\frac{4\lambda_1^2}{\eta}\right)}\right\}, \tag{A.17}$$

resulting in

$$\xi_1^2 > \frac{1}{2}\left\{\left(1+\lambda_1+\frac{2\lambda_1}{\eta}\right)+\left|1-\frac{2\lambda_1}{\eta}\right|\right\} > 1. \tag{A.18}$$

By referring to equation (A.16), the second root, ξ_2, can be rearranged as

$$\xi_2^2 = \frac{1}{2}\left\{\left(1+\lambda_1+\frac{2\lambda_1}{\eta}\right)-\sqrt{\left(1-\lambda_1-\frac{2\lambda_1}{\eta}\right)^2+4\lambda_1}\right\}, \tag{A.19}$$

which can directly lead to

$$\xi_2^2 < \frac{1}{2}\left\{\left(1+\lambda_1+\frac{2\lambda_1}{\eta}\right)-\left|1-\lambda_1-\frac{2\lambda_1}{\eta}\right|\right\} \leq 1. \tag{A.20}$$

Then, the following relation can be obtained,

$$\xi_1 > 1 > \xi_2. \tag{A.21}$$

Chapter 4: A new two-dimensional elastic metamaterial system with multiple local resonances

As the extension of the developed one-dimensional model in Chapter 3, this chapter introduces a new two-dimensional elastic metamaterial with multiple local resonances, which can generate simultaneously negative effective mass, bulk modulus and shear modulus in certain frequency ranges. Analytical study of the new metamaterial system is performed based on a simplified model to investigate the effects of the main material and geometric parameters. Numerical analysis is further conducted to simulate elastic wave propagation in the current metamaterial. Typical examples of the current metamaterial under different loading conditions are presented to show both the modal response and the property of elastic wave propagation in the metamaterial.

4.1 Introduction

Metamaterials are artificially structured materials, which have peculiar effective properties not commonly seen in nature. These unconventional properties are generated from the representative cell, the basic building blocks of the metamaterials (Cummer et al., 2016). Early studies of metamaterial have been focussed mainly on electromagnetic metamaterials, which have negative permittivity and/or negative permeability under certain frequencies, and make the negative refractive index achievable (Veselago, 1968). Many advanced applications of metamaterials for electromagnetic wave manipulation have been proposed over the last two decades, such as the invisible cloak based on the designed gradient-index (Pendry et al., 2006; Schurig et al., 2006)

and superlenses with sub-wavelength resolution using the concept of negative index (Kundtz and Smith, 2010; Shelby et al., 2001). In recent years, efforts have also been extended to explore the possible unconventional properties of acoustic/elastic metamaterials, the mechanical counterpart of the electromagnetic metamaterials. In the field of acoustic metamaterials, many promising applications have also been proposed or realized, such as sound isolating (Nateghi et al., 2017; Peng and Frank Pai, 2014; Sui et al., 2015; Tang et al., 2017), acoustic surface wave manipulation (Christensen et al., 2007), acoustic cloaking (Popa et al., 2011; Zhang et al., 2011), and the sub-wavelength imaging associated with negative phase velocity (Guenneau et al., 2007; Zhang et al., 2009).

Comparing with the intensive efforts in acoustic metamaterials, relatively less attention has been paid to elastic metamaterials, which are characterized by the coexistence and coupling of the longitudinal and transverse waves in the elastic mediums (Zhu et al., 2015). In the design of elastic metamaterials, to achieve the desired unconventional functionalities, negative effective material parameters are usually required (Zhou et al., 2012). Different metamaterial models have been proposed to achieve negative effective mass density and/or moduli by designing specific representative cells, mainly based on local resonances (Lee and Wright, 2016; Li and Wang, 2016; Ma and Sheng, 2016; Wang, 2014). These representative cells are usually highly frequency-dependent and the desired negative parameters can be obtained in certain frequency ranges (Chen et al., 2017; Liu et al., 2015; Oh et al., 2016). Following the first experimental design of elastic metamaterials, where the negative effective mass density is achieved by embedding heavy spheres coated with soft silicon rubber in epoxy (Liu et al., 2000), it is now well established that the negative effective mass density can be generated by the out-of-phase

translation motion between the main structure and the resonator, under the so-called dipolar resonance (Lu et al., 2017; Mitchell et al., 2014; Wang and Wang, 2016).

Negative effective bulk modulus was first experimentally illustrated in a one-dimensional acoustic metamaterial composed of periodic cavities, which serve as Helmholtz resonators (Fang et al., 2006). Similar phenomenon has also been observed for acoustic wave propagation in a tube with a periodic array of interspaced membranes and side holes (Lee et al., 2010). The similar mechanism, i.e. generating volumetric resonance, has been used to design elastic metamaterials (Liu et al., 2011a; Wu et al., 2007). Theoretical models have been developed based on spring-mass systems to illustrate the mechanisms of generating negative effective mass and modulus (Li and Wang, 2016; Wang, 2014). The negative effective shear modulus, exclusive to the elastic metamaterials can also be realized through local resonances in the representative cells of the elastic metamaterials (Zhou and Hu, 2009).

Double negative behaviour of elastic metamaterials can be achieved if the local resonances associated with negative effective mass and modulus can be excited simultaneously. Many efforts have been made to develop various metamaterial structures with such properties. An elastic metamaterial formed by arrays of rubber-coated-gold spheres or bubble-contained water spheres embedded in epoxy matrix, is reported to possess simultaneously negative effective mass density and bulk modulus due to the combined effect of the monopolar and dipolar resonances (Ding et al., 2007). Similar results have been obtained in an elastic metamaterial made of only solid materials, which implements the rotational motion of the resonators in its chiral microstructures to realize negative effective bulk modulus (Liu et al., 2011a). In an elastic metamaterial with its representative cells featuring fluid-solid inclusions, the negative shear

modulus associated with quadrupolar resonance, as well as the negative effective mass density, has been demonstrated (Wu et al., 2011). A hybrid elastic model has been reported to possess negative effective mass density, and negative effective bulk modulus or negative effective shear modulus in different frequency ranges (Lai et al., 2011). However, in the existing works discussed above, these three effective parameters, effective mass density, bulk modulus and shear modulus, are not allowed to turn negative simultaneously.

In the current study, a new two-dimensional elastic metamaterial system has been designed with its representative cells featuring only translational motions. The periodic structures of the proposed metamaterial system can induce dipolar, monopolar and quadrupolar resonances in overlapping frequencies, directly leading to simultaneous negative effective mass density, bulk modulus and shear modulus. Due to anisotropic nature of the metamaterial structure, various dynamic behaviour can be observed when elastic waves propagating in different directions. This new elastic metamaterial can behave like a solid with negative phase velocities for longitudinal and transverse waves and also can behave like a fluid mainly supporting longitudinal waves with negative phase velocities.

4.2 The two-dimensional elastic metamaterial model

Unlike traditional periodic materials, the overall properties of metamaterials are dominated by the dynamic behaviour of their representative cells. The structural design of the representative cells plays a vital role in achieving the desired properties. In the current work, a new two-dimensional elastic metamaterial is proposed to generate single negative (negative effective mass or modulus) or double negative (negative effective mass and modulus) mechanical prop-

erties. Negative effective mass and modulus are achieved through only translational motion of two types of local resonators introduced. This two-dimensional metamaterial system can induce strong wave mitigation and generate negative phase velocities in a controlled manner. The current new metamaterial model provides a more realistic design with simpler structures and more flexibility for controlling the desired dynamic behaviour represented by negative effective parameters.

4.2.1 The proposed representative cell

The proposed two-dimensional elastic metamaterial is schematically depicted in figure 4.1(a), in which the governing geometrical parameters have been labelled. It consists of periodic local structures with its representative cell being shown in figure 4.1(b). The cell has been designed to include multiple resonators to achieve negative effective mass and moduli. To generate the local resonance, four different materials are used. Materials I and II have higher mass densities and higher stiffnesses. Materials III and IV have lower mass densities and lower stiffnesses.

4.2.2 A simplified metamaterial model

When materials I and II are much heavier and stiffer than materials III and IV, I and II can be treated as rigid bodies and III and IV can be regarded as massless linear springs. In this simplified case, the representative cell can be modelled as a spring-mass system, as illustrated in figure 4.1(b), with the effective mass and stiffness of the springs determined from the original metamaterial model analytically or numerically (Liu et al., 2015).

In the representative cell of the simplified spring-mass model, four end rigid masses have the same mass M. A centre resonator with mass m_1 is attached to the rigid boundaries through

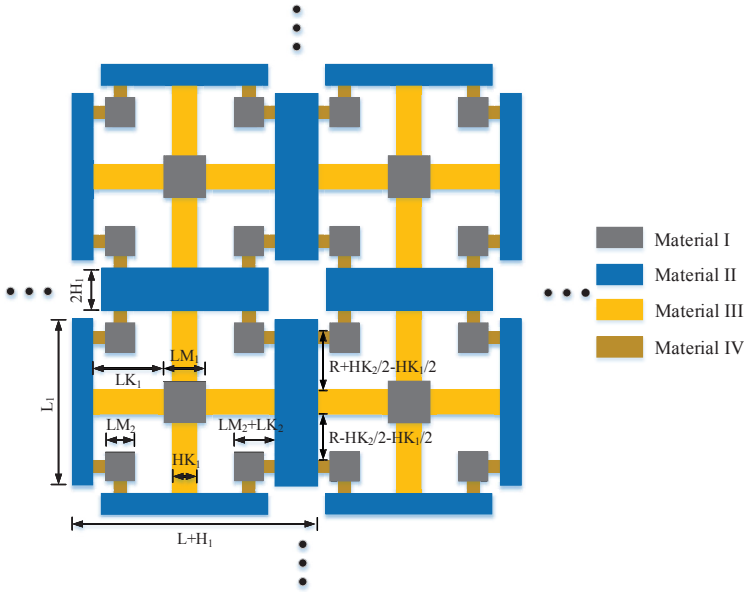

(a)

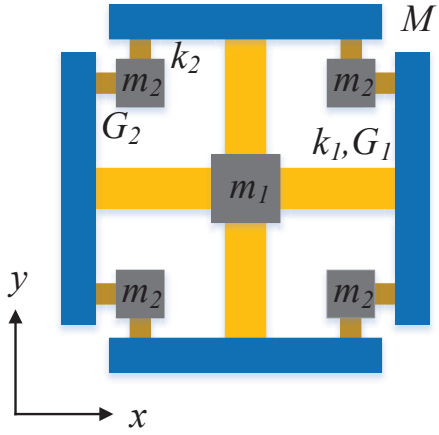

(b)

Figure 4.1: The two-dimensional elastic metamaterial system, (a) periodic cells, (b) the representative cell.

four identical springs with longitudinal and shear stiffnesses k_1 and G_1, along and perpendicular to the spring direction, respectively, as identified in figure 4.1(b). Four identical masses (resonators), m_2, are also attached with each of them being connected to its two adjacent end

rigid masses through springs with stiffness constants k_2 and G_2. The representative cells are connected to each other through the rigid boundaries with a periodic length L.

Formulation of the simplified model

A representative cell of the simplified spring-mass model, as schematically shown in figure 4.1(b), is labelled with the unit number (n,h), in which n and h are the order of the cell in horizontal and vertical directions, corresponding to x and y, respectively. The horizontal and vertical displacements of the boundary mass on the left are denoted as $u^M_{x1(n,h)}$ and $u^M_{y1(n,h)}$, and those of the lower boundary mass are denoted as $u^M_{x2(n,h)}$ and $u^M_{y2(n,h)}$. As a general notation used in the following discussion, subscripts '1' and '2' represent the boundary masses on the left/right and top/down, respectively. As an example, the equations of motion of the left boundary mass are

$$\begin{aligned} 2M\frac{\partial^2 u^M_{x1(n,h)}}{\partial t^2} =& k_1\left(u^{m1}_{x(n,h)} + u^{m1}_{x(n-1,h)} - 2u^M_{x1(n,h)}\right) \\ &+ k_2\left(u^{m2}_{x(n,h)-ul} + u^{m2}_{x(n-1,h)-ur} - 2u^M_{x1(n,h)}\right) \\ &+ k_2\left(u^{m2}_{x(n,h)-ll} + u^{m2}_{x(n-1,h)-lr} - 2u^M_{x1(n,h)}\right), \end{aligned} \tag{4.1}$$

$$\begin{aligned} 2M\frac{\partial^2 u^M_{y1(n,h)}}{\partial t^2} =& G_1\left(u^{m1}_{y(n,h)} + u^{m1}_{y(n-1,h)} - 2u^M_{y1(n,h)}\right) \\ &+ G_2\left(u^{m2}_{y(n,h)-ul} + u^{m2}_{y(n-1,h)-ur} - 2u^M_{y1(n,h)}\right) \\ &+ G_2\left(u^{m2}_{y(n,h)-ll} + u^{m2}_{y(n-1,h)-lr} - 2u^M_{y1(n,h)}\right). \end{aligned} \tag{4.2}$$

The displacements with superscripts 'm1' and 'm2' in equations (4.1) and (4.2) are associated with the internal resonators m_1 and m_2, respectively. The equations of motion of other boundary masses can be similarly determined. As shown in Appendix B, the displacements of the internal

resonators m_1 and m_2 can be expressed in terms of the displacements of the boundary masses by using the equations of motion of these internal resonators. Therefore, the equations of motion of the representative cell are in terms of the displacements of the boundary masses only.

Dispersion Relation

The dynamic behaviour of the two-dimensional elastic metamaterial in response to wave propagation can be described by the dispersion relation. For this metamaterial system, the dispersion relation is determined by evaluating the wave form of the propagating wave based on the equations of motion of the boundary masses.

Here, consider a plane harmonic wave propagating in the two-dimensional elastic metamaterial system, which can be generally expressed in the form of

$$\mathbf{u} = \mathbf{U}e^{i(K_1 x + K_2 y - \omega t)}, \tag{4.3}$$

where $\mathbf{u} = \left\{ u^M_{x1(n,h)},\ u^M_{y1(n,h)},\ u^M_{x2(n,h)},\ u^M_{y2(n,h)} \right\}^T$ is the displacement of the boundary masses and vector $\mathbf{U}$ contains the corresponding amplitudes of the displacements. In this two-dimensional system, the cell at the origin of (x,y) has the cell number $(0,0)$. The distance of the left end of the n^{th} cell to the origin in the horizontal direction is denoted as $x = nL$, and the distance of the lower end of the h^{th} cell to the origin in the vertical direction is $y = nL$. ω is the circular frequency of the wave. K_1 and K_2 are the wave numbers in x and y directions, respectively.

Substituting the wave form shown in equation (4.3) into equations of motion of all four boundary masses and making using of the periodic boundary conditions (Brillouin, 1953), the

following homogeneous equations of the boundary displacements for cell (n,h) are obtained,

$$p_{11}u^{M}_{x1(n,h)} + p_{13}u^{M}_{x2(n,h)} = 0, \tag{4.4}$$

$$p_{22}u^{M}_{y1(n,h)} + p_{24}u^{M}_{y2(n,h)} = 0, \tag{4.5}$$

$$p_{31}u^{M}_{x1(n,h)} + p_{33}u^{M}_{x2(n,h)} = 0, \tag{4.6}$$

$$p_{42}u^{M}_{y1(n,h)} + p_{44}u^{M}_{y2(n,h)} = 0, \tag{4.7}$$

where p_{ij} are the nonzero components of a 4×4 matrix $\mathbf{P}$, which contains the frequency ω, the wave numbers K_1 and K_2, and five independent material parameters, as given in Appendix C. The five material parameters are the stiffness ratios, η_1, η_2 and η_3, and the mass ratios, λ_1 and λ_2, defined by

$$\eta_1 = \frac{G_1}{k_1},\ \eta_2 = \frac{G_2}{k_2},\ \eta_3 = \frac{k_1}{k_2},\ \lambda_1 = \frac{m_1}{M},\ \lambda_2 = \frac{m_2}{M}. \tag{4.8}$$

Equations (4.4)-(4.7) can be reorganized in a matrix form,

$$[\mathbf{P}(K_1L, K_2L, \gamma)]\,\mathbf{U} = 0, \tag{4.9}$$

where $\gamma = \omega/\omega_1$ is a normalized frequency with $\omega_1 = \sqrt{2k_1/m_1}$. The dispersion relation, i.e. the relation between the frequency and the wave number, can then be determined by solving the eigenvalue problem given by equation (4.9). Due to the periodicity of the metamaterial formed by the square representative cell, the normalized wave numbers need to be determined only in the first Brillouin zone, which has a shape of square in (K_1L, K_2L) space with $-\pi \leq (K_1L, K_2L) \leq \pi$ (Brillouin, 1953). Two specific directions in the first Brillouin zone, ΓX and ΓM shown in figure 4.2, are particularly interesting because of their high symmetry. Along

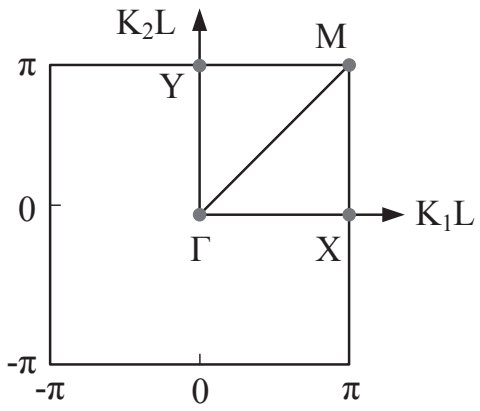

Figure 4.2: The sketch of the first Brillouin zone.

ΓX ($\Gamma \rightarrow$ X) direction, K_1L varies from 0 to π with $K_2L = 0$, while along ΓM ($\Gamma \rightarrow$ M) direction, K_1L and K_2L increase simultaneously from 0 to π.

To illustrate the single or double negative properties of the proposed metamaterial, the dispersion relation for specific material combinations and geometric configurations is evaluated. The dispersion relation along the ΓX and ΓM directions are shown in figures 4.3, 4.4 and 4.5 for $\eta_3 = k_1/k_2 = 2.0$, 4.0 and 8.0, respectively, for cases where $\eta_1 = G_1/k_1 = 0.5$, $\eta_2 = G_2/k_2 = 0.3$, $\lambda_1 = m_1/M = 1.4$, $\lambda_2 = m_2/M = 0.8$. For the case of $\eta_3 = 2.0$, figure 4.3, it is observed that along ΓX direction there are two frequency ranges with negative dispersion, from $\gamma = \omega/\omega_1 = 0.631$ to 0.754 (lower frequency range) and from 1.295 to 1.558 (upper frequency range), respectively. Among the four branches shown in the figure, three of them possess negative dispersion. Along ΓM direction, two similar frequency ranges with negative dispersion exist. When η_3 increases to 4.0, similar dispersion behaviour can be observed in figure 4.4. The branches with negative dispersion in the upper frequency range are almost unchanged. While, the width of the lower frequency range and the magnitude of the slopes of

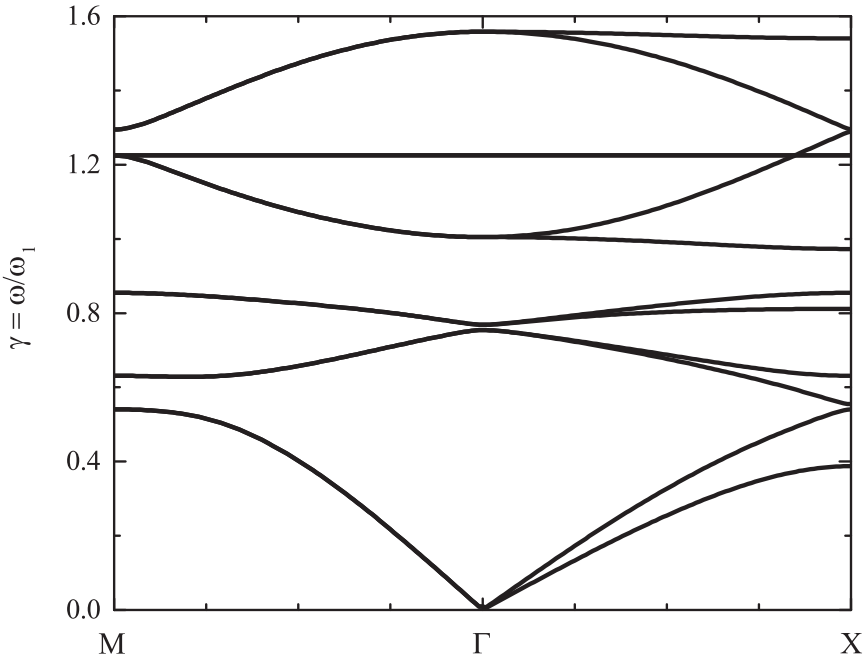

Figure 4.3: The dispersion relation of the simplified spring-mass model for case 1 (ΓX: wave number K_1L, ΓM: wave numbers $K_1L = K_2L$).

the curves (corresponding to group velocities) decrease substantially. As η_3 reaches 8.0, the slopes of the two branches in the lower frequency range are almost zero, as shown in figure 4.5, indicating no wave can propagate in the elastic metamaterial. The increase of η_3 has very limited influence on the two branches with negative dispersion in the upper frequency range.

4.3 Numerical analysis of the developed elastic metamaterial model

In this section, the original metamaterial system shown in figure 4.1(a) is analyzed using Finite Element Method (FEM) with the commercial software package COMSOL Multiphysics 5.2a to evaluate the dispersion relation and the property of wave propagation.

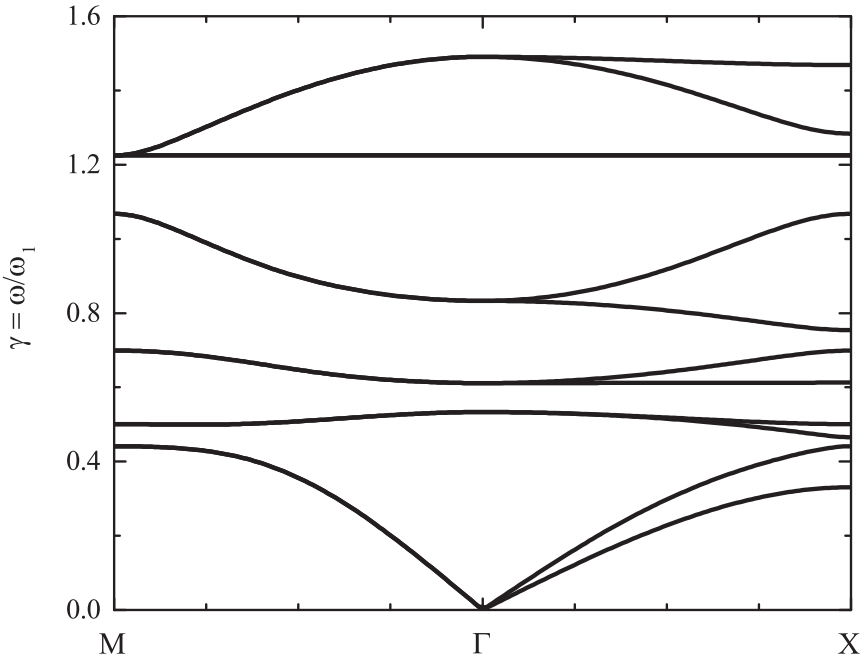

Figure 4.4: The dispersion relation of the simplified spring-mass model for case 2 (ΓX: wave number K_1L, ΓM: wave numbers $K_1L = K_2L$).

4.3.1 FEM model

The representative cell of the original elastic metamaterial is illustrated in figure 4.1(b). The geometrical parameters used are listed in table 4.1. Considering the requirements on the masses and stiffnesses of the components, tungsten, steel, Al-SiC foam and Polyethylene foam are chosen as material I, II, III and IV, respectively, as shown in table 4.2. In the FEM model, quad elements are utilized with element size being around $1.0 \times 10^{-2}L$, as illustrated in figure 4.6(a).

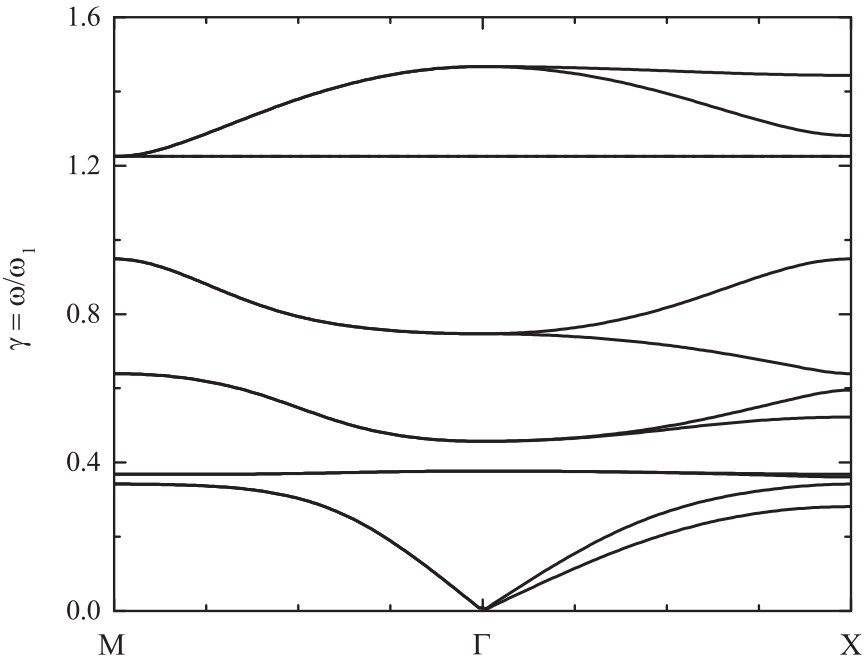

Figure 4.5: The dispersion relation of the simplified spring-mass model for case 3 (ΓX: wave number K_1L, ΓM: wave numbers $K_1L = K_2L$).

Table 4.1: Geometrical parameters

	L	L_1	H_1	LM_1	LM_2	LK_1	HK_1	LK_2	HK_2	R
Values (mm)	50.0	40.0	4.0	10.0	7.6	16.0	5.5	4.7	3.0	12.5

4.3.2 Equivalent stiffness of the spring model

In the simplified spring-mass model, the masses and stiffnesses need to be determined from the properties of the original representative cell. The values of the masses m_1, m_2 and M can be readily obtained. The stiffness constants of the springs, k_1, k_2, G_1 and G_2, can be determined

by evaluating the static deformation of the cell in response to properly applied tensile or shear loads, with the left boundary of the cell fixed in the FEM analysis, as shown in figures 4.6(b) and 4.6(c). For the current configuration, the determined masses are, $m_1 = 1.780$ Kg, $m_2 = 1.028$ Kg and $M = 0.432$ Kg, and the effective stiffnesses are, $k_1 = 2.666 \times 10^7$ N/m, $k_2 = 5.866 \times 10^6$ N/m, $G_1 = 7.190 \times 10^5$ N/m and $G_2 = 4.440 \times 10^5$ N/m. It should be noted that the materials used are assumed to be linear elastic and damping effect will be not considered. For all the local elements, unit thickness is assumed.

Table 4.2: Material parameters (Lai et al., 2011; Zhou et al., 2014)

	Material	Density $(\mathrm{Kg/m^3})$	Young's Modulus (Pa)	Poisson's ratio
Material I	Tungsten	17800	3.6E11	0.28
Material II	Aluminum	2700	7.0E10	0.33
Material III	Al-SiC foam	72	7.0E7	0.30
Material IV	Polyethylene foam	115	8.0e6	0.33

4.3.3 Dispersion relation

The dispersion relation of the elastic metamaterial model was determined by conducting modal analysis of the periodic metamaterial system using COMSOL. The dispersion relation for different wave numbers K_1L and K_2L are studied. The dispersion curves along the ΓX and ΓM directions, as shown in figure 4.2, are plotted in figure 4.7(a). The results are also compared with that from the simplified spring-mass model with the black dots representing the FEM results and the solid lines representing the analytical results from the simplified model. It can

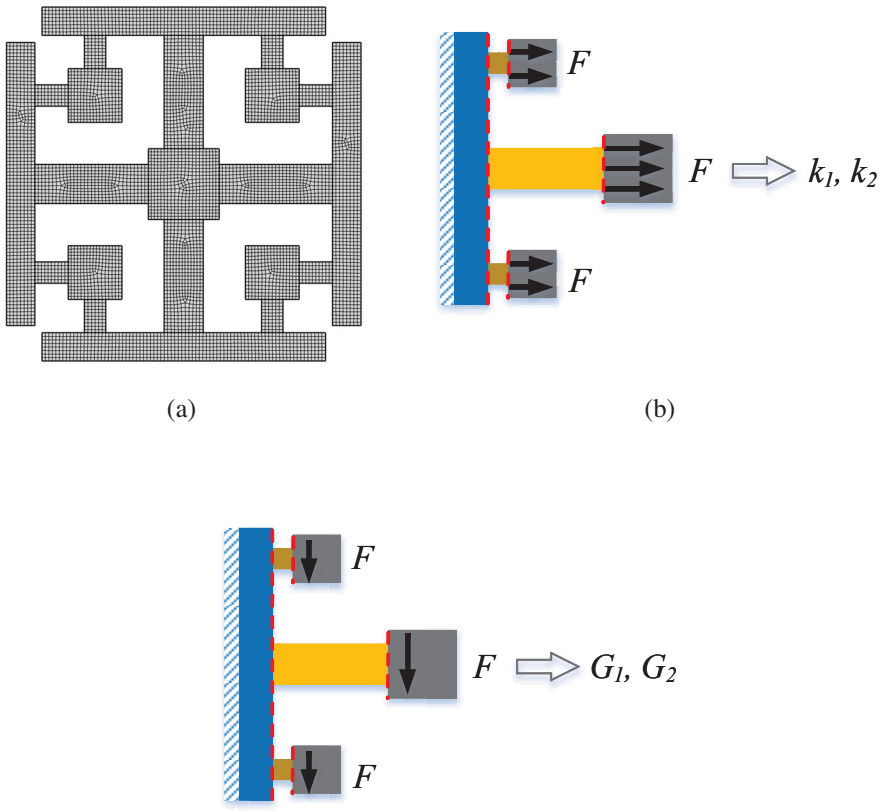

Figure 4.6: Numerical calculation, (a) FEM mesh, (b) calculating stiffness k_1 and k_2, (b) calculating stiffness G_1 and G_2.

be observed that the branches predicted by the spring-mass model agree well with the FEM results, especially in the frequency ranges with negative dispersion. FEM study reveals more branches of dispersion curves in other frequency ranges, as shown in 4.7(a). This might be related to the effect of the rotational motion of the masses in the representative cell, ignored in the spring-mass model. To evaluate in detail the dispersion relation of the current metamaterial, three branches with negative dispersion, predicted from the FEM, have been plotted in figure 4.7(b), with branch *A* in circle, branch *B* in triangle and branch *C* in star, respectively. Branch

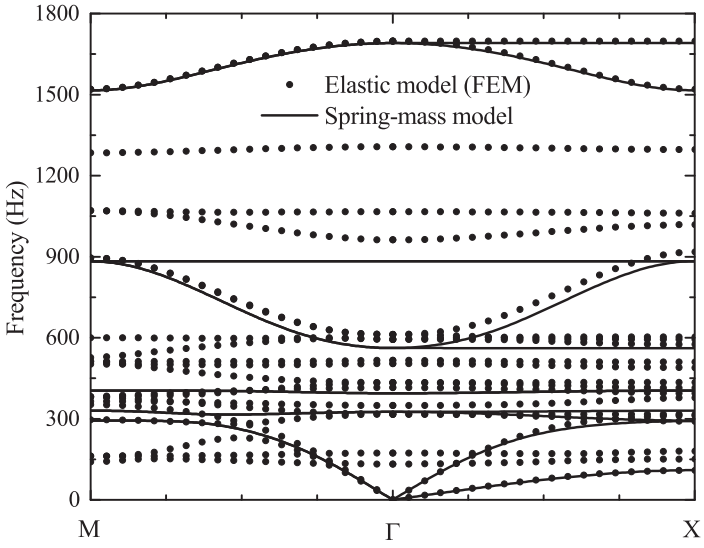

(a)

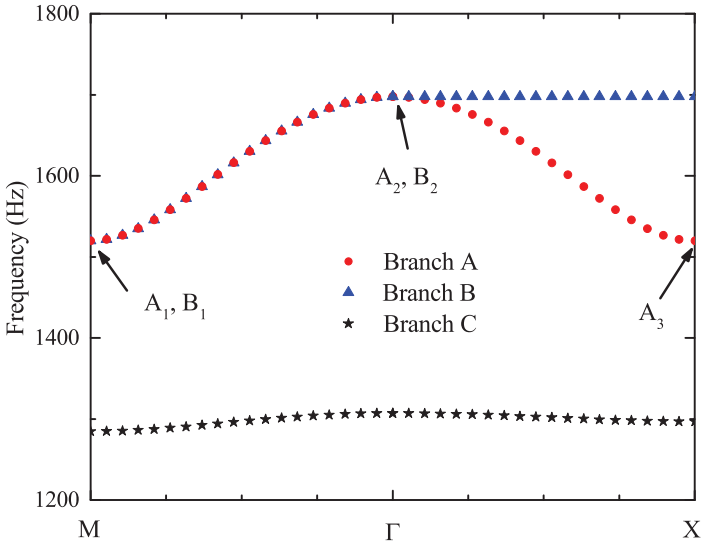

(b)

Figure 4.7: (a) The dispersion relation of the elastic metamaterial model along the ΓM and the ΓX directions, (b) the branches of the dispersion relation with negative dispersions (ΓX: wave number K_1L, ΓM: wave numbers $K_1L = K_2L$).

A and branch *B* almost overlap with a negligible difference along the ΓM direction. Along the ΓX direction, however, branches *A* and *B* differ significantly. For branch *A*, the frequency varies from 1519.8 Hz to 1697.7 Hz, while branch *B* exists under a almost constant frequency, as shown in figure 4.7(b), indicating that for branch B the energy transmission inside the metamaterial along the ΓX direction is very low. Branch C exhibits negative dispersion behaviour within a very narrow frequency range. Therefore, the negative dispersion of the current elastic metamaterial is mainly represented by branches *A* and *B*. It is interesting to mention that the spring-mass model, agrees well with the FEM results for branches *A* and *B*, suggesting that it can serve as an effective tool for predicting the desired negative dispersion behaviour of the two-dimensional elastic metamaterial.

Eigenstates of the representative cell

To illustrate the dynamic response of the metamaterial, during wave propagation, as given by the branches with negative dispersion, the eigenstates of the representative cell, i.e. the vibration modes, are investigated for specific frequency ranges. First, the displacement eigenstates of branches *A* and *B* at the boundary points along the ΓM direction (points M and Γ in figure 4.7(b)) are plotted in figure 4.8, where blue colour indicates low displacement amplitude and red colour represents high displacement amplitude with the arrow showing the direction of the displacement vector. At point M for branches *A* and *B*, although the frequencies are almost the same, the modes of motion (eigenstates) are very different. Figure 4.8(a) shows the displacement field for point A_1 (point M of branch *A*), where the four boundary masses moves in an inwards-outwards manner (quadrupolar). At point B_1 (point M of branch *B*), the eigenstate

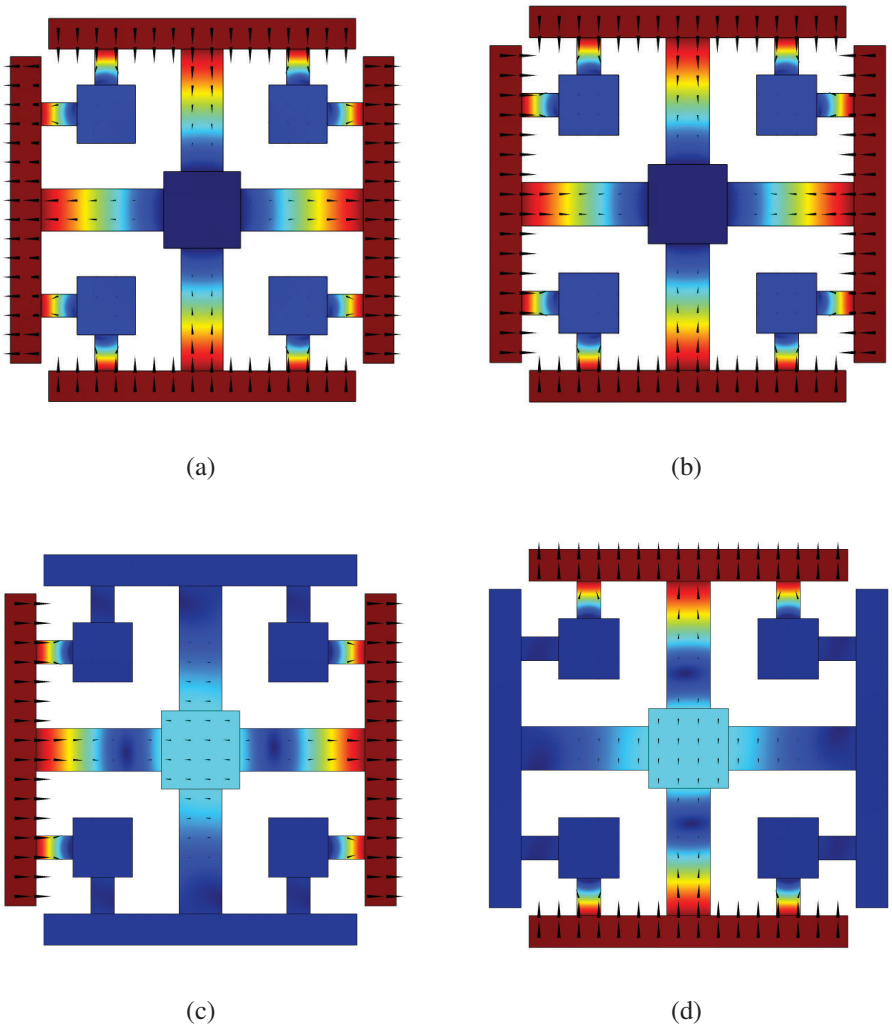

Figure 4.8: Displacement distribution of the eigenstates at, (a) point A_1 ($f = 1519.8$ Hz), (b) point B_1 ($f = 1519.8$ Hz), (c) point A_2 ($f = 1697.7$ Hz), (d) point B_2 ($f = 1697.7$ Hz).

shown in 4.8(b) clearly demonstrates an inwards-inwards motion (monopolar). For points A_2 and B_2 (point Γ of branches A and B), the frequencies are almost the same while the eigenstates are different, as shown in figures 4.8(c) and 4.8(d). For A_2, figure 4.8(c) shows that the boundary masses move mainly in the horizontal direction with the centre resonators moving in opposite direction (dipolar). For B_2, figure 4.8(d) shows, in contrast, mainly vertical motions in a similar manner. For other points along ΓM between the boundary points of branches A and

B, the hybridization of the monopolar, dipolar and quadrupolar resonances exists. For point A_3 of branch A in the ΓX direction, the displacement eigenstate shows an almost monopolar resonance without significant vertical motion, as illustrated in figure 4.9. Along the ΓX direction, the combined effect of monopolar and dipolar resonances is expected.

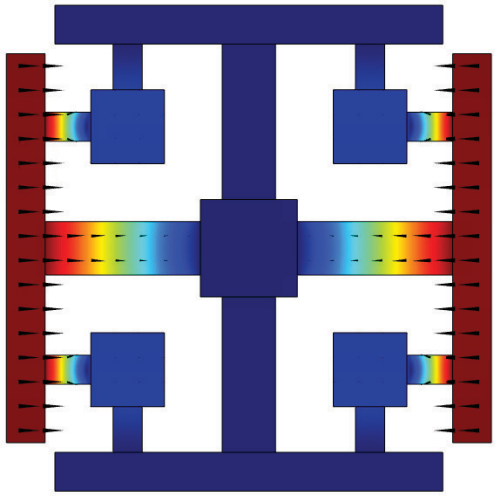

Figure 4.9: Displacement distribution of the eigenstate at point A_3 $(f = 1519.8Hz)$.

4.3.4 Effective mass and modulus of the metamaterial

Since the dynamic behaviour of the metamaterial can be represented by the response of the boundary masses of the representative cell (Lai et al., 2011; Li and Wang, 2016; Wang, 2014), the effective force, displacement and acceleration on the boundaries of the representative cell are evaluated carefully using FEM to determine the overall effective mass and moduli at specific frequencies. In the following discussion, only the magnitudes of these effective parameters are considered for the harmonic response of the metamaterial.

Effective mass density

The effective mass density can be defined from the relation between the net force applied to the representative cell and its average acceleration (Li and Wang, 2016; Wang, 2014). Considering the motion of the cell in x direction leads to the following effective mass density ρ^e,

$$\rho^e = \frac{F_x^e}{(a_x^e)^2 L^2}, \tag{4.10}$$

where F_x and a_x^e are the net force and the average acceleration calculated along the boundaries of the representative cell, given by

$$F_x^e = \int \sigma_{xx} dy|_{x=L} - \int \sigma_{xx} dy|_{x=0} + \int \sigma_{xy} dx|_{y=L} - \int \sigma_{xy} dx|_{y=0}, \tag{4.11}$$

$$a_x^e = \frac{1}{2}\left(\int \bar{a}_x|_{x=0} + \int \bar{a}_x|_{x=L} \right), \tag{4.12}$$

where σ and a represent stress and acceleration, respectively.

Effective moduli

The effective moduli are defined from the relation between the average force applied to the representative cell and the average deformation of it (Li and Wang, 2016; Wang, 2014). The effective stresses of the cell can be calculated as

$$\sigma_{xx}^e = \left(\int \sigma_{xx} dy|_{x=0} + \int \sigma_{xx} dy|_{x=L} \right) / (2L), \tag{4.13}$$

$$\sigma_{yy}^e = \left(\int \sigma_{yy} dx|_{y=0} + \int \sigma_{yy} dx|_{y=L} \right) / (2L), \tag{4.14}$$

$$\sigma_{xy}^e = \left(\int \sigma_{xy} dx|_{y=0} + \int \sigma_{xy} dx|_{y=L} + \int \sigma_{xy} dy|_{x=0} + \int \sigma_{xy} dy|_{x=L} \right) / (4L). \tag{4.15}$$

The effective strains of the cell can be expressed in the form of

$$\varepsilon_{xx}^{e} = \left(\int u_x dy|_{x=L} - \int u_x dy|_{x=0} \right) / \left(L^2 \right), \tag{4.16}$$

$$\varepsilon_{yy}^{e} = \left(\int u_y dx|_{y=L} - \int u_y dx|_{y=0} \right) / \left(L^2 \right), \tag{4.17}$$

$$\varepsilon_{xy}^{e} = \left(\int u_x dx|_{y=L} - \int u_x dx|_{y=0} + \int u_y dy|_{x=L} - \int u_y dy|_{x=0} \right) / \left(2L^2 \right), \tag{4.18}$$

where u is the displacement measured along the boundaries of the representative cell.

Due to the structural symmetry of the metamaterial system, the effective medium can be modelled as a two-dimensional cubic material (Lai et al., 2011; Ting, 1996). The constitutive relation with respect to the principle directions takes the following general form

$$\begin{Bmatrix} \sigma_{xx}^{e} \\ \sigma_{yy}^{e} \\ \sigma_{xy}^{e} \end{Bmatrix} = \begin{bmatrix} C_{11}^{e} & C_{12}^{e} & 0 \\ C_{12}^{e} & C_{11}^{e} & 0 \\ 0 & 0 & C_{44}^{e} \end{bmatrix} \begin{Bmatrix} \varepsilon_{xx}^{e} \\ \varepsilon_{yy}^{e} \\ 2\varepsilon_{xy}^{e} \end{Bmatrix}, \tag{4.19}$$

where three independent effective moduli, C_{11}^{e}, C_{12}^{e} and C_{44}^{e}, exist.

In x and y directions, for the two-dimensional elastic metamaterial, two effective moduli, C_{11}^{e} and C_{12}^{e}, describe the relation between the normal stresses and normal strains, and C_{44}^{e} describes the shear deformation. In the following, three effective parameters, the effective bulk modulus κ^{e}, the effective shear moduli μ^{e} and μ_{44}^{e} are used, which are defined by

$$\kappa^{e} = \frac{C_{11}^{e} + C_{12}^{e}}{2}, \quad \mu^{e} = \frac{C_{11}^{e} - C_{12}^{e}}{2}, \quad \mu_{44}^{e} = C_{44}^{e}. \tag{4.20}$$

The two effective moduli μ^{e} and μ_{44}^{e} play different roles in controlling wave propagation in the metamaterial system, when the direction of wave propagation changes.

Frequency dependency of the effective moduli and mass

By considering the case where $K_2L = 0$, i.e. along ΓX direction, as shown in figure 4.2, the eigenstates of branch A are used to calculate the effective mass and moduli of the metamaterial for different frequencies. It is observed that for branch A along ΓX, the motion of the representative cell is mainly in the horizontal direction $\left(\varepsilon^e_{yy} = 0\right)$ for all frequencies considered, as shown by the eigenstates at points A_2 and A_3 (points Γ and X in figure 4.7(b)), in figures 4.8(c) and 4.9. Accordingly, the effective mass ρ^e can be obtained by using equation (4.10) and C^e_{11} can be determined by using equation (4.19) based on the calculated σ^e_{xx} and ε^e_{xx}.

To determine C^e_{12}, consider the eigenstates corresponding to $K_1L = K_2L$, i.e. along ΓM direction (figure 4.2). For these eigenstates, the normal deformation are significant and the effective stress and strain components, σ^e_{xx}, σ^e_{yy}, ε^e_{xx} and ε^e_{yy}, are calculated using equations (4.13), (4.14), (4.16) and(4.17). Equation (4.19) is then used to determine the effective moduli C^e_{11} and C^e_{12}. It was found that the calculated C^e_{11} is almost the same as that from the previous calculation from ΓX direction.

Figure 4.10 shows the variation of the effective mass density with frequency within branches A and B. Negative effective mass density can be observed due to the dipolar resonance of the centre resonators. In figure 4.11, negative effective bulk modulus κ^e associated with monopolar resonance is observed. Negative effective shear modulus μ^e associated with quadrupolar resonance is also observed for branches A and B, which is illustrated in figure 4.12.

In the frequency ranges considered, higher order modes are involved for shear deformation associated with μ^e_{44}. For the current configuration of the metamaterial system, the shear stiffness of the spring components, G_1 and G_2, are small compared to the longitudinal stiffness,

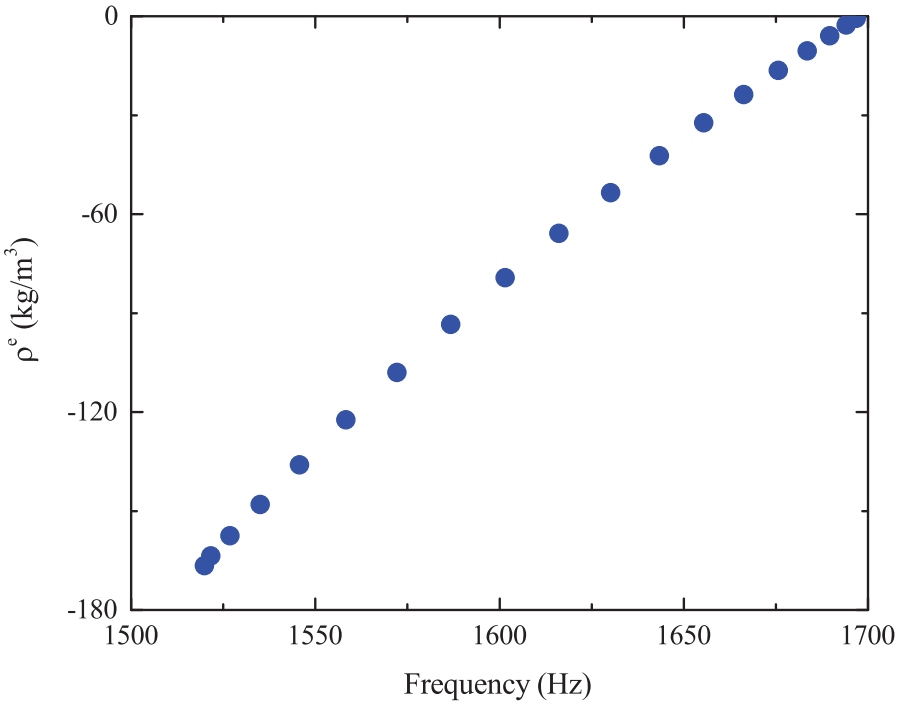

Figure 4.10: The effective mass density ρ^e of the representative cell.

k_1 and k_2, with $\eta_1 = G_1/K_1 = 0.027$ and $\eta_2 = G_2/K_2 = 0.076$, as given in section 3.2. This is consistent with the FEM result that transverse wave can hardly propagate in the metamaterial along ΓX direction. For the current metamaterial, among the three effective moduli, the effective bulk modulus κ^e and the effective shear modulus μ^e play dominating roles in controlling the dynamic behaviour of the metamaterial system in the frequency ranges with negative dispersion.

4.3.5 Wave propagation in the metamaterial

Numerical simulations are conducted to study the detailed process of wave propagation in the current metamaterial system. The two models are considered in FEM simulations, which are

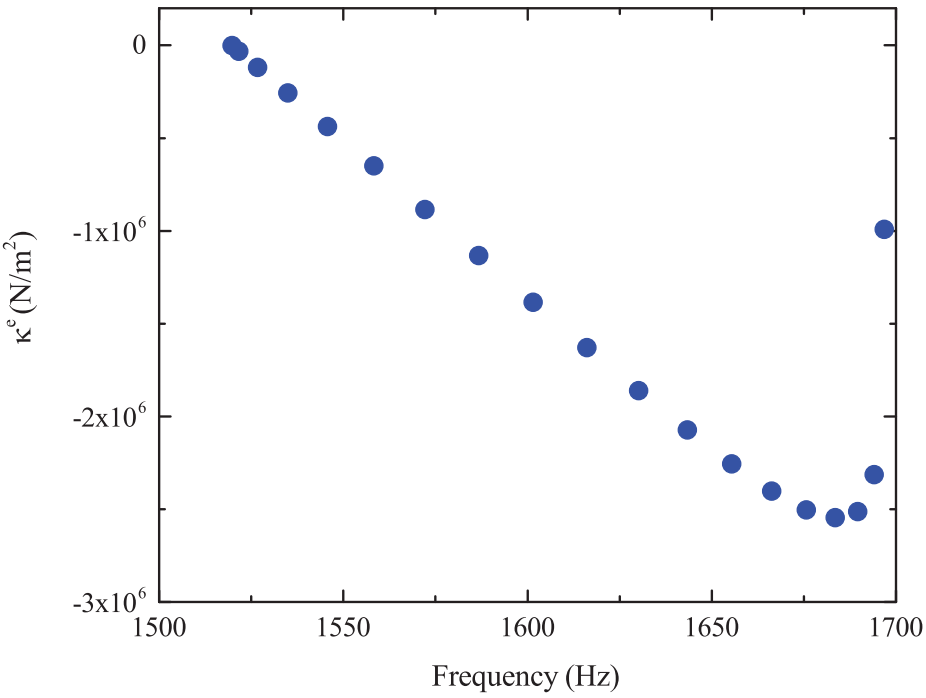

Figure 4.11: The effective bulk modulus κ^e of the representative cell.

illustrated in figure 4.13, corresponding to wave propagation in ΓX and ΓM directions, respectively. For both cases, the models consist of 100 representative cells in the horizontal direction. The selection of 100 representative cells has been shown sufficient to model infinitely long metamaterials with periodical structures. For case (a) shown in figure 4.13(a), the representative cells are oriented in the horizontal direction while for case (b) shown in figure 4.13(b), the representative cells are oriented 45^o from the horizontal direction. The periodic boundary conditions are placed on the upper and lower boundaries of the metamaterial system. Normal/tangent harmonic displacements are applied at the left boundary to generate wave propagation in the system, as shown in figure 4.13.

Transmission analysis

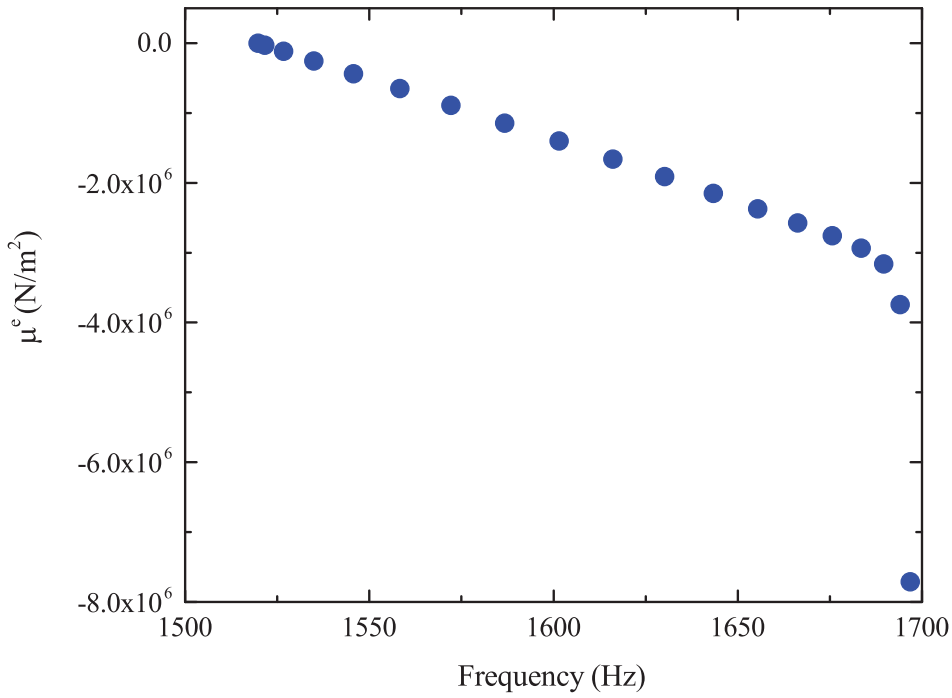

Figure 4.12: The effective shear modulus μ^e of the representative cell.

The output displacements of the metamaterial at the right end are used to evaluate the transmission ratio of the waves, which is defined as the ratio between the output displacements to the applied displacement at the left end.

Figure 4.14 illustrates the transmission ratio when only horizontal displacement is applied to the left boundary of the metamaterial system, shown in figure 4.13(a). The results show that longitudinal wave (denoted as *P* wave) can propagate in the metamaterial system along the ΓX direction, when the frequency is in the frequency range of branch *A* (ΓX) between the two vertical dashed lines. When a vertical displacement is applied at the left end, which corresponds to a shear wave, the respond at the right end is very weak, indicating low transmission ratio for a transverse wave (denoted as *S* wave).

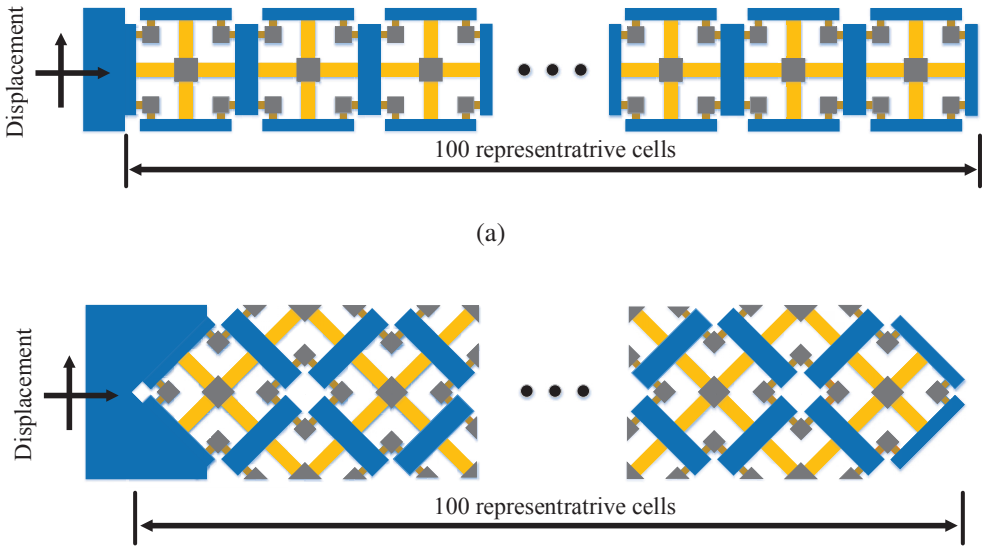

Figure 4.13: The numerical set-up for transmission, (a) along the ΓX direction, (b) along the ΓM direction.

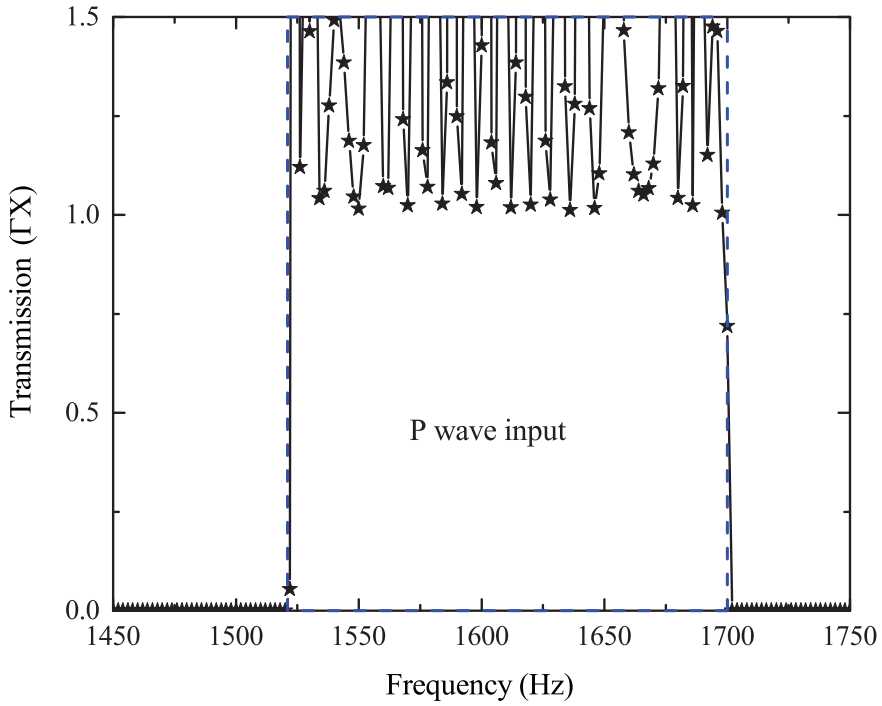

Figure 4.14: Transmission along the ΓX direction for P wave input.

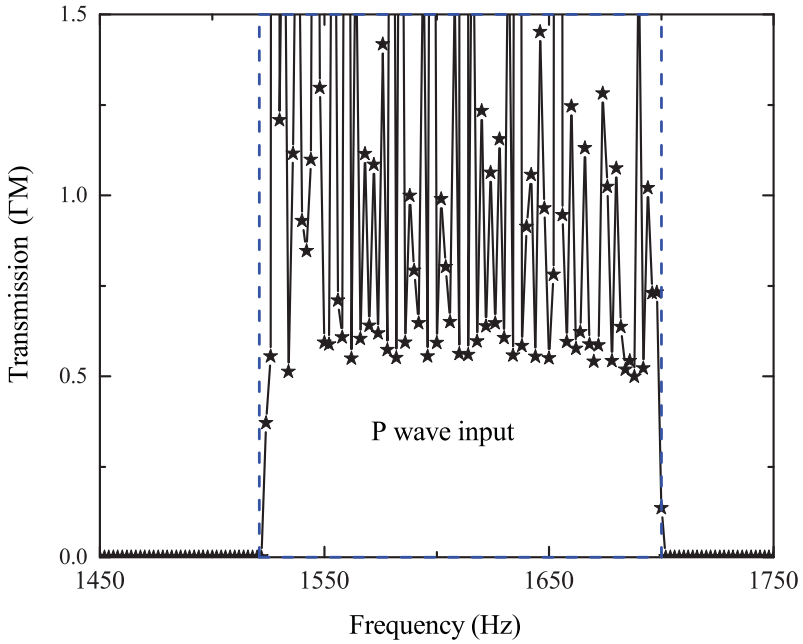

(a)

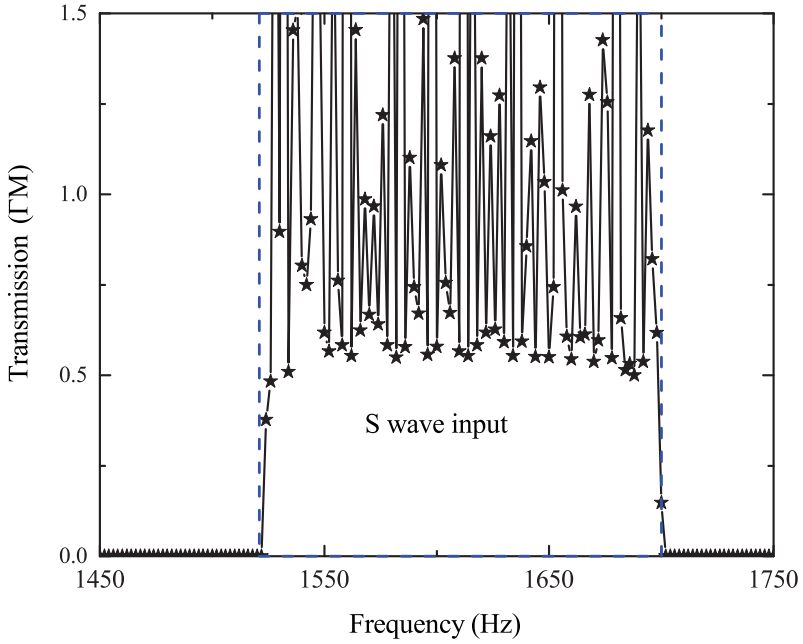

(b)

Figure 4.15: Transmission along the ΓM direction for, (a) P wave input, (b) S wave input.

For the case shown in figure 4.13(b), when only a horizontal (vertical) displacement is applied at the left boundary, only the horizontal (vertical) displacement output can be observed, as shown in figure 4.15. In this case, both longitudinal and transverse waves can propagate in the metamaterial system, which is controlled by the effective mass density ρ^e, the effective bulk modulus κ^e and the effective shear modulus μ^e.

Negative phase velocity

In the proposed elastic metamaterial, the simultaneous occurrence of negative effective mass density ρ^e and negative effective moduli, indicates negative phase velocities. To show the phenomena of negative phase velocity, transient wave propagation in the current elastic metamaterial is studied using FEM simulation. Normal/tangent displacements are applied to the left boundaries of the metamaterial systems shown in figure 4.13. The excitation frequency applied is equal to 1690 Hz, which is within branches *A* and *B*. The normalized displacements of the propagating waves are used to illustrate the wave propagation with properly selected time increments to identify the propagating direction of the wave. Figure 4.16 shows the longitudinal wave propagation in the metamaterial shown in figure 4.13(a) in response to the normal input displacement. At the initial stage of the excitation, the wavefront moves forward, indicating positive energy flow, but the peaks of the normalized displacement move to the left showing negative phase velocity. When the wave propagation is stabilized, as illustrated in figure 4.16(b), backward wave can be clearly observed. Figures 4.17 and 4.18 show the wave propagation of longitudinal and transverse waves in the metamaterial shown in figure 4.13(b). These results are in agreement with the prediction by the effective parameters analysis and the transmission ratio analysis.

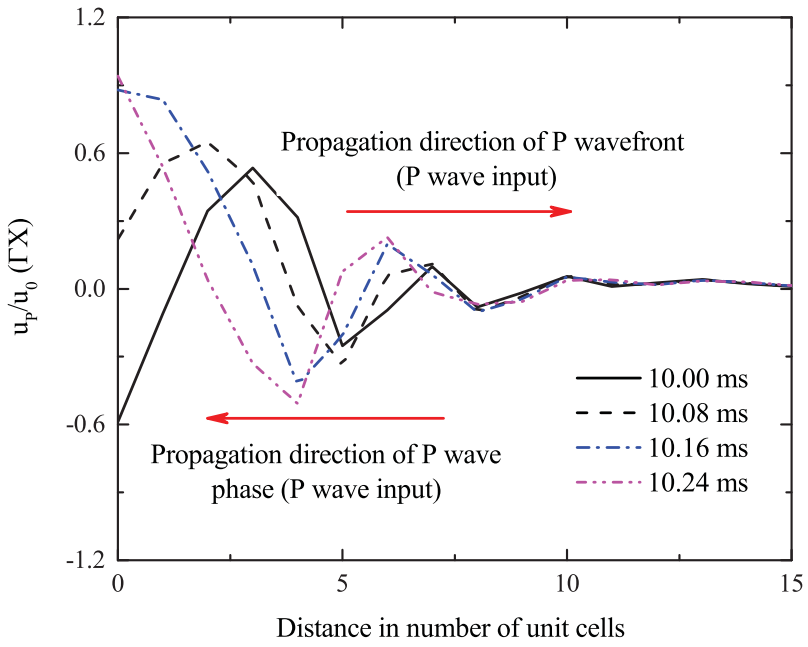

(a)

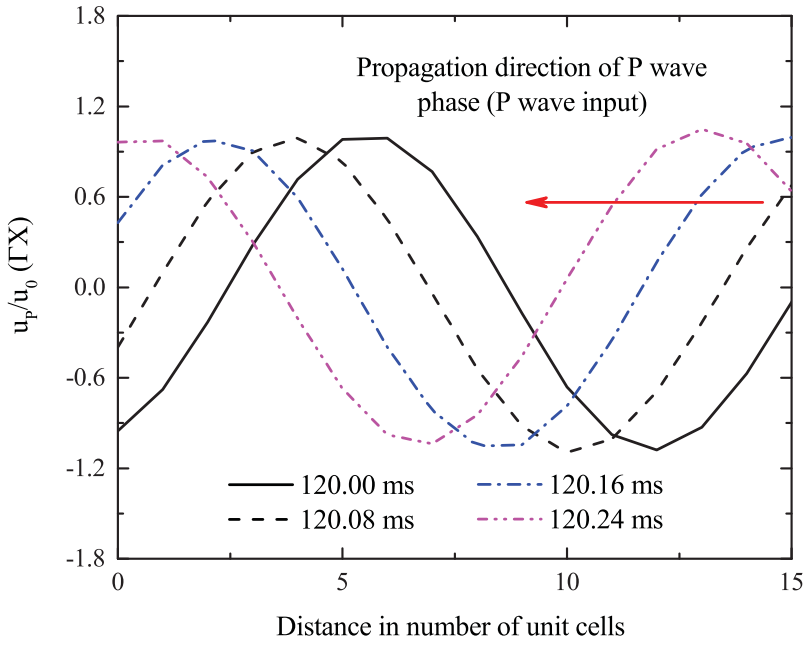

(b)

Figure 4.16: Snapshots of the P wave propagating along the ΓX direction with P wave input, (a) around 10 ms, (b) around 120 ms.

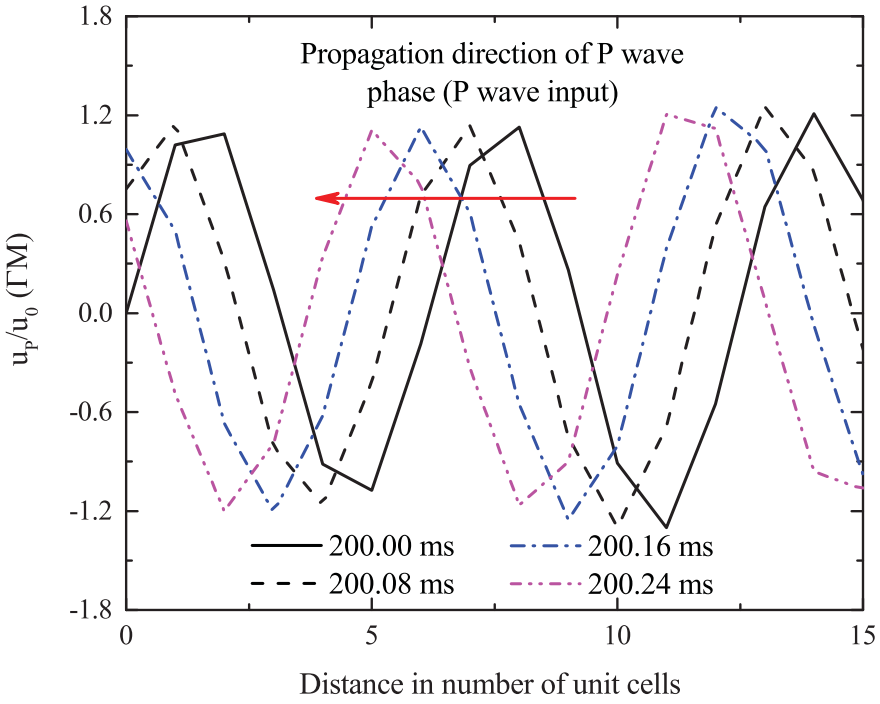

Figure 4.17: Snapshots of the P wave propagating along the ΓM direction with P wave input around 200 ms.

4.4 Conclusion

A new two-dimensional elastic metamaterial system has been developed showing the desired negative properties, which can be well described by a simplified spring-mass model. In specific frequency ranges, the elastic metamaterial possesses simultaneous negative effective mass, bulk modulus and shear modulus. The relations between the effective material parameters and the different types of local resonances have also been investigated. The current metamaterial can induce dipolar resonances, monopolar resonances and quadrupolar resonances, corresponding to negative effective mass density, negative effective bulk modulus and negative

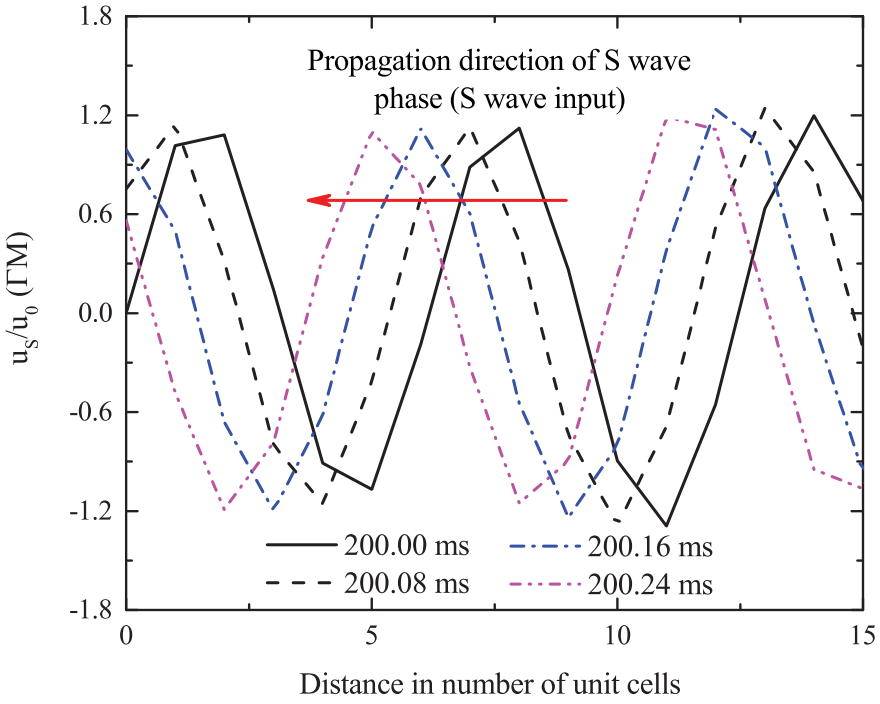

Figure 4.18: Snapshots of the S wave propagating along the ΓM direction with S wave input around 200 ms.

effective shear modulus, respectively. These three negative effective parameters are realized through only the translational motion of the resonators in the proposed representative cell, which makes the current metamaterial system easier to fabricate and provides more flexibility in design.

The metamaterial is anisotropic. Along the ΓX direction, the absence of the dispersion branch supporting transverse waves endows the elastic model with fluid-like material property and makes it a good candidate for a wave polarization filter. Along ΓM direction, both longitudinal and transverse waves can propagate in the metamaterial system with negative phase velocities. The current elastic metamaterial system can be used in the design of new elastic

metamaterials featuring negative refractions. Compared with the one-dimensional elastic metamaterial model developed in Chapter 3, this two-dimensional elastic metamaterial model can support elastic wave propagation in multiple directions and show richer dynamic behaviour. For example, negative refraction caused by negative velocities of the longitudinal and transverse waves can be observed, which does not exist in the one-dimensional model.

Appendix B

By considering the kinetic relation of the representative cell in figure 4.1(b), the equations of motion of the centre resonator, m_1, can be expressed as

$$\begin{aligned} m_1 \frac{\partial^2 u^{m1}_{x(n,h)}}{\partial t^2} =& k_1 \left(u^{M}_{x1(n,h)} + u^{M}_{x1(n+1,h)} - 2u^{m1}_{x(n,h)} \right) \\ &+ G_1 \left(u^{M}_{x2(n,h)} + u^{M}_{x2(n,h+1)} - 2u^{m1}_{x(n,h)} \right), \end{aligned} \tag{B1}$$

$$\begin{aligned} m_1 \frac{\partial^2 u^{m1}_{y(n,h)}}{\partial t^2} =& k_1 \left(u^{M}_{y2(n,h)} + u^{M}_{y2(n,h+1)} - 2u^{m1}_{y(n,h)} \right) \\ &+ G_1 \left(u^{M}_{y1(n,h)} + u^{M}_{y1(n+1,h)} - 2u^{m1}_{y(n,h)} \right), \end{aligned} \tag{B2}$$

where $u^{m1}_{x(n,h)}$ and $u^{m1}_{y(n,h)}$ represent the displacements of m_1 in x and y directions, respectively.

Similarly, the following relations of the four identical resonators, m_2, can be obtained as

$$\begin{aligned} m_2 \frac{\partial^2 u^{m2}_{x(n,h)-ul}}{\partial t^2} =& k_2 \left(u^{M}_{x1(n,h)} + R\theta^{M}_{1(n,h)} - u^{m2}_{x(n,h)-ul} \right) \\ &+ G_2 \left(u^{M}_{x2(n,h+1)} - u^{m2}_{x(n,h)-ul} \right), \end{aligned} \tag{B3}$$

$$\begin{aligned} m_2 \frac{\partial^2 u^{m2}_{y(n,h)-ul}}{\partial t^2} =& k_2 \left(u^{M}_{y2(n,h+1)} + R\theta^{M}_{2(n,h+1)} - u^{m2}_{y(n,h)-ul} \right) \\ &+ G_2 \left(u^{M}_{y1(n,h)} - u^{m2}_{y(n,h)-ul} \right), \end{aligned} \tag{B4}$$

$$m_2\frac{\partial^2 u^{m2}_{x(n,h)-ur}}{\partial t^2} = k_2\left(u^M_{x1(n+1,h)} + R\theta^M_{1(n+1,h)} - u^{m2}_{x(n,h)-ur}\right) + G_2\left(u^M_{x2(n,h+1)} - u^{m2}_{x(n,h)-ur}\right), \tag{B5}$$

$$m_2\frac{\partial^2 u^{m2}_{y(n,h)-ur}}{\partial t^2} = k_2\left(u^M_{y2(n,h+1)} - R\theta^M_{2(n,h+1)} - u^{m2}_{y(n,h)-ur}\right) + G_2\left(u^M_{y1(n+1,h)} - u^{m2}_{y(n,h)-ur}\right), \tag{B6}$$

$$m_2\frac{\partial^2 u^{m2}_{x(n,h)-ll}}{\partial t^2} = k_2\left(u^M_{x1(n,h)} - R\theta^M_{1(n,h)} - u^{m2}_{x(n,h)-ll}\right) + G_2\left(u^M_{x2(n,h)} - u^{m2}_{x(n,h)-ll}\right), \tag{B7}$$

$$m_2\frac{\partial^2 u^{m2}_{y(n,h)-ll}}{\partial t^2} = k_2\left(u^M_{y2(n,h)} + R\theta^M_{2(n,h)} - u^{m2}_{y(n,h)-ll}\right) + G_2\left(u^M_{y1(n,h)} - u^{m2}_{y(n,h)-ll}\right), \tag{B8}$$

$$m_2\frac{\partial^2 u^{m2}_{x(n,h)-lr}}{\partial t^2} = k_2\left(u^M_{x1(n+1,h)} - R\theta^M_{1(n+1,h)} - u^{m2}_{x(n,h)-lr}\right) + G_2\left(u^M_{x2(n,h)} - u^{m2}_{x(n,h)-lr}\right), \tag{B9}$$

$$m_2\frac{\partial^2 u^{m2}_{y(n,h)-lr}}{\partial t^2} = k_2\left(u^M_{y2(n,h)} - R\theta^M_{2(n,h)} - u^{m2}_{y(n,h)-lr}\right) + G_2\left(u^M_{y1(n+1,h)} - u^{m2}_{y(n,h)-lr}\right), \tag{B10}$$

where the displacements with subscripts 'ul', 'ur', 'll' and 'lr' are associated with distributed resonators m_2 in upper left, upper right, lower left and lower right sides of the representative cell, respectively. It should be mentioned that the possible rotational motions of the resonators, m_1 and m_2, are not considered in this study.

Appendix C

The nonzero components of the 4×4 matrix $\mathbf{P}$ can be expressed as

$$p_{11} = -2\left(\eta_3 + 2 - \frac{2\eta_3\gamma^2}{\lambda_1}\right) + \frac{\eta_3\left(1+\cos K_1 L\right)}{(1+\eta_1)-\gamma^2} + \frac{4}{(1+\eta_2)-\theta^2\gamma^2}, \tag{C1}$$

$$p_{13} = -p_{24} = \frac{\left(1+e^{-iK_1L}\right)\left(1+e^{iK_2L}\right)}{2}\left\{\frac{\eta_1\eta_3}{(1+\eta_1)-\gamma^2} + \frac{2\eta_2}{(1+\eta_2)-\theta^2\gamma^2}\right\}, \tag{C2}$$

$$p_{22} = 2\left(\eta_1\eta_3 + 2\eta_2 - \frac{2\eta_3\gamma^2}{\lambda_1}\right) - \frac{\eta_1^2\eta_3\left(1+\cos K_1 L\right)}{(1+\eta_1)-\gamma^2} - \frac{4\eta_2^2}{(1+\eta_2)-\theta^2\gamma^2}, \tag{C3}$$

$$p_{31} = p_{42} = \frac{\left(1+e^{iK_1L}\right)\left(1+e^{-iK_2L}\right)}{2}\left\{\frac{\eta_1\eta_3}{(1+\eta_1)-\gamma^2} + \frac{2\eta_2}{(1+\eta_2)-\theta^2\gamma^2}\right\}, \tag{C4}$$

$$p_{33} = -2\left(\eta_1\eta_3 + 2\eta_2 - \frac{2\eta_3\gamma^2}{\lambda_1}\right) + \frac{\eta_1^2\eta_3\left(1+\cos K_2 L\right)}{(1+\eta_1)-\gamma^2} + \frac{4\eta_2^2}{(1+\eta_2)-\theta^2\gamma^2}, \tag{C5}$$

$$p_{44} = -2\left(\eta_3 + 2 - \frac{2\eta_3\gamma^2}{\lambda_1}\right) + \frac{\eta_3\left(1+\cos K_2 L\right)}{(1+\eta_1)-\gamma^2} + \frac{4}{(1+\eta_2)-\theta^2\gamma^2}, \tag{C6}$$

where θ is given by

$$\theta = \sqrt{\frac{2\lambda_2\eta_3}{\lambda_1}}. \tag{C7}$$

Chapter 5: Wave propagation in the two-dimensional elastic metamaterial

A two-dimensional elastic metamaterial model with triple negative effective material parameters is previously designed in Chapter 4. In this chapter, numerical analysis of such elastic metamaterials is performed to further study the wave propagation in the metamaterial systems with large number of representative cells. The unusual dynamic property of the elastic metamaterial at frequency with negative dispersion is investigated and the wave attenuation ability of an anisotropic case of the metamaterial model is studied in detail.

5.1 Introduction

One of the main features of elastic metamaterials is that they can be used to manipulate waves. Different from acoustic metamaterials which can only support longitudinal waves, elastic metamaterials with the coupling between the longitudinal and transvserse waves can show richer dynamic behaviour and provide more advanced applications, such as elastic wave filter, vibration isolators, sub-wavelength imaging and cloaking (Mitchell et al., 2014; Zhang and Parnell, 2018; Zhu et al., 2014a). The origin of the unusual elastic metamaterials' functionalities mostly lies in the delicately engineered structures of their representative cells (Lee and Wright, 2016; Li and Wang, 2016). Through the interacting between the elastic waves and the designed structures, elastic metamaterials can possibly exhibit three effective material parameters, i.e. effective mass density, effective bulk modulus and effective shear modulus, which can vary with excitation frequency and even turn negative in certain frequency ranges. To realize the

desired functionalities, various elastic metamaterial structures have been developed with negative effective parameters by introducing a large enough collection of identical resonators to control wave propagation (Cummer et al., 2016; Ge et al., 2018; Zhou et al., 2012). From the perspective of effective material parameters, elastic metamaterials will usually possess single negative, or double negative, or triple negative effective parameters.

The extraodinary wave filtering phenonmenon of elastic metamaterial is firstly demonstrated in a composite with rubber-coated lead spheres embedded in an expoxy matrix and its nagative mass density can explain the band gaps resulting from the local resonance (Liu et al., 2000). Various elastic metamaterial models have been developed to realize negative mass density or negative modulus (Tan et al., 2014; Wu et al., 2007; Zhou et al., 2012). Among these efforts, anisotropic elasic metamaterial can show unusual wave attenuation ability due to their varying effective material property along different principle directions. The possibility of anisotropic mass density is initially investigated with simplified spring-mass model (Milton and Willis, 2007). In what follows, elliptic cylinders with circular silicone rubber coating in a rigid matrix is shown to exhibit anisotropic mass density (Gu et al., 2009), and then similar results have been obtained in an elastic metamaterial made of lead cylinders coated with elliptical rubbers in an expoxy matrix (Liu et al., 2012). Recently, a single-phase elastic metamaterial is developed to show anisotropic mass density (Zhu et al., 2016b), and eccentric resonators have been introduced into a composite to generate band gaps in the low frequency range (Li et al., 2017). Basically, the anisotropicity of elastic metamaterials can be introduced by generating different resonant frequencies along various directions of their representative cells (Huang and Sun, 2011b; Liu et al., 2015).

From the mechanisms of generating negative effective mass density or effective modulus, various metamaterials with double negative effective parameters have been designed. These metamaterials can show negative phase velocities in certain frequency ranges, resulting negative refraction, and this unique property can be utilized to design superlens with high spatial resolution (Ma and Sheng, 2016). An elastic metamaterial with chiral resonators is developed to possess simultaneously negative effective mass density and bulk modulus through the translational and rotational resonances of the resoators, and the phenomenon of negative refraction of longitudinal waves is numerically observed due to the resulting double negative property (Liu et al., 2011a). This unusual phenomenon is further experimentally demonstrated in a single-phase elastic metamaterial with chiral microstructures (Zhu et al., 2014b). Water cylinders with silicone rubber coating have been embedded in foam matrix to induce simultaneously negative effective mass density and shear modulus, and negative refraction of transverse waves is numerically realized (Wu et al., 2011). Plane elastic wave propagation along the interface between the semi-infinite conventional material and semi-infinite elastic metamaterials with double or triple negative material properties assigned is analytially and numerically studied to show the general dynamic properties of these elastic metamaterials (Zhu et al., 2015). However, similar numerical analysis of elastic metamaterial with triple negative effective material parameters is still lacking.

In the previous work, a two-dimensional elastic metamaterials is proposed to possess simultaneously negative effective mass density, bulk modulus and shear modulus. It can behave like solid by supporting longitudinal and transverse waves with negative phase velocities along ΓM direction (K_1L and K_2L increase simultaneously from 0 to π), whereas it also can behave like

fluid by only supporting longitudinal waves with negative phase velocities along ΓX direction (K_1L varies from 0 to π with $K_2L = 0$). In this study, the main focus is placed on the wave propagation in the elastic metamaterial developed, especially the negative refraction phenonmenon due to the negative phase velocities. Also, the elastic metamaterial model can show anisotropic effective material property by changing the material assignment in some components of the representative cell, resulting in unique wave filtering ability.

5.2 Negative wave refraction

A two-dimensional elastic metamaterial is previously developed with its representative cell schematically shown in figure 5.1. The geometrical parameters of the representative cell are provided in table 4.1. As illustrated in figure 5.1, four different materials have been assigned to the components and the related material parameters are given in table 4.2. Under this specific configuration, the elastic metamaterial can show negative dispersion relation in the frequency range, $(1519.8\text{ Hz}, 1697.7\text{ Hz})$, along ΓX and ΓM directions. At these frequencies, this metamaterial possesses simultaneously negative effective mass density, bulk modulus and shear modulus, which are induced by the bipolar, monopolar and quadrupolar resonances in the representative cell, respectively. The resulting triple negative effective material property can generate backward propagating waves, i.e. propagating waves with negative phase velocities, which can enable negative wave refraction under harmonic wave excitations. In this section, the attention will be focused on the unusual dynamic behavior of the metamaterial model in the frequency range with negative dispersion.

To numerically simulate the phenomonenon of negative refraction in COMSOL, a 45^o

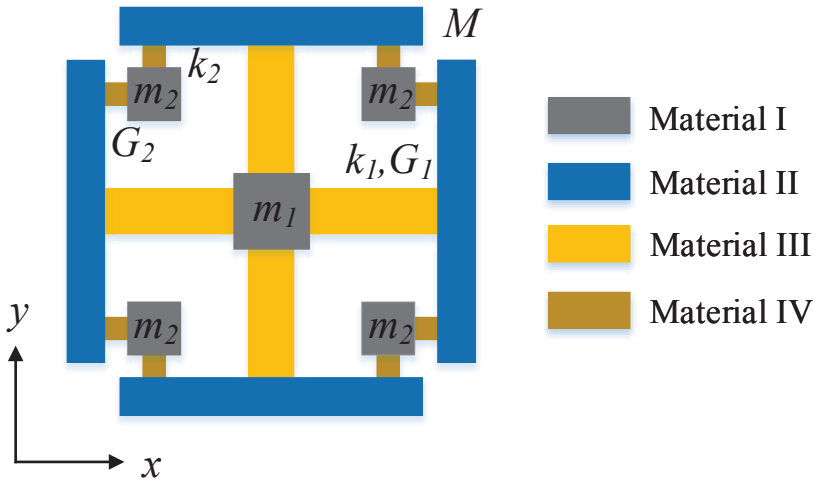

Figure 5.1: The representative cell of the two-dimensional elastic metamaterial.

prism-shaped elastic metamaterial sample with 200 unit cells embedded in a matrix is designed, as illustrated in figure 5.2, and the simulations are conducted through the commercial software package COMSOL Multiphysica 5.2a. The material of the matrix possesses the same phase velocity with the metamaterial model for longitudinal waves at frequency 1680 Hz. Perfect matched layers (PML) are artificial absorbing layers, which can strongly absorb outgoing waves from the interior region without reflecting waves back. To simulate a system with open boundaries, they have been added in the outside boundaries of the matrix. Displacement excitations are applied to the central part of the left side of the prism to simulate incident plane waves along ΓX direction, whereas displacement excitations are applied to the central part of the upper right side of the prism to simulate incident plane waves along ΓM direction. The displacement excitations have width of $9L$ and they are applied with a distance of $2L$ from the incident interface, where L is the length of the representative cell of the elastic metamaterial systems.

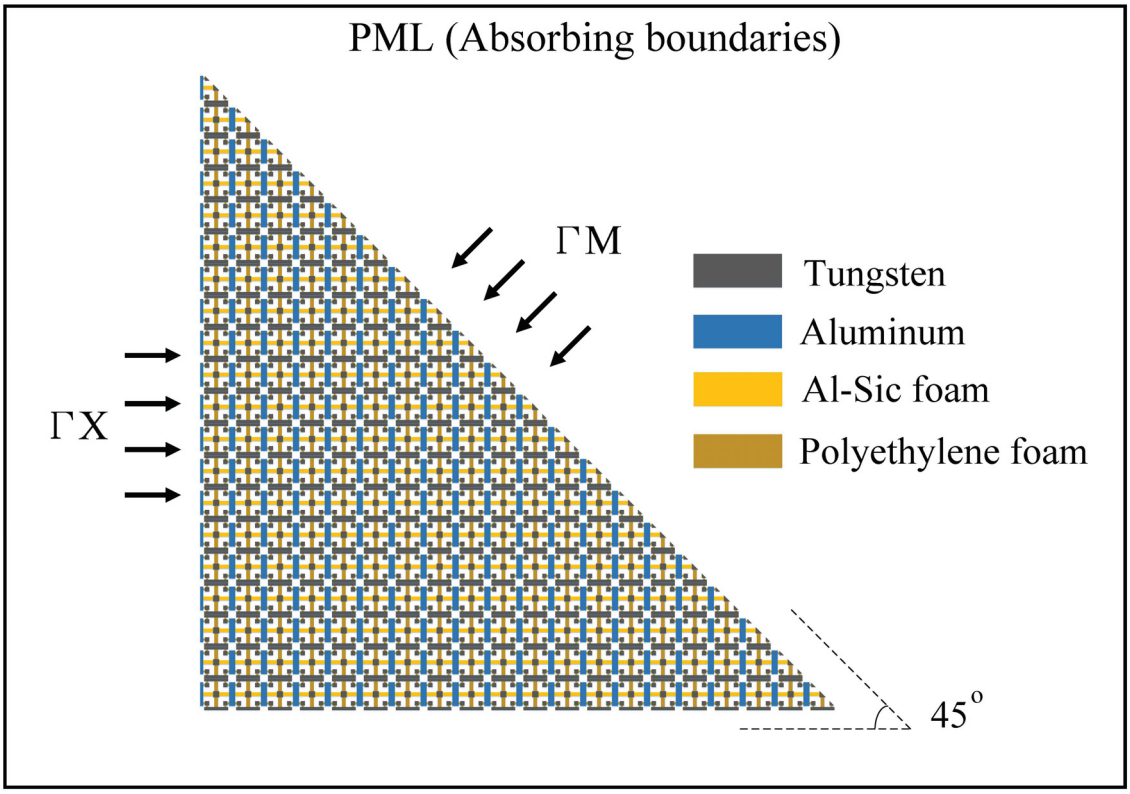

Figure 5.2: The numerical set-up of a system for negative refraction.

Figure 5.3 shows the wave field of the elastic metamaterial sample for incident longitudinal wave along ΓX direction at frequency 1680 Hz. In the wave field, red color indicates high displacement amplitude and blue color represents very low displacement amplitude. The black dashed line shows the direction vertical to the interface and the black arrow indicates the wave propagating direction of the refracted waves. In figure 5.3, it can be clearly observed that the incident wave passes through the wedge and generate negatively refracted longitudinal and transverse waves. Along ΓX direction, the elastic metamaterial will behave like fluid and the incident plane transverse wave cannot propagate through the elastic metamaterial sample. In what follows, the displacement distribution of this case is not presented for brevity.

Figure 5.4 shows the wave field of the elastic metamaterial sample for incident longitudinal

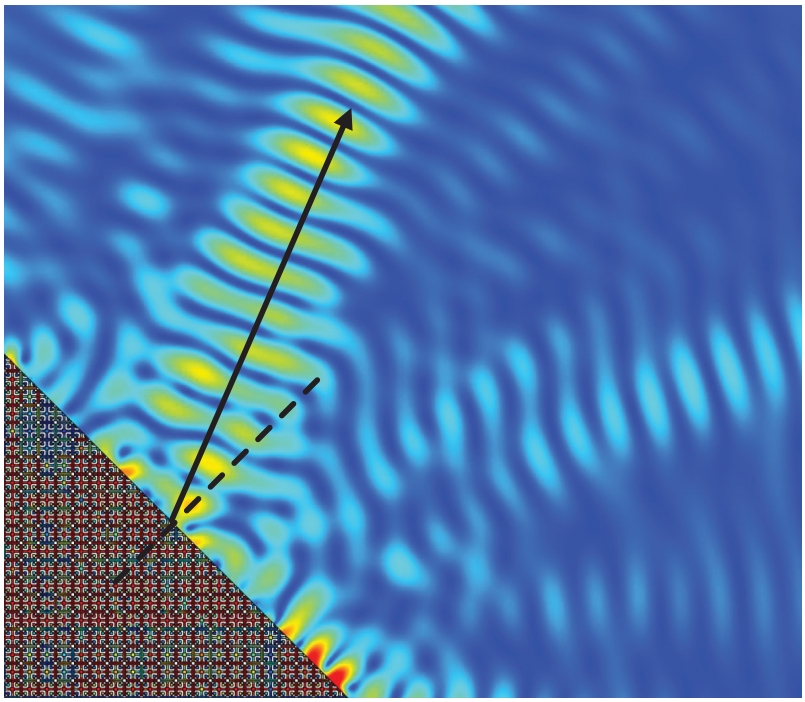

Figure 5.3: The displacement distribution of the elastic metamaterial sample for longitudinal wave incidence at frequency 1680 Hz along ΓX direction.

wave along ΓM direction at frequency 1680 Hz. The corresponding wave field for the case of incident transvese wave is illustrated in figure 5.5. Similar phenomena can be clearly observed and elastic waves are negatively refracted.

As discussed in this section, negative refraction of elastic waves can be induced in the developed elastic metamaterial system at frequency located in the negative dispersion range.

5.3 Wave filtering

Due to the unique structural feature of the two-dimensional elastic metamaterial system developed, it can be easily revised to describe the case of anisotropic material properties by adjusting the masses and stiffnesses of the components in the two main directions, exhibiting

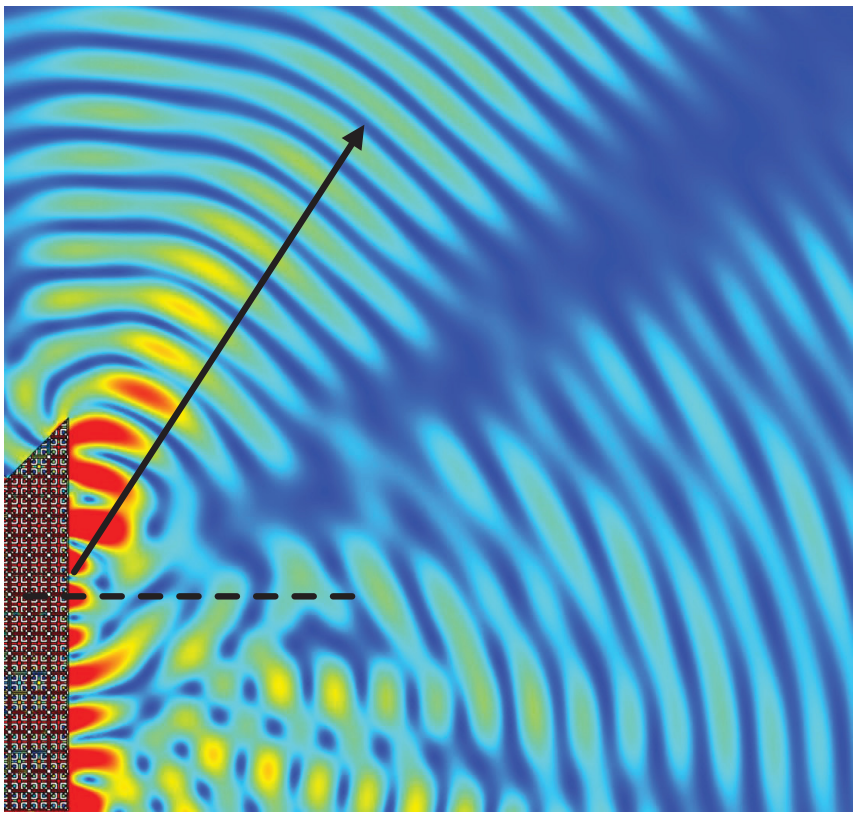

Figure 5.4: The displacement distribution of the elastic metamaterial sample for longitudinal wave incidence at frequency 1680 Hz along ΓM direction.

unique functionalities in wave filtering. The anisotropic representative cell with square shape and spatial periodicity of L, as shown in figure 5.6, serves as a typical example to illustrate the wave propagation in such a two-dimensional anisotropic metamaterial.

Compared with the original two-dimensional elastic metamaterial system illustrated in figure 5.1, this anisotropic model keeps the same geometrical parameters and material selections with slight change of the material assignment in the components. These geometrical and material parameters are illustrated in tables 4.1 and 4.2, respectively. It can be directly observed in figure 5.6 that the effective material properties of the anisotropic representative cell will have

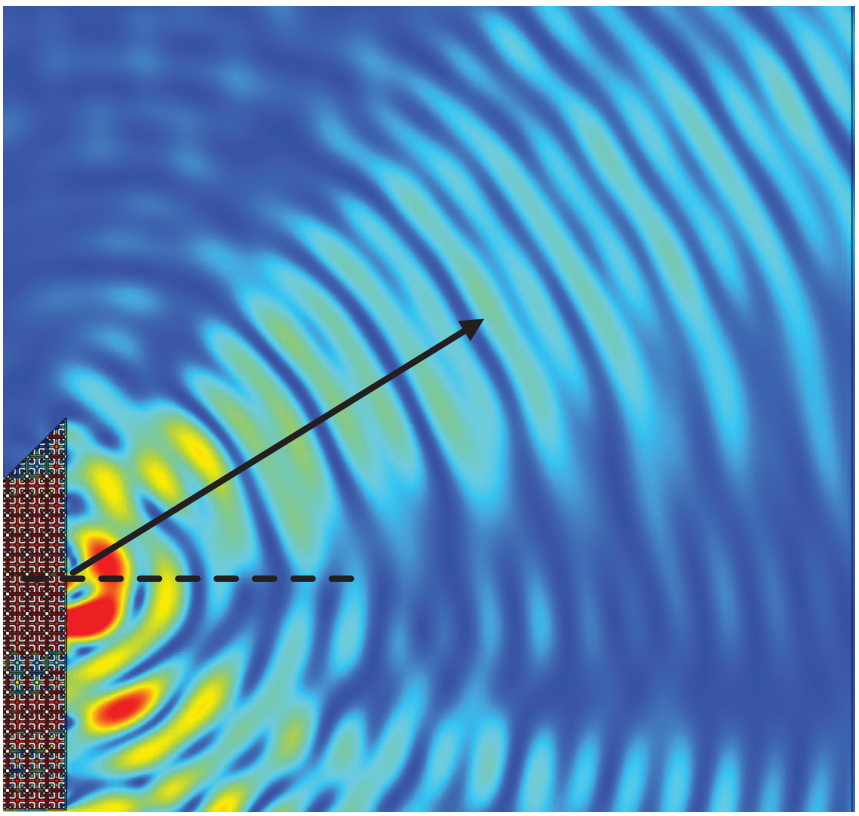

Figure 5.5: The displacement distribution of the elastic metamaterial sample for transvese wave incidence at frequency 1680 Hz along ΓM direction.

stronger dependency on the incident angles of the propagating elastic waves. In what follows, the dispersion relation of this model should be illustrated in the first Brillouin zone (ΓXMY) shown in figure 4.2, not just in the first irreducible Brillouin zone (ΓXM), due to the property variation between the two main directions, i.e. x and y directions. In light of this point, the corresponding dispersion relation is plotted in figure 5.7 with black dots through the modal analysis of the periodic metamaterial system by using COMSOL. In figure 5.7, K_1L and K_2L represent the normalized wave number of the elastic waves in x and y direction, respectively. In this configuration, the developed metamaterial can generate two wide band gaps for elastic waves, the areas of which have been filled with light grey color. These two band gaps are

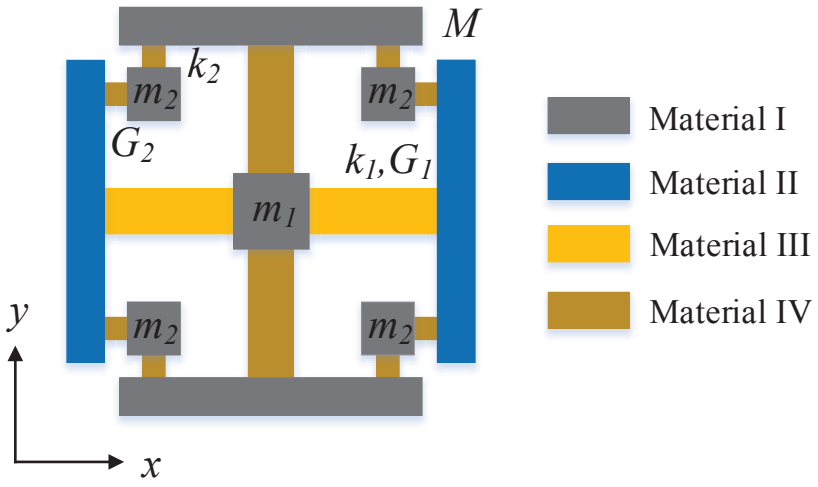

Figure 5.6: The representative cell of the anisotropic elastic metamaterial.

$(1118.8\ \text{Hz}, 1519.9\ \text{Hz})$ and $(1692.6\ \text{Hz}, \infty)$.

This anisotropic elastic metamaterial model shows different dispersion relation in x and y directions, as shown in figure 5.7. To investigate its wave filtering ability, two numerical systems have been built for transmission simulations along the two main directions, as shown in figure 5.8. In these models, one layer of ten representative cells are embedded in the matrix and external horizontal/vertical harmonic displacements are placed in the left sides to provide longitudinal/transverse wave inputs. Perfect matched layers (PML) have been added at the two ends of the models to abosrb outgoing waves and periodic boundary conditions have been applied at the upper and lower edges. The output displacements at the data lines are collected to calculate the corresponding transmission ratios. When only a horizontal/vertical displacement is applied, the amplitude of the horizontal/vertical displacement at the dataline is much larger than that of the vertical/horizontal displacement, and in this case only the horizontal/vertical displacement at the dataline is regarded as the displacement output in the following analysis.

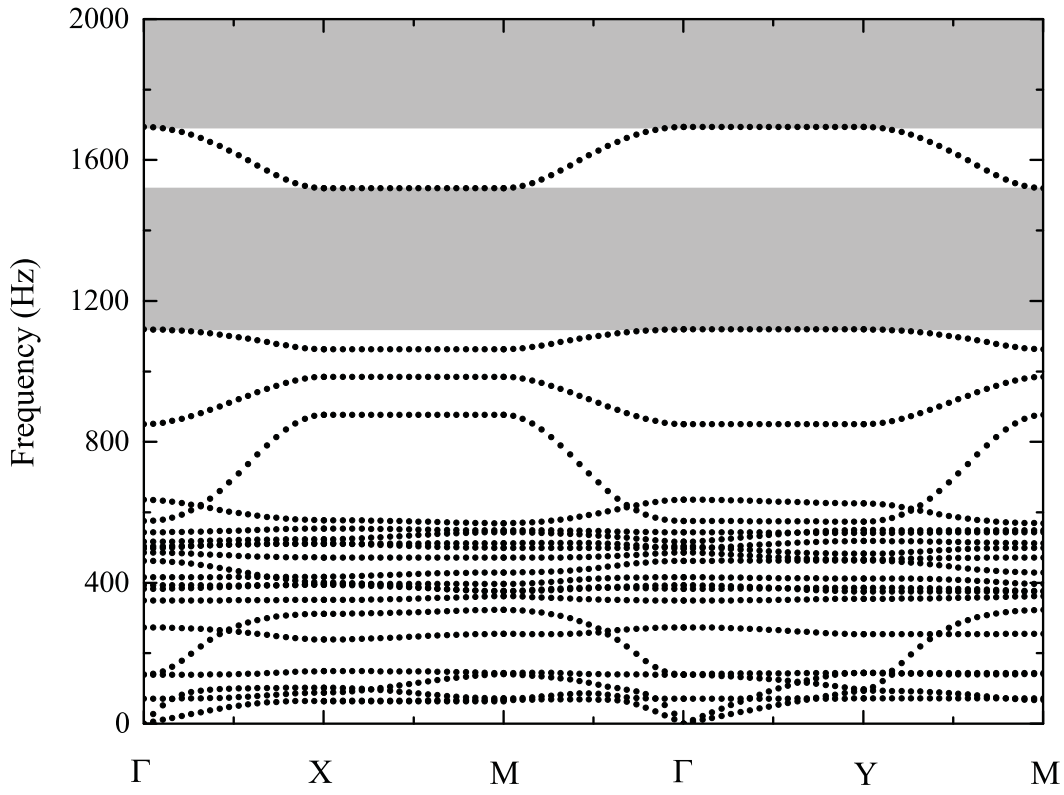

Figure 5.7: The dispersion relation of the two-dimensional anisotropic elastic metamaterial (ΓX: wave number K_1L, XM: wave numbers K_2L and $K_1L=\pi$, ΓM: wave numbers $K_1L=K_2L$, ΓY: wave number K_2L, YM: wave numbers K_1L and $K_2L=\pi$).

It should be mentioned that unlike the transmission models with big sizes in figure 4.13, these systems in figure 5.8 have much smaller size and also can well validate the transmission property of the developed anisotropic model along the two main directions.

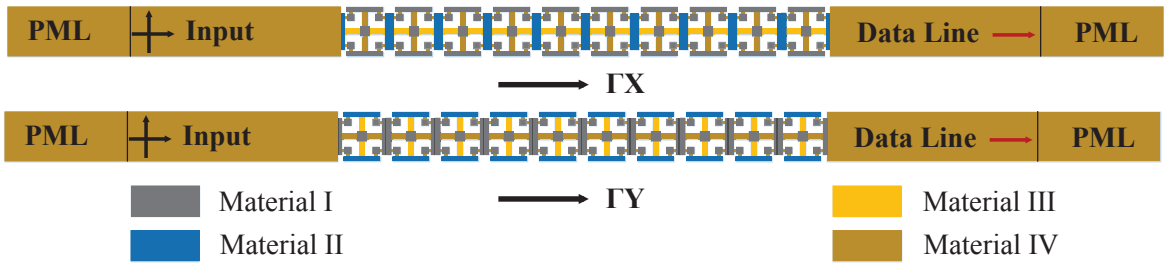

Figure 5.8: The numerical set-up for transmission simulation along ΓX and ΓY directions.

The transmission ratio along ΓX direction has been plotted in figure 5.9 with the correponding diserpsion relation for better comparison. It can be observed that the transmission of the model under vertical displacement input is very small, indicating that transverse waves cannot propagate through the model along ΓX direction at any frequency. For horizontal displacement input, the frequency ranges with very low transmission ratios are $(102.0\text{ Hz}, 139.1\text{ Hz})$, $(314.9\text{ Hz}, 384.2\text{ Hz})$, $(397.5\text{ Hz}, 499.2\text{ Hz})$, $(517.6\text{ Hz}, 525.4\text{ Hz})$, $(529.7\text{ Hz}, 569.8\text{ Hz})$, $(901.8\text{ Hz}, 1519.9\text{ Hz})$ and $(1698.2\text{ Hz}, +\infty)$, which well match the ranges of the band gaps in the dispersion relation. The band gaps in interest are the last two with wide ranges. It is worth to note that some modes cannot be excited by the horizontal displacement input and

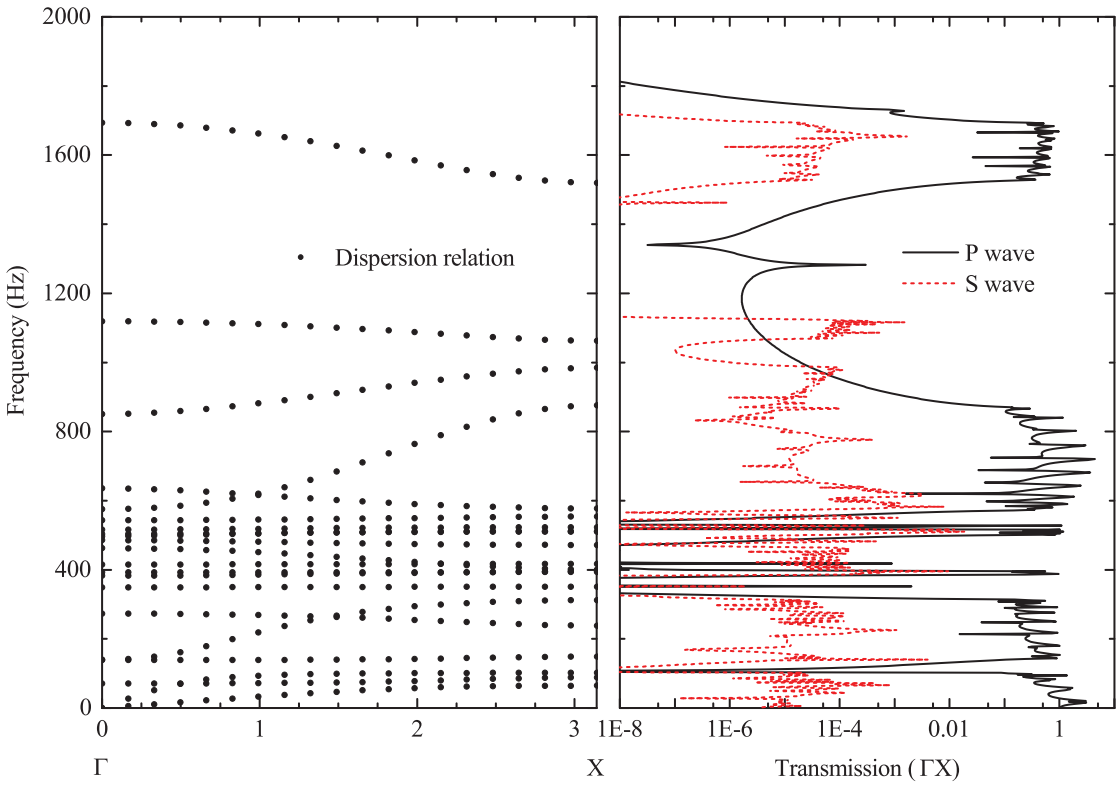

Figure 5.9: The dispersion relation and transmission along ΓX direction.

several dispersion curves with near zero slope indicate no wave propagation. To vividly illus-

trate the wave propagation in the model, figure 5.10 shows the displacement distribution of the metamaterial model with elastic waves propagating along ΓX direction based on the numerical simulation set-up depicted in figure 5.8. Here, red color represents high displacement amplitude and blue color indicates very low displacement amplitude. As shown in figure 5.10, longitudinal wave at frequency 300 Hz can propagate through the system, whereas longitudinal wave at frequency 1000 Hz is totally blocked. Also, the transverse waves at these two frequencies cannot proapgate in the system. In this regard, the anisotropic metamaterial model can behave like fluid along the ΓX direction at any frequency and this unusual property can be implemented to efficiently filter transverse waves.

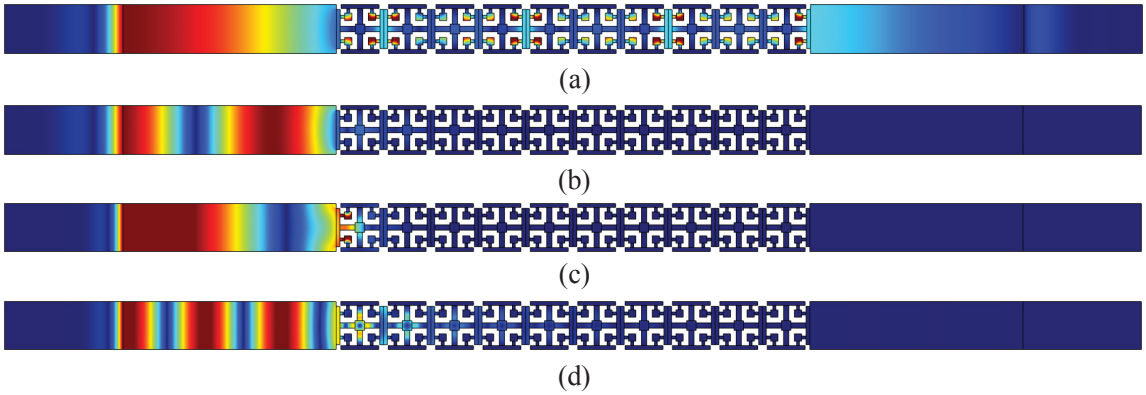

Figure 5.10: The displacement distribution along ΓX direction at, (a) 300 Hz for P wave input, (b) 1000 Hz for P wave input, (c) 300 Hz for S wave input, and (d) 1000 Hz for S wave input.

The transmission ratio and the dispersion curves along ΓY direction have been plotted in figure 5.11. It should be mentioned that there are several dispersive curves in high frequencies with zero slopes, which have no effect on the band gaps. For horizontal displacement input, the frequency ranges with very low transmission ratios are $(156.7\text{ Hz}, 255.2\text{ Hz})$, $(275.3\text{ Hz}, 377.1\text{ Hz})$, $(395.2\text{ Hz}, 484.6\text{ Hz})$, $(555.3\text{ Hz}, 629.1\text{ Hz})$ and $(643.5\text{ Hz}, +\infty)$, as

shown in figure 5.11. For vertical displacement input, the frequency ranges with very low transmission ratios are $(145.8\text{ Hz}, 474.8\text{ Hz})$, $(492.0\text{ Hz}, 499.1\text{ Hz})$ and $(525.7\text{ Hz}, +\infty)$. These frequency ranges fit the band gaps in the dispersion relation well.

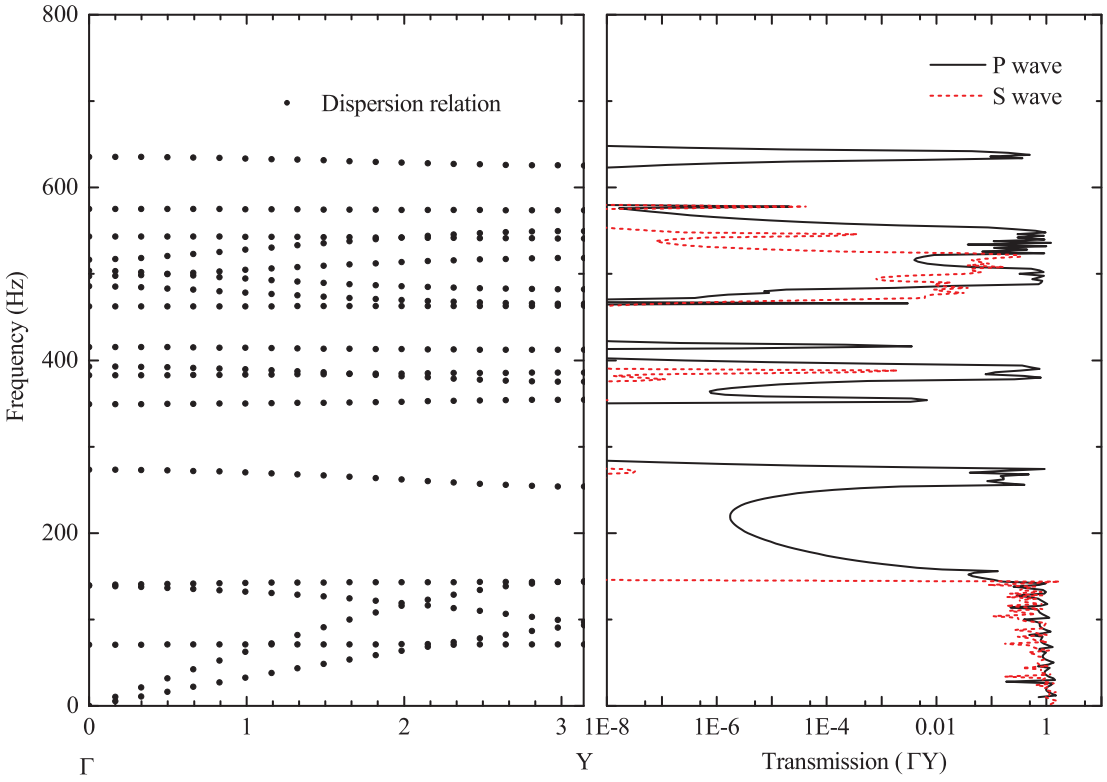

Figure 5.11: The dispersion relation and transmission along ΓY direction.

The displacement distribution of the system under longitudinal and transverse wave inputs has been illustrated in figure 5.12 for excitation frequencies 100 Hz and 600 Hz, which are located in the pass band and band gap, respectively. As expected, the phenomena of wave propagation and wave filtering are clearly observed. To this end, this anisotropic metamaterial model has broad band gaps for elastic waves progating along ΓY direction, which range from low frequencies to infinity and they can be effciently used to attenuate elastic waves.

In the developed anisotropic metamaterial, it shows various transmission ratios along ΓX

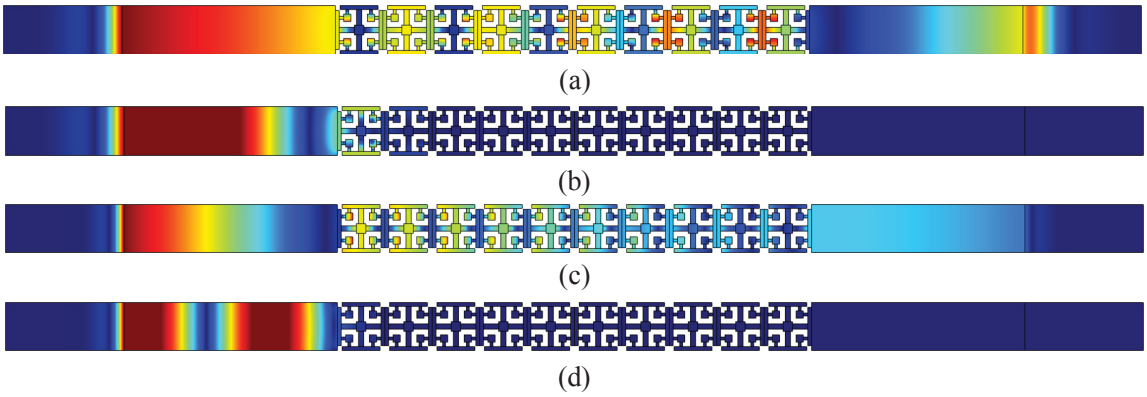

Figure 5.12: The displacement distribution along ΓY direction at, (a) 100 Hz for P wave input, (b) 600 Hz for P wave input, (c) 100 Hz for S wave input, and (d) 600 Hz for S wave input.

and ΓY directions. This unique property can be utilized to separate elastic waves with different frequencies. To show this phenonmenon, numerical simulations have been conducted based on the system shown in figure 5.13. In this system, normal/tangential harmonic displacement can be applied to generate longitudinal/transverse wave input and perfect matched layers are added to absorb outgoing waves. As designed, elastic waves with frequencies located in the pass bands along ΓX direction will propagate into the matrix in the right side, whereas elastic waves with frequencies located in the pass bands along ΓY direction will propagate into the matrix in the lower side.

The displacement distribution of the system under longitudinal wave input at several frequencies has been plotted in figuer 5.14 as an example to show its special dynamic behavior. In this figure, red color indicates large displacement amplitude and blue color represents very small displacement amplitude. As shown in figure 5.14, displacement output can be observed in the right and lower sides of the system for incident wave with excitation frequency 50 Hz. When the excitation frequency is increased to 1250 Hz, the incident wave is totally blocked.

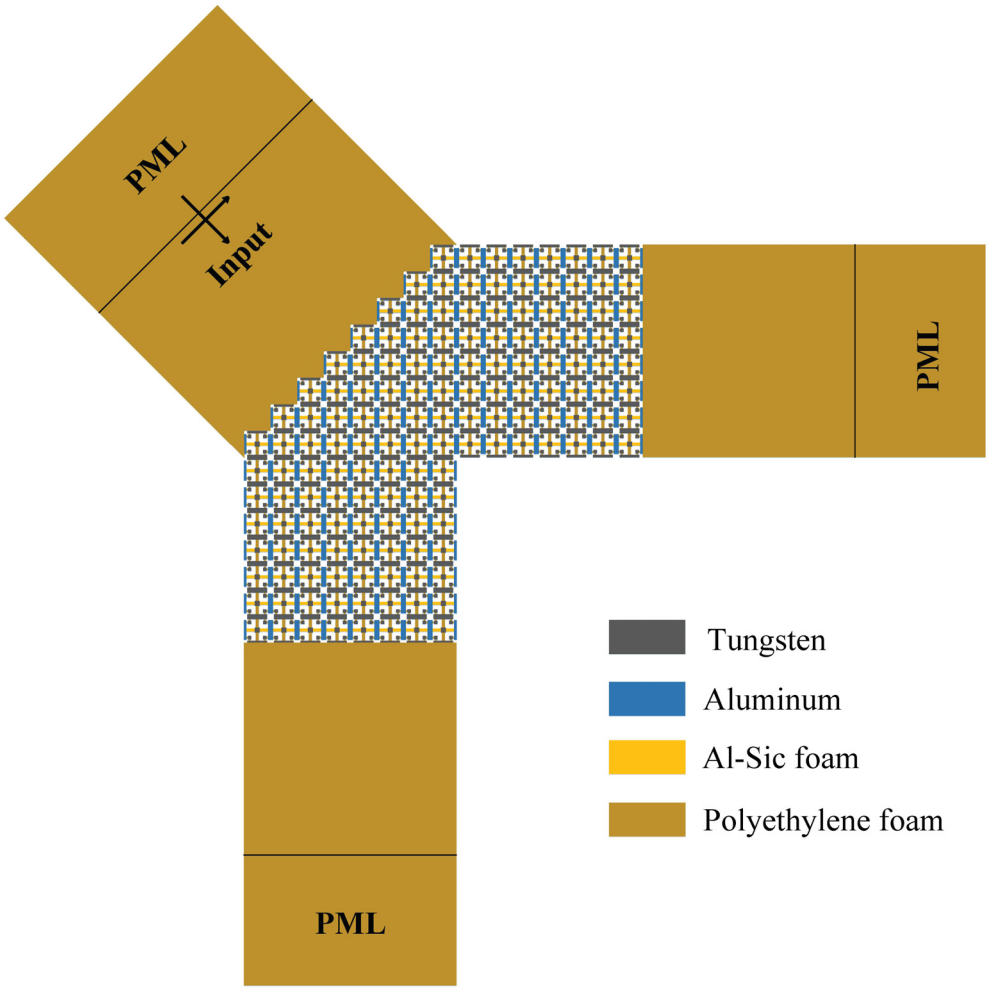

Figure 5.13: The numerical set-up of a system controlling elastic wave propagating directions.

These two frequencies, 50 Hz and 1250 Hz are located in the pass bands and stop bands of the model along any direction, respectively. When the excitation frequency is 110 Hz, the waves only can propagate to the lower side and when the excitation frequency is 980 Hz, the waves only can propagate to the right side. Then, this model can be utilized to separeate elastic waves for certain frequencies.

As discussed, this anisotropic elastic metamaterial can extract longitudinal waves by filtering transverse waves from the propagating mixed waves along ΓX direction. Also, it possesses broad band gaps ranging from lower frequencies to infinity, which can efficiently attenuate

elastic waves along ΓY direction. Due to the material property variation along the two main directions, this metamaterial model can separate elastic waves for certain frequencies.

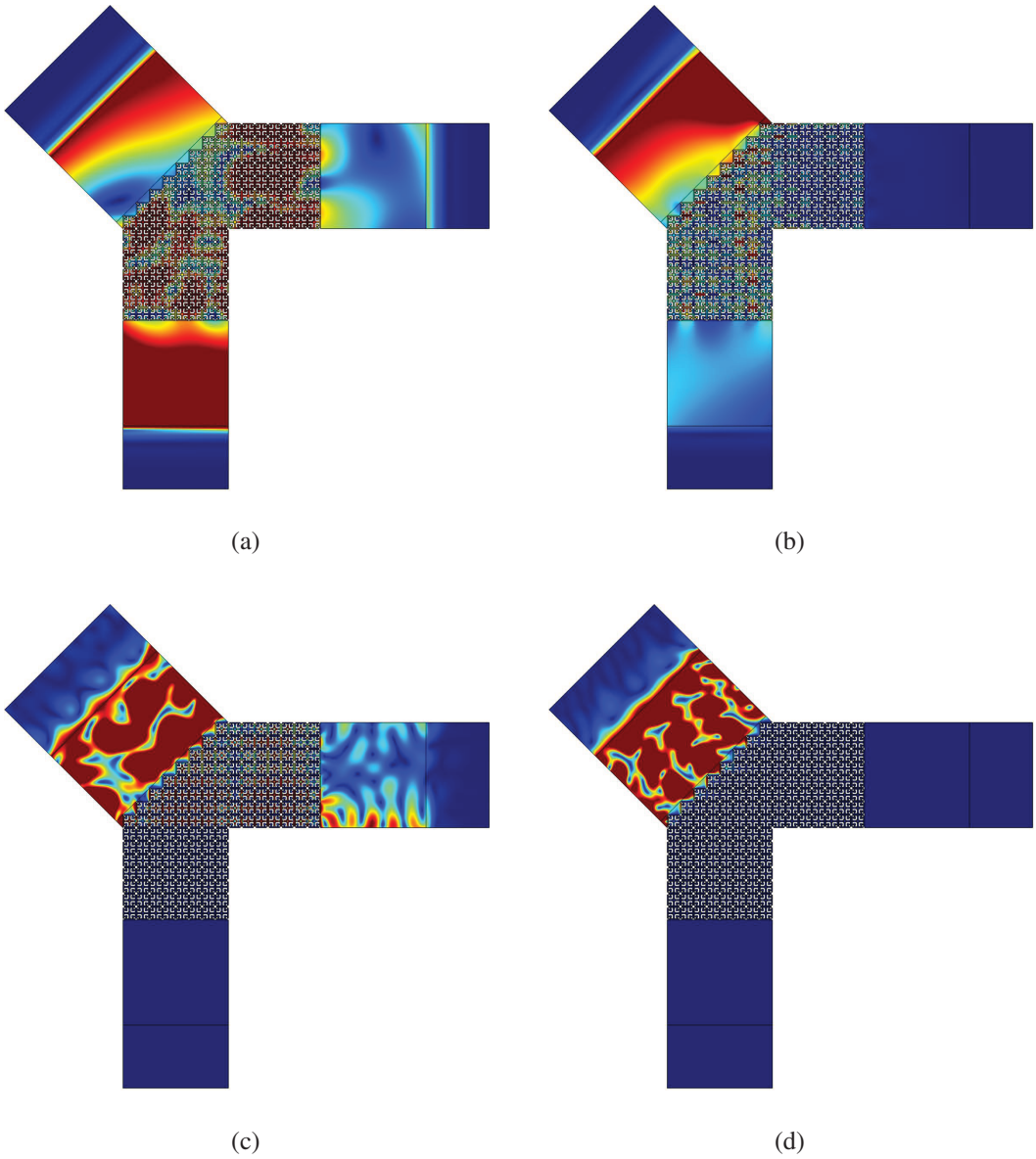

Figure 5.14: The displacement distribution of the system under longitudinal wave input at, (a) 50 Hz, (b) 110 Hz, (c) 980 Hz and (d) 1250 Hz.

5.4 Conclusion

In this chapter, the wave propagation of the two-dimensional elastic metamaterial developed is numerically studied. At the frequencies with negative dispersion, negative wave refraction for longitudinal and transverse waves can be clearly observed due to the triple negative effective material properties. The negative elastic wave refraction phenomenon can be potentially implemented to design superlense with high spatial resolution. When the elastic metamaterial is adjusted to obtain anisotropic material properties, it can show unique wave filtering abilities, such as attenuating elasic waves in broad frequecy ranges, and filtering transverse waves by behaving like fluid.

Chapter 6: Contributions and future work

This chapter summarizes the main contributions of this thesis on the elastic metamaterial modelling and describes several issues that remain to be addressed in the subsequent research.

6.1 Main contributions

This thesis aims to design elastic metamaterials with negative effective mass and/or modulus, and investigate the unusual dynamic behaviour of these metamaterials. Throughout this study, four major issues essential to the research of elastic metamaterials have been considered, (i) the underlying mechanism of generating independent negative effective parameters; (ii) how to model the one-dimensional elastic metamaterials with double negative behavior; (iii) how to model the two-dimensional elastic metamaterials with simultaneously negative effective mass, bulk modulus and shear modulus; (iv) how the elastic waves propagate in such a two-dimensional elastic metamaterial.

The main contributions of this thesis are summarized as follows.

6.1.1 Underlying mechanism of generating negative effective parameters

The first two-dimensional elastic metamaterial structure based on spring-mass system has been developed to illustrate the underlying mechanism of generating negative effective mass and/or negative effective modulus. In the model, the translational resonance of the resonators induces overall motion of the cells to obtain negative effective mass and the rotational resonance gives rise to the local deformation of the cells without overall motion to generate negative effective

modulus. Examples of harmonic elastic waves in this metamaterial system are studied to illustrate the effect of the generated negative mass and/or modulus on wave propagation. This model can provide a guideline for designing two-dimensional elastic metamaterials.

6.1.2 A new one-dimensional elastic metamaterial with double negative behavior

The new one-dimensional elastic metamaterial model has been developed to obtain negative effective mass and/or modulus, and at most two frequency ranges double negative behavior exists based on two types of translational resonances. One resonance contributes directly to the negative effective modulus and the coupled effect of the two resonances dominates the negative effective mass, which endows the elastic metamaterial with great flexibility to generate negative effective parameters in different frequency ranges. Due to the unique feature of the proposed representative cells, the independent control of the effective mass and modulus can be realized to some extent. Typical examples are presented to illustrate the dynamic properties of the developed metamaterisl, such as wave mitigating ability and negative phase velocity of the propagating waves. This model mainly serves as a stepping stone to more interesting properties in higher dimensions.

6.1.3 A new two-dimensional elastic metamaterial with triple negative behavior

This new two-dimensional elastic metamaterial has been developed, exhibiting multiple local resonances. In certain frequency ranges, negative effective mass, bulk modulus and shear modulus can be achieved simultaneously only through the translational motion of the resonators in the representative cell. Numerical analysis has been conducted to evaluate the association between the negative effective parameters and the modes of local resonance. A simplified ana-

lytical model is also formed to study the effects of the main material and geometric parameters and it can be utilized as an effective tool for predicting the desired negative dispersion behavior of the elastic metamaterial. Featuring simple design and easy fabrication, this new elastic metamaterial can behave like solids or fluid with negative phase velocities for longitudinal and/or transverse waves in different wave propagating directions.

6.1.4 Wave propagation of the two-dimensional elastic metamaterial

This new two-dimensional elastic metamaterials can exhibit negative refraction for longitudinal and transverse waves due to the negative phase velocities, which are associated with the negative effective parameters. This model can be potentially implemented to design superlense that can beat the diffraction limit. The phenomenon of elastic wave attenuation in broad frequency ranges also has been observed in the anisotropic metamaterial model.

6.2 Future work

Despite the tremendous growth of research during the last decade, the development of elastic metamaterials is still in its early stage. Although the research of this thesis has tried to cover some important challenges and limitations of the current models in elastic metamaterials with negative effective parameters, there are still some issues that need to be further addressed. Attentions will be paid on the following as the research directions in the future.

6.2.1 Experimental validation

This thesis is mainly based on the analytical modelling of the developed elastic metamaterials and the corresponding numerical simulations have been conducted to support these analytical

results. However, certain assumptions have been made in this study. For this reason, related experiments are recommended to further validate the effectiveness of the elastic metamaterials designed.

6.2.2 Consideration of material damping

Material damping, as an intrinsic feature of the material components in the representative cells, is directly associated with energy loss of the metamaterial structures. It is of interest to understand the combined effect of local resonance and material damping on the dynamic behaviour of the elastic metamaterials. The utilization of material damping may lead to more useful engineering applications.

6.2.3 Active control of elastic metamaterial

In this thesis, the elastic models developed can only provide passive control over the propagating waves with fixed material properties, which cannot be timely tuned in response to the possible variation of the external environment. This limits their practical applications due to the absence of reconfigurability and tunability. To address this inherent limitation and get closer to the real engineering designs, active elastic metamaterials with tunable effective material parameters are desired. As designed, these effective parameters can be timely adjusted through the controllable external excitations applied, such as voltage and temperature. The introduction of active control can endow the elastic metamaterials with more flexibility to generate negative effective mass and/or modulus, and broad band gap in the low frequency range may be formed.

Bibliography

Ambati, M., Fang, N., Sun, C., and Zhang, X. Surface resonant states and superlensing in acoustic metamaterials. *Physical Review B*, 75(19):195447, 2007.

An, X. Y., Sun, F. F., Yu, P. S., Fan, H. L., He, S. P., and Fang, D. N. Negative effective mass density of one-dimensional hierarchical metacomposite. *Journal of Applied Mechanics-Transactions of the Asme*, 82(3):8, 2015.

An, X., Fan, H., and Zhang, C. Wave dispersion in one-dimensional periodic graded metacomposites. *Journal of Sound and Vibration*, 409:217–226, 2017.

Antonakakis, T., Craster, R. V., and Guenneau, S. Homogenisation for elastic photonic crystals and dynamic anisotropy. *Journal of the Mechanics and Physics of Solids*, 71:84–96, 2014.

Ao, X. and Chan, C. T. Far-field image magnification for acoustic waves using anisotropic acoustic metamaterials. *Physical Review E*, 77(2):025601, 2008.

Auld, B. A. *Acoustic fields and waves in solids*. Krieger Publishing Company, Malabar, FL, 1973.

Babaee, S., Shim, J., Weaver, J. C., Chen, E. R., Patel, N., and Bertoldi, K. 3d soft metamaterials with negative poisson's ratio. *Advanced Materials*, 25(36):5044–5049, 2013.

Banerjee, A., Das, R., and Calius, E. P. Frequency graded 1d metamaterials: A study on the attenuation bands. *Journal of Applied Physics*, 122(7):12, 2017.

Banerjee, B. *An Introduction to Metamaterials and Waves in Composites*. CRC Press, Taylor and Francis Group, Boca Raton, 2011.

Baravelli, E. and Ruzzene, M. Internally resonating lattices for bandgap generation and low-frequency vibration control. *Journal of Sound and Vibration*, 332(25):6562–6579, 2013.

Bell, J. S., Summers, I. R., Murray, A. R. J., Hendry, E., Sambles, J. R., and Hibbins, A. P. Low acoustic transmittance through a holey structure. *Physical Review B*, 85(21):214305, 2012.

Bi, Y., Jia, H., Sun, Z., Yang, Y., Zhao, H., and Yang, J. Experimental demonstration of three-dimensional broadband underwater acoustic carpet cloak. *Applied Physics Letters*, 112(22): 223502, 2018.

Bigoni, D., Guenneau, S., Movchan, A. B., and Brun, M. Elastic metamaterials with inertial locally resonant structures: Application to lensing and localization. *Physical Review B*, 87 (17):6, 2013.

Bonnet, G. and Monchiet, V. Dynamic mass density of resonant metamaterials with homogeneous inclusions. *The Journal of the Acoustical Society of America*, 142(2):890–901, 2017.

Brillouin, L. *Wave propagation in periodic structures*. Dover, 1953.

Brun, M., Guenneau, S., and Movchan, A. B. Achieving control of in-plane elastic waves. *Applied Physics Letters*, 94(6):061903, 2009.

Brunet, T., Merlin, A., Mascaro, B., Zimny, K., Leng, J., Poncelet, O., Aristegui, C., and Mondain-Monval, O. Soft 3d acoustic metamaterial with negative index. *Nature Materials*, 14:384, 2014.

Carcione, J. and Cavallini, F. On the acoustic-electromagnetic analogy. *Wave Motion*, 21(2): 149–162, 1995.

Chan, C. T., Li, J., and Fung, K. H. On extending the concept of double negativity to acoustic waves. *Journal of Zhejiang University-Science A*, 7(1):24–28, 2006.

Cheer, J., Daley, S., and McCormick, C. Feedforward control of sound transmission using an active acoustic metamaterial. *Smart Materials and Structures*, 26(2):025032, 2017.

Chen, H., Zhai, S., Ding, C., Liu, S., Luo, C., and Zhao, X. Meta-atom cluster acoustic metamaterial with broadband negative effective mass density. *Journal of Applied Physics*, 115(5):054905, 2014.

Chen, H. and Chan, C. T. Acoustic cloaking in three dimensions using acoustic metamaterials. *Applied Physics Letters*, 91(18):183518, 2007.

Chen, H., Chan, C. T., and Sheng, P. Transformation optics and metamaterials. *Nature Materials*, 9:387, 2010.

Chen, Y. Y., Barnhart, M. V., Chen, J. K., Hu, G. K., Sun, C. T., and Huang, G. L. Dissipative elastic metamaterials for broadband wave mitigation at subwavelength scale. *Composite Structures*, 136:358–371, 2016.

Chen, Y., Hu, G., and Huang, G. A hybrid elastic metamaterial with negative mass density and tunable bending stiffness. *Journal of the Mechanics and Physics of Solids*, 105:179–198, 2017.

Cheng, Y., Xu, J. Y., and Liu, X. J. Broad forbidden bands in parallel-coupled locally resonant ultrasonic metamaterials. *Applied Physics Letters*, 92(5):051913, 2008.

Christensen, J., Fernandez-Dominguez, A. I., de Leon-Perez, F., Martin-Moreno, L., and Garcia-Vidal, F. J. Collimation of sound assisted by acoustic surface waves. *Nature Physics*, 3:851, 2007.

Christensen, J., Martin-Moreno, L., and Garcia-Vidal, F. J. All-angle blockage of sound by an acoustic double-fishnet metamaterial. *Applied Physics Letters*, 97(13):134106, 2010.

Colquitt, D. J., Brun, M., Gei, M., Movchan, A. B., Movchan, N. V., and Jones, I. S. Transformation elastodynamics and cloaking for flexural waves. *Journal of the Mechanics and Physics of Solids*, 72:131–143, 2014.

Colquitt, D. J., Craster, R. V., and Makwana, M. High frequency homogenisation for elastic lattices. *Quarterly Journal of Mechanics and Applied Mathematics*, 68(2):203–230, 2015.

Craster, R. V. and Guenneau, S. *Acoustic Metamaterials: Negative Refraction, Imaging, Lensing, and Cloaking*. Springer Series in Materials Science. Springer, Dordrecht, 2013.

Cselyuszka, N., Secujski, M., and Crnojevic-Bengin, V. Novel negative mass density resonant metamaterial unit cell. *Physics Letters A*, 379(1-2):33–36, 2015.

Cummer, A., Steven and Schurig, D. One path to acoustic cloaking. *New Journal of Physics*, 9(3):45, 2007.

Cummer, S. A., Popa, B.-I., Schurig, D., Smith, D. R., and Pendry, J. Full-wave simulations of electromagnetic cloaking structures. *Physical Review E*, 74(3):036621, 2006.

Cummer, S. A., Christensen, J., and Alu, A. Controlling sound with acoustic metamaterials. *Nature Reviews Materials*, 1:16001, 2016.

Deymier, P. A. *Acoustic Metamaterials and Phononic Crystals*. Springer Series in Solid-State Sciences. Springer-Verlag Berlin Heidelberg, 2013.

Diatta, A., Kadic, M., Wegener, M., and Guenneau, S. Scattering problems in elastodynamics. *Physical Review B*, 94(10):100105, 2016.

Ding, C. and Zhao, X. Multi-band and broadband acoustic metamaterial with resonant structures. *Journal of Physics D: Applied Physics*, 44(21):215402, 2011.

Ding, C., Hao, L., and Zhao, X. Two-dimensional acoustic metamaterial with negative modulus. *Journal of Applied Physics*, 108(7):074911, 2010.

Ding, Y., Liu, Z., Qiu, C., and Shi, J. Metamaterial with simultaneously negative bulk modulus and mass density. *Physical Review Letters*, 99(9):093904, 2007.

Drugan, W. J. Elastic composite materials having a negative stiffness phase can be stable. *Physical Review Letters*, 98(5):055502, 2007.

Drugan, W. J. Wave propagation in elastic and damped structures with stabilized negative-stiffness components. *Journal of the Mechanics and Physics of Solids*, 106:34–45, 2017.

Fang, N., Xi, D., Xu, J., Ambati, M., Srituravanich, W., Sun, C., and Zhang, X. Ultra metamaterials with negative modulus. *Nature Materials*, 5(6):452–456, 2006.

Fey, J. and Robertson, W. M. Compact acoustic bandgap material based on a subwavelength collection of detuned helmholtz resonators. *Journal of Applied Physics*, 109(11):114903, 2011.

Fleury, R., Monticone, F., and Alu, A. Invisibility and cloaking: Origins, present, and future perspectives. *Physical Review Applied*, 4(3):037001, 2015.

Fok, L. and Zhang, X. Negative acoustic index metamaterial. *Physical Review B*, 83(21): 214304, 2011.

Gan, W. S. *New acoustics based on metamaterials*. Springer Singapore, Singapore, 2018.

Garcia-Chocano, V. M., Gracia-Salgado, R., Torrent, D., Cervera, F., and Sanchez-Dehesa, J. Quasi-two-dimensional acoustic metamaterial with negative bulk modulus. *Physical Review B*, 85(18):184102, 2012.

Ge, H., Yang, M., Ma, C., Lu, M.-H., Chen, Y.-F., Fang, N., and Sheng, P. Breaking the barriers: advances in acoustic functional materials. *National Science Review*, 5(2):159–182, 2018.

Gracia-Salgado, R., Garcia-Chocano, V. M., Torrent, D., and Sanchez-Dehesa, J. Negative mass density and ρ-near-zero quasi-two-dimensional metamaterials: Design and applications. *Physical Review B*, 88(22):224305, 2013.

Graeme, W. M., Marc, B., and John, R. W. On cloaking for elasticity and physical equations with a transformation invariant form. *New Journal of Physics*, 8(10):248, 2006.

Gu, Y. W., Luo, X. D., and Ma, H. R. Low frequency elastic wave propagation in two dimensional locally resonant phononic crystal with asymmetric resonator. *Journal of Applied Physics*, 105(4):7, 2009.

Guenneau, S., Movchan, A., Petursson, G., and Ramakrishna, S. A. Acoustic metamaterials for sound focusing and confinement. *New Journal of Physics*, 9(11):399, 2007.

Huang, G. L. and Sun, C. T. Band gaps in a multiresonator acoustic metamaterial. *Journal of Vibration and Acoustics-Transactions of the Asme*, 132(3):6, 2010.

Huang, H. H. and Sun, C. T. Wave attenuation mechanism in an acoustic metamaterial with negative effective mass density. *New Journal of Physics*, 11:15, 2009b.

Huang, H. H. and Sun, C. T. Theoretical investigation of the behavior of an acoustic metamaterial with extreme young's modulus. *Journal of the Mechanics and Physics of Solids*, 59 (10):2070–2081, 2011a.

Huang, H. H. and Sun, C. T. Locally resonant acoustic metamaterials with 2d anisotropic effective mass density. *Philosophical Magazine*, 91(6):981–996, 2011b.

Huang, H. H. and Sun, C. T. Anomalous wave propagation in a one-dimensional acoustic metamaterial having simultaneously and young's modulus. *The Journal of the Acoustical Society of America*, 132(4):2887–2895, 2012.

Huang, H. H., Sun, C. T., and Huang, G. L. On the negative effective mass density in acoustic metamaterials. *International Journal of Engineering Science*, 47(4):610–617, 2009a.

Huang, T. Y., Shen, C., and Jing, Y. Membrane- and plate-type acoustic metamaterials. *Journal of the Acoustical Society of America*, 139(6):3239–3249, 2016.

Hussein, M. I., Leamy, M. J., and Ruzzene, M. Dynamics of phononic materials and structures: Historical origins, recent progress, and future outlook. *Applied Mechanics Reviews*, 66(4): 040802–040802–38, 2014.

Islam, M. T. and Newaz, G. Metamaterial with mass-stem array in acoustic cavity. *Applied Physics Letters*, 100(1):011904, 2012.

Jiang, X., Liang, B., Li, R.-q., Zou, X.-y., Yin, L.-l., and Cheng, J.-c. Ultra-broadband absorption by acoustic metamaterials. *Applied Physics Letters*, 105(24):243505, 2014.

Kaina, N., Lemoult, F., Fink, M., and Lerosey, G. Negative refractive index and acoustic superlens from multiple scattering in single negative metamaterials. *Nature*, 525(7567): 77–+, 2015.

Kochmann, D. M. and Drugan, W. J. Dynamic stability analysis of an elastic composite material having a negative-stiffness phase. *Journal of the Mechanics and Physics of Solids*, 57 (7):1122–1138, 2009.

Kundtz, N. and Smith, D. R. Extreme-angle broadband metamaterial lens. *Nature Materials*, 9(2):129–132, 2010.

Lai, Y., Wu, Y., Sheng, P., and Zhang, Z.-Q. Hybrid elastic solids. *Nature Materials*, 10(8): 620–624, 2011.

Lakes, R. S., Lee, T., Bersie, A., and Wang, Y. C. Extreme damping in composite materials with negative-stiffness inclusions. *Nature*, 410(6828):565–567, 2001.

Landy, N. and Smith, D. R. A full-parameter unidirectional metamaterial cloak for microwaves. *Nature Materials*, 12:25, 2012.

Larabi, H., Pennec, Y., Djafari-Rouhani, B., and Vasseur, J. O. Multicoaxial cylindrical inclusions in locally resonant phononic crystals. *Physical Review E*, 75(6):066601, 2007.

Lee, D., Nguyen, D. M., and Rho, J. Acoustic wave science realized by metamaterials. *Nano Convergence*, 4(1):3, 2017.

Lee, S. H. and Wright, O. B. Origin of negative density and modulus in acoustic metamaterials. *Physical Review B*, 93(2):024302, 2016.

Lee, S. H., Park, C. M., Seo, Y. M., Wang, Z. G., and Kim, C. K. Acoustic metamaterial with negative density. *Physics Letters A*, 373(48):4464–4469, 2009a.

Lee, S. H., Park, C. M., Seo, Y. M., Wang, Z. G., and Kim, C. K. Acoustic metamaterial with negative modulus. *Journal of Physics: Condensed Matter*, 21(17):175704, 2009b.

Lee, S. H., Park, C. M., Seo, Y. M., Wang, Z. G., and Kim, C. K. Composite acoustic medium with simultaneously negative density and modulus. *Physical Review Letters*, 104(5):054301, 2010.

Leonhardt, U. Optical conformal mapping. *Science*, 312(5781):1777–1780, 2006.

Li, J. and Chan, C. T. Double-negative acoustic metamaterial. *Physical Review E*, 70(5): 055602, 2004.

Li, J., Fok, L., Yin, X., Bartal, G., and Zhang, X. Experimental demonstration of an acoustic magnifying hyperlens. *Nature Materials*, 8(12):931–934, 2009.

Li, Z., Wang, C., and Wang, X. Dynamic behaviour of a two-dimensional elastic metamaterial with eccentric local resonators. *The 8th International Conference on Metamaterial, photonic Crystals and Plasmonics*, 2017.

Li, Z. and Wang, X. On the dynamic behaviour of a two-dimensional elastic metamaterial system. *International Journal of Solids and Structures*, 78-79:174–181, 2016.

Liang, Z., Willatzen, M., Li, J., and Christensen, J. Tunable acoustic double negativity metamaterial. *Scientific Reports*, 2:859, 2012.

Liu, A. P., Zhu, R., Liu, X. N., Hu, G. K., and Huang, G. L. Multi-displacement microstructure continuum modeling of anisotropic elastic metamaterials. *Wave Motion*, 49(3):411–426, 2012.

Liu, X. N., Hu, G. K., Huang, G. L., and Sun, C. T. An elastic metamaterial with simultaneously negative mass density and bulk modulus. *Applied Physics Letters*, 98(25):251907, 2011a.

Liu, X. N., Hu, G. K., Sun, C. T., and Huang, G. L. Wave propagation characterization and design of two-dimensional elastic chiral metacomposite. *Journal of Sound and Vibration*, 330(11):2536–2553, 2011b.

Liu, X. and Hu, G. Elastic metamaterials making use of chirality: A review. *Journal of Mechanical Engineering*, 62(7/8):403–418, 2016.

Liu, Y. Q., Su, X. Y., and Sun, C. T. Broadband elastic metamaterial with single negativity by mimicking lattice systems. *Journal of the Mechanics and Physics of Solids*, 74:158–174, 2015.

Liu, Y. and Zhang, X. Metamaterials: a new frontier of science and technology. *Chemical Society Reviews*, 40(5):2494–2507, 2011.

Liu, Z. Y., Zhang, X. X., Mao, Y. W., Zhu, Y. Y., Yang, Z. Y., Chan, C. T., and Sheng, P. Locally resonant sonic materials. *Science*, 289(5485):1734–1736, 2000.

Liu, Z., Lee, H., Xiong, Y., Sun, C., and Zhang, X. Far-field optical hyperlens magnifying sub-diffraction-limited objects. *Science*, 315(5819):1686–1686, 2007.

Liu, Z., Chan, C. T., and Sheng, P. Analytic model of phononic crystals with local resonances. *Physical Review B*, 71(1):014103, 2005.

Lu, L., Ru, C. Q., and Guo, X. Negative effective mass of a filled carbon nanotube. *International Journal of Mechanical Sciences*, 134:174–181, 2017.

Lu, M.-H., Feng, L., and Chen, Y.-F. Phononic crystals and acoustic metamaterials. *Materials Today*, 12(12):34–42, 2009.

Ma, G. and Sheng, P. Acoustic metamaterials: From local resonances to broad horizons. *Science Advances*, 2(2), 2016.

Ma, G., Yang, M., Yang, Z., and Sheng, P. Low-frequency narrow-band acoustic filter with large orifice. *Applied Physics Letters*, 103(1):011903, 2013.

Mei, J., Liu, Z., Wen, W., and Sheng, P. Effective mass density of fluid-solid composites. *Physical Review Letters*, 96(2):024301, 2006.

Mei, J., Liu, Z., Wen, W., and Sheng, P. Effective dynamic mass density of composites. *Physical Review B*, 76(13):134205, 2007.

Mei, J., Ma, G., Yang, M., Yang, Z., Wen, W., and Sheng, P. Dark acoustic metamaterials as super absorbers for low-frequency sound. *Nature Communications*, 3:756, 2012.

Milton, G. W. and Willis, J. R. On modifications of newton's second law and linear continuum elastodynamics. *Proceedings of the Royal Society of London A: Mathematical, Physical and Engineering Sciences*, 463(2079):855–880, 2007.

Mitchell, S. J., Pandolfi, A., and Ortiz, M. Metaconcrete: designed aggregates to enhance dynamic performance. *Journal of the Mechanics and Physics of Solids*, 65:69–81, 2014.

Moleron, M. and Daraio, C. Acoustic metamaterial for subwavelength edge detection. *Nature Communications*, 6:8037, 2015.

Movchan, A. B. and Slepyan, L. I. Band gap green's functions and localized oscillations. *Proceedings of the Royal Society A: Mathematical, Physical and Engineering Science*, 463 (2086):2709–2727, 2007.

Nateghi, A., Van Belle, L., Claeys, C., Deckers, E., Pluymers, B., and Desmet, W. Wave propagation in locally resonant cylindrically curved metamaterial panels. *International Journal of Mechanical Sciences*, 127:73–90, 2017.

Norris, A. N. and Parnell, W. J. Hyperelastic cloaking theory: transformation elasticity with pre-stressed solids. *Proceedings of the Royal Society A: Mathematical, Physical and Engineering Science*, 468(2146):2881–2903, 2012.

Norris, A. N. and Shuvalov, A. L. Elastic cloaking theory. *Wave Motion*, 48(6):525–538, 2011.

Oh, J. H., Kwon, Y. E., Lee, H. J., and Kim, Y. Y. Elastic metamaterials for independent realization of negativity in density and stiffness. *Scientific Reports*, 6:23630, 2016.

Pai, P. F. and Huang, G. *Theory and Design of Acoustic Metamaterials*, volume PM260. SPIE, 2015.

Park, C. M., Park, J. J., Lee, S. H., Seo, Y. M., Kim, C. K., and Lee, S. H. Amplification of acoustic evanescent waves using metamaterial slabs. *Physical Review Letters*, 107(19): 194301, 2011.

Park, J. J., Park, C. M., Lee, K. J. B., and Lee, S. H. Acoustic superlens using membrane-based metamaterials. *Applied Physics Letters*, 106(5):051901, 2015.

Parnell, W. J. and Shearer, T. Antiplane elastic wave cloaking using metamaterials, homogenization and hyperelasticity. *Wave Motion*, 50(7):1140–1152, 2013.

Pendry, J. B. Negative refraction makes a perfect lens. *Physical Review Letters*, 85(18):3966–3969, 2000.

Pendry, J. B., Schurig, D., and Smith, D. R. Controlling electromagnetic fields. *Science*, 312 (5781):1780–1782, 2006.

Peng, H. and Frank Pai, P. Acoustic metamaterial plates for elastic wave absorption and structural vibration suppression. *International Journal of Mechanical Sciences*, 89:350–361, 2014.

Popa, B.-I., Zigoneanu, L., and Cummer, S. A. Experimental acoustic ground cloak in air. *Physical Review Letters*, 106(25):253901, 2011.

Popa, B.-I., Shinde, D., Konneker, A., and Cummer, S. A. Active acoustic metamaterials reconfigurable in real time. *Physical Review B*, 91(22):220303, 2015.

Schurig, D., Mock, J. J., Justice, B. J., Cummer, S. A., Pendry, J. B., Starr, A. F., and Smith, D. R. Metamaterial electromagnetic cloak at microwave frequencies. *Science*, 314(5801): 977–980, 2006.

Shalaev, V. M. Optical negative-index metamaterials. *Nature Photonics*, 1:41, 2007.

Shelby, R. A., Smith, D. R., and Schultz, S. Experimental verification of a negative index of refraction. *Science*, 292(5514):77–79, 2001.

Shen, C., Xie, Y., Sui, N., Wang, W., Cummer, S. A., and Jing, Y. Broadband acoustic hyperbolic metamaterial. *Physical Review Letters*, 115(25):254301, 2015.

Sheng, P., Mei, J., Liu, Z., and Wen, W. Dynamic mass density and acoustic metamaterials. *Physica B: Condensed Matter*, 394(2):256–261, 2007.

Sklan, R., Sophia, Pak, Y. S., Ronald, and Li, B. Seismic invisibility: elastic wave cloaking via symmetrized transformation media. *New Journal of Physics*, 20(6):063013, 2018.

Smith, D. R., Padilla, W. J., Vier, D. C., Nemat-Nasser, S. C., and Schultz, S. Composite medium with simultaneously negative permeability and permittivity. *Physical Review Letters*, 84(18):4184–4187, 2000.

Song, Y. B., Feng, L. P., Wen, J. H., Yu, D. L., and Wen, X. S. Reduction of the sound transmission of a periodic sandwich plate using the stop band concept. *Composite Structures*, 128:428–436, 2015.

Srivastava, A. and Nemat-Nasser, S. Overall dynamic properties of three-dimensional periodic elastic composites. *Proceedings of the Royal Society a-Mathematical Physical and Engineering Sciences*, 468(2137):269–287, 2012.

Srivastava, A. Elastic metamaterials and dynamic homogenization: a review. *International Journal of Smart and Nano Materials*, 6(1):41–60, 2015.

Su, Y. C. and Sun, C. T. Design of double negativity elastic metamaterial. *International Journal of Smart and Nano Materials*, 6(1):61–72, 2015.

Sui, N., Yan, X., Huang, T.-Y., Xu, J., Yuan, F.-G., and Jing, Y. A lightweight yet sound-proof honeycomb acoustic metamaterial. *Applied Physics Letters*, 106(17):171905, 2015.

Tan, K. T., Huang, H. H., and Sun, C. T. Blast-wave impact mitigation using negative effective mass density concept of elastic metamaterials. *International Journal of Impact Engineering*, 64:20–29, 2014.

Tang, Y., Ren, S., Meng, H., Xin, F., Huang, L., Chen, T., Zhang, C., and Lu, T. J. Hybrid acoustic metamaterial as super absorber for broadband low-frequency sound. *Scientific Reports*, 7:43340, 2017.

Ting, T. C. T. *Anisotropic Elasticity Theory and Application*. Oxford University Press, Oxford, 1996.

Torrent, D., Pennec, Y., and Djafari-Rouhani, B. Effective medium theory for elastic metamaterials in thin elastic plates. *Physical Review B*, 90(10):15, 2014.

Veselago, V. G. The electrodynaics of substances with simultaneously negative of ε and μ. *Soviet Physics Uspekhi*, 10(4):509, 1968.

Wang, C. and Wang, X. Modeling and simulation of wave scattering of multiple inhomogeneities in composite media. *Composites Part B: Engineering*, 90:341–350, 2016.

Wang, G., Wen, X., Wen, J., Shao, L., and Liu, Y. Two-dimensional locally resonant phononic crystals with binary structures. *Physical Review Letters*, 93(15):154302, 2004.

Wang, X. D. Dynamic behaviour of a metamaterial system with negative mass and modulus. *International Journal of Solids and Structures*, 51(7-8):1534–1541, 2014.

Wang, X. D. and Gan, S. Effective antiplane dynamic properties of fiber-reinforced composites. *Journal of Applied Mechanics*, 69(5):696–699, 2002.

Wang, Y. F., Wang, Y. S., and Zhang, C. Z. Two-dimensional locally resonant elastic metamaterials with chiral comb-like interlayers: Bandgap and simultaneously double negative properties. *Journal of the Acoustical Society of America*, 139(6):3310–3318, 2016.

Wu, Y., Lai, Y., and Zhang, Z.-Q. Effective medium theory for elastic metamaterials in two dimensions. *Physical Review B*, 76(20):205313, 2007.

Wu, Y., Lai, Y., and Zhang, Z.-Q. Elastic metamaterials with simultaneously negative effective shear modulus and mass density. *Physical Review Letters*, 107(10):105506, 2011.

Wu, Y., Yang, M., and Sheng, P. Perspective: Acoustic metamaterials in transition. *Journal of Applied Physics*, 123(9):090901, 2018.

Xiao, S., Li, Y., Yang, Z., and Sheng, P. Active control of membrane-type acoustic metamaterial by electric field. *Applied Physics Letters*, 106(9):091904, 2015.

Xiao, Y., Wen, J., and Wen, X. Longitudinal wave band gaps in metamaterial-based elastic rods containing multi-degree-of-freedom resonators. *New Journal of Physics*, 14(3):033042, 2012.

Yang, Z., Mei, J., Yang, M., Chan, N. H., and Sheng, P. Membrane-type acoustic metamaterial with negative dynamic mass. *Physical Review Letters*, 101(20):204301, 2008.

Yang, Z., Dai, H. M., Chan, N. H., Ma, G. C., and Sheng, P. Acoustic metamaterial panels for sound attenuation in the 50-1000 hz regime. *Applied Physics Letters*, 96(4):041906, 2010.

Yao, S., Zhou, X., and Hu, G. Experimental study on negative effective mass in a 1d mass-spring system. *New Journal of Physics*, 10(4):043020, 2008.

Yao, S., Zhou, X., and Hu, G. Investigation of the negative-mass behaviors occurring below a cut-off frequency. *New Journal of Physics*, 12(10):103025, 2010.

Zadpoor, A. A. Mechanical meta-materials. *Materials Horizons*, 3(5):371–381, 2016.

Zhang, P. and Parnell, W. J. Hyperelastic antiplane ground cloaking. *The Journal of the Acoustical Society of America*, 143(5):2878–2885, 2018.

Zhang, S., Xia, C. G., and Fang, N. Broadband acoustic cloak for ultrasound waves. *Physical Review Letters*, 106(2):4, 2011.

Zhang, S., Yin, L., and Fang, N. Focusing ultrasound with an acoustic metamaterial network. *Physical Review Letters*, 102(19):194301, 2009.

Zhang, X. and Liu, Z. Superlenses to overcome the diffraction limit. *Nature Materials*, 7:435, 2008.

Zhao, H. G., Liu, Y. Z., Wang, G., Wen, J. H., Yu, D. L., Han, X. Y., and Wen, X. S. Resonance modes and gap formation in a two-dimensional solid phononic crystal. *Physical Review B*, 72(1):4, 2005.

Zhou, X. and Hu, G. Analytic model of elastic metamaterials with local resonances. *Physical Review B*, 79(19):195109, 2009.

Zhou, X., Liu, X., and Hu, G. Elastic metamaterials with local resonances: an overview. *Theoretical and Applied Mechanics Letters*, 2(4):041001, 2012.

Zhou, X., Assouar, M. B., and Oudich, M. Acoustic superfocusing by solid phononic crystals. *Applied Physics Letters*, 105(23):233506, 2014.

Zhu, R., Huang, H. H., Huang, G. L., and Sun, C. T. Microstructure continuum modeling of an elastic metamaterial. *International Journal of Engineering Science*, 49(12):1477–1485, 2011.

Zhu, R., Liu, X. N., Hu, G. K., Sun, C. T., and Huang, G. L. A chiral elastic metamaterial beam for broadband vibration suppression. *Journal of Sound and Vibration*, 333(10):2759–2773, 2014a.

Zhu, R., Liu, X. N., Hu, G. K., Sun, C. T., and Huang, G. L. Negative refraction of elastic waves at the deep-subwavelength scale in a single-phase metamaterial. *Nature Communications*, 5:8, 2014b.

Zhu, R., Liu, X. N., and Huang, G. L. Study of anomalous wave propagation and reflection in semi-infinite elastic metamaterials. *Wave Motion*, 55:73–83, 2015.

Zhu, R., Chen, Y. Y., Barnhart, M. V., Hu, G. K., Sun, C. T., and Huang, G. L. Experimental study of an adaptive elastic metamaterial controlled by electric circuits. *Applied Physics Letters*, 108(1):011905, 2016a.

Zhu, R., Chen, Y. Y., Wang, Y. S., Hu, G. K., and Huang, G. L. A single-phase elastic hyperbolic metamaterial with anisotropic mass density. *The Journal of the Acoustical Society of America*, 139(6):3303–3310, 2016b.

Zigoneanu, L., Popa, B.-I., and Cummer, S. A. Three-dimensional broadband omnidirectional acoustic ground cloak. *Nature Materials*, 13(4):352–355, 2014.